DISSERTATION | DOCTORAL THESIS

Titel | Title

Structural studies of the Z-disc complex FATZ-1/α-actinin-2

verfasst von | submitted by

Ariadna Rodriguez Chamorro

angestrebter akademischer Grad | in partial fulfilment of the requirements for the degree of

Doctor of Philosophy (PhD)

Wien | Vienna, 2024

Studienkennzahl lt. Studienblatt | Degree programme code as it appears on the student record sheet:	UA 794 620 490
Dissertationsgebiet lt. Studienblatt | Field of study as it appears on the student record sheet:	Molekulare Biologie
Betreut von | Supervisor:	Univ.-Prof. Dipl.-Ing. Dr. Kristina Djinovic-Carugo

…to my three boys

ACKNOWLEDGEMENTS

I would like to thank my former colleagues from Krisitina's Group, who supported me as a Ph.D. student, especially Dr. Euripides De Almeida Ribeiro, Claudia Schreiner and Dr. Julius Kostan. They guided my experimental journey with FATZ-1 and α-actinin-2**,** and gave me helpful advice to tackle the challenges of experimental work with difficult proteins.

I am also grateful to my PhD committee, Dr. Bojan Zagrovic, Prof. Robert Konrant and Dr. Dieter O. Fürst. I appreciate their advice and suggestions, which helped me decipher the purpose of this work.

Furthermore, I would like to thank my collaborators. For cross-linking and mass spectrometry analyses, Dr. Friedel Drepper and Prof. Bettina Warsheid at the University of Freiburg. For NMR experiments and analysis, Prof. Robert Konrat's group at the University of Vienna.

Many thanks to my supervisor, Prof. Kristina Djinovic-Carugo, for giving me two opportunities to accomplish my Ph.D. I first learned structural biology and scientific methodology; second, I learned to persevere. I also learned one Italian saying, "meglio tardi che mai."

TABLE OF CONTENTS

ABSTRACT

FATZ-1 is a protein expressed in the Z-disc of fast-twitch fibres with multiple binding partners such as α-actinin, filamin-C, telethonin, ZASP, myotilin and calcineurin. FATZ-1 is an essential player in Z-disc signalling as a negative modulator of the calcineurin/NFAT signalling cascade that controls the muscle fibre composition in response to biomechanical stress. In addition, FATZ-1 may play an essential role in the Z-disc assembly by interacting with α-actinin-2 since the complex appears in the early stages of myofibrillogenesis, where it may recruit other proteins to the Z-disc. Its C-terminal region appears as a functional domain, named CD2, where α-actinin-2 and other binding partners interact. How the structure of the FATZ-1 CD2 region can support multiple binding partners and achieve the recruitment of other proteins to the Z-disc while still binding to α-actinin-2 remains to be discovered.

We performed a structural study of the complex FATZ-1/α-actinin-2 to understand this complex supports the Z-disc structure. Since predictions indicated large unstructured regions in FATZ-1, we employed several biophysical methods, such as CD and SAXS, to study its structure. We found that FATZ-1 has characteristics of an intrinsically disordered protein with residual secondary structure content and can better be described as a conformational ensemble. In addition, we found that FATZ-1 and α-actinin-2 form a high-affinity complex with two different binding events. We identified contact residues of the complex FATZ-1/α-actinin-2 binding interface employing chemical crosslinking combined with mass spectrometry. Finally, our CD and SAXS data suggested that FATZ-1 remains flexible rather than compact after binding to α-actinin-2.

Our study hypothesizes that the high affinity of the complex FATZ-1/α-actinin-2 and the flexibility of FATZ-1 may be advantageous to the Z-disc assembly and signalling, by allowing FATZ-1 to stay anchored to the Z-disc while interacting with other binding partners that would exchange in its CD2 region in response to signalling events or according to the Z-disc developing stages.

ABBREVIATIONS

BME: 2-Mercaptoethanol

BSA: Bovine Serum Albumin

CD: circular dichroism

CBB: Coomassie Brilliant Blue

Dmax: maximum intramolecular distance

DLS: Dynamic Light Scattering

IDP: intrinsically disordered protein

ITC: isothermal titration calorimetry

NMR: nuclear magnetic resonance

NRMSD: normalized root mean square deviation

PMSF: Phenylmethanesulfonyl fluoride

R_h: hydrodynamic radius

Rg: radius of gyration

RT: room temperature

SAXS: a small angle X-ray scattering

SDS: sodium dodecyl sulphate

SDS-PAGE: SDS-polyacrylamide gel electrophoresis

SEC: size exclusion chromatography

SEC-MALS: Size exclusion chromatography combined with multiple angle light scattering

TCEP: Tris(2-carboxyethyl)phosphine hydrochloride

XL-MS: Cross-linking combined with mass spectrometry

2D-HSQC: 2D 1H 15N heteronuclear single-quantum coherence spectroscopy

INTRODUCTION

The sarcomere

Sarcomeres are the striated muscle's basic structural unit, linked in continuous long strands forming the myofibrils. Several myofibrils are packed in bundles to form the muscles that move body parts (Squire, 1997). Under the microscope, muscle fibres appear in a striated pattern due to the arrangement of the myosin and actin filaments, alternating a dark band and a light band within each sarcomere, named A-band and I-band respectevely. The A-bands consist of thick filaments of myosin interlaced with thin actin filaments. The M-band is at the center of the A-band, where transverse, electron-dense M-bridges cross-link the myosin filaments (Luther, 2009; Squire, 1997). The I-bands comprise actin filaments, and the Z-disc connects oppositely polarized actin filaments in the middle of the I-band (Clark et al., 2002), as shown in **Figure 1**.

Other filament systems also exist in the sarcomere, formed by two giant proteins. Titin (3 MDa) spans half of the sarcomere, and nebulin (800 kDa) spans the length of the actin filaments (Clark et al., 2002; Luther, 2009). Titin forms the template for the sarcomere, and nebulin forms the template for the thin filament assembly (Clark et al., 2002). Moreover, the Z-discs define the lateral boundaries of the sarcomere where the actin, titin, and nebulin filaments are anchored (Luther, 2009).

The sarcomere is the unit where muscle contraction occurs. The interactions between the actin filaments and the myosin filaments support this role. Hundreds of myosin molecules form the myosin filaments, the molecular motor for muscle contraction (Clark et al., 2002). The myosin protein comprises two functional regions: the N-terminal head and the C-terminal rod. The myosin head domain forms the catalytic motor ATPase domain and bears the binding sites for actin. The myosin C-terminal comprises a two-chain coiled-coil rod involved in myosin polymerization and attachment to the M-band (Squire, 1997).

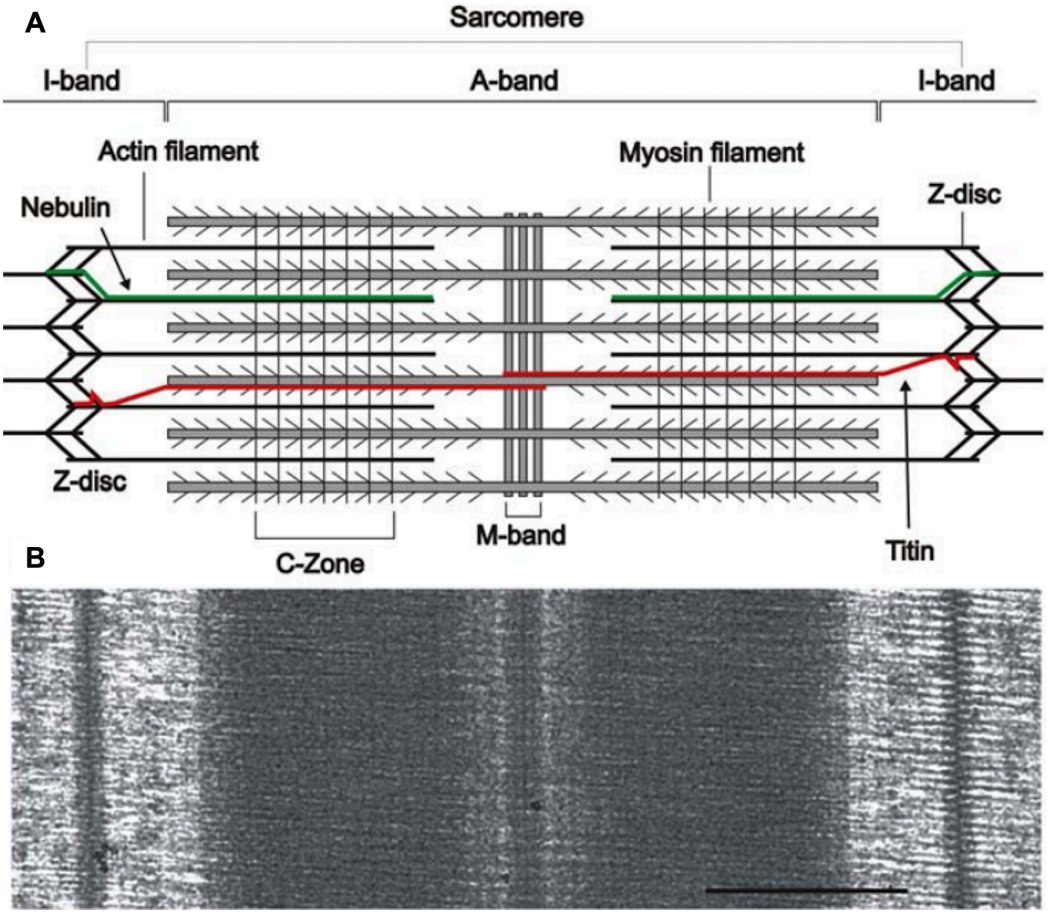

Figure 1. Striated muscle sarcomere. (Modified from Luther, 2009). A) Diagram showing the main components of the sarcomere. The A-bands consist of thick filaments of myosin crosslinked at the centre by the M-band. Myosin filaments are interlaced with thin filaments of actin, which spann the I-bands and are crosslinked at the Z-disc. Additionally, two giant proteins contribute to the structure of the Z-disc. Nebulin (800 kDa) runs along the thin filaments and overlaps in the Z-disc, and titin (3 MDa) runs between the M-line and the Z-disc. B) Electron micrograph of a fish white fast oxidative fibre sarcomere.

Upon ATP hydrolysis, the head domain undergoes a significant angular rotation, displacing 100 Å over the actin filament and forming a cross-bridge. A power stroke reaction allows the myosin to pull the actin filament towards the M-line, shortening the sarcomere. After the power stroke is completed, Pi and ADP are released, and a new ATP molecule binds myosin, returning the complex to a relaxed state, ready for a new power stroke cycle (Huxley, 1969). The muscle contraction is controlled by Ca2+, which binds regulatory proteins tropomyosin and troponin attached to the actin filaments and exposes the actin-binding site to myosin heads. When actin filaments slide towards the M-band, the sarcomere reduces its lengths,

and the entire myofibril shortens, provided muscles are attached at their ends. When many myofibrils undergo a contraction at the same time, a muscle can build up enough force to move parts of the body. (Holmes, 1995).

Although skeletal and cardiac muscle fibres appear very different, they are made from the same building block, the sarcomere. However, each muscle type has unique cellular components, physiology, and regulation mechanisms, allowing them to perform specific functions (Clark et al., 2002).

Skeletal muscles are classified by their contraction speed and metabolic energy pathways. They respond to voluntary stimuli to move the body. Type 1 fibres are also called slow oxidative fibres, which contract relatively slowly and use the oxidative metabolic pathway to generate ATP. They are in charge of low-power contractions over long periods and resits longer to fatigue. Type 2A fibres, also known as fast oxidative fibres, contract fast and use the primary oxidative metabolic pathway to produce ATP. They undergo fatigue more quickly than slow oxidative fibres. However, they can switch rapidly to the glycolytic pathway to produce ATP and respond faster to contraction. The last type is type 2 B, also called fast glycolytic fibres because they have rapid contractions and primarily use the glycolytic pathway. They are in charge of high-power contraction over a short period and undergo fatigue more quickly than the others (Schiaffino & Reggiani, 2011).

Cardiac muscles, or myocardium, are involuntary, striated muscles that cover the heart chambers. They comprise individual cardiomyocytes connected through intercalated discs. These highly adherent complexes allow the cardiac muscle cells to receive rapid electrical transmission and contract as a single unit, allowing the myocardium to perform the fast and continuous contractions needed for the heart function (Frank & Frey, 2011).

The Z-disc: structural anchor and signalling hub

In skeletal and cardiac muscle, the Z-disc is in charge of similar functions, the crosslink of actin filaments and the regulation of signalling pathways that control de myofibril physiology and phenotype (Clark et al., 2002; Luther, 2009). The crosslinks of oppositely polarized actin filaments are created by α-actinin molecules (Takahashi & Hattori, 1989). They form a network that resembles a basketweave described as a

“small-square lattice” (Goldstein et al., 1986; Luther, 2000), and their width varies with fibre and muscle type: fast muscles have narrow widths (*30–50 nm), and slow and cardiac fibres have wide Z-bands (*100–140 nm) (Luther et al., 2003). The widths are determined by the overlap of the interlaced actin filaments and by the number of crosslinking layers of α-actinin, which range from two in fast muscle to six in slow muscle (Luther et al., 2003).

Apart from the actin filaments and α-actinin, many other sarcomeric proteins, like the giant titin and nebulin, overlap in the Z-disc (Clark et al., 2002; Squire, 1997). It is thought that nebulin plays an essential role in the assembly, structure and function of the Z-disc in skeletal muscle (McElhinny et al., 2003). In cardiac muscle, nebulin is present as nebulette, a 107 kDa nebulin homologue. During myofibrillogenesis, nebulin emerges in Z bodies, precursors of Z-discs, before the actin filaments are formed (McElhinny et al., 2003). Experimental evidence indicates that nebulin is required for the localization of CapZ in the Z-disc, which caps the barbed ends of the actin filaments and interacts strongly with α-actinin (Pappas et al., 2008). Since nebulin traverses the I-band until the Z-disc, it may contribute to the tension-bearing role of the Z-disc (Luther, 2009).

The titin N-terminus (90 kDa) is located at the Z-disc (Young et al., 1998), where the Ig domains Z1 and Z2 are located at the distal end of the Z-disc and Z-repeats span the width of the Z-disc (Gregorio et al., 1998). The Z-repeats are differentially expressed in fibre types (Gautel et al., 1996), and their role in the Z-disc assembly has been debated (Luther, 2009). Nevertheless, since they have specific expression patterns in different fibre types, the Z-repeats and the nebulin Z-disc regions can be used as start and end markers of the different Z-disc fibre types (Luther, 2009).

Besides being the lateral boundaries of the sarcomere, the Z-disc is a signal transduction center of the myofibrils. This function is supported by several other proteins that find housing in the Z-disc and modulate signalling pathways connecting the sarcomere to the nucleus (Clark et al., 2002; Frank & Frey, 2011; Sanger et al., 2010). The diversity of proteins present in the Z-disc, with its multiple interactions involved in signalling and structural support, is illustrated schematically in **Figure 2.** Signalling proteins such as the phosphatase calcineurin and the protein kinase C

(PKC) have positive and negative modulators in the Z-disc (Frank & Frey, 2011). The phosphatase calcineurin was found to play a crucial role in the skeletal muscle response to biomechanical stress and the cardiomyocyte's response to pressure overload by controlling the NFAT (nuclear factor of activated T-cells) activity. Moreover, the failure to fine-tune the calcineurin/NFAT signalling cascade leads to a hypertrophic response in cardiomyocytes, and the development of an hypertrophic cardiomyopathy (Frey et al., 2000, 2004).

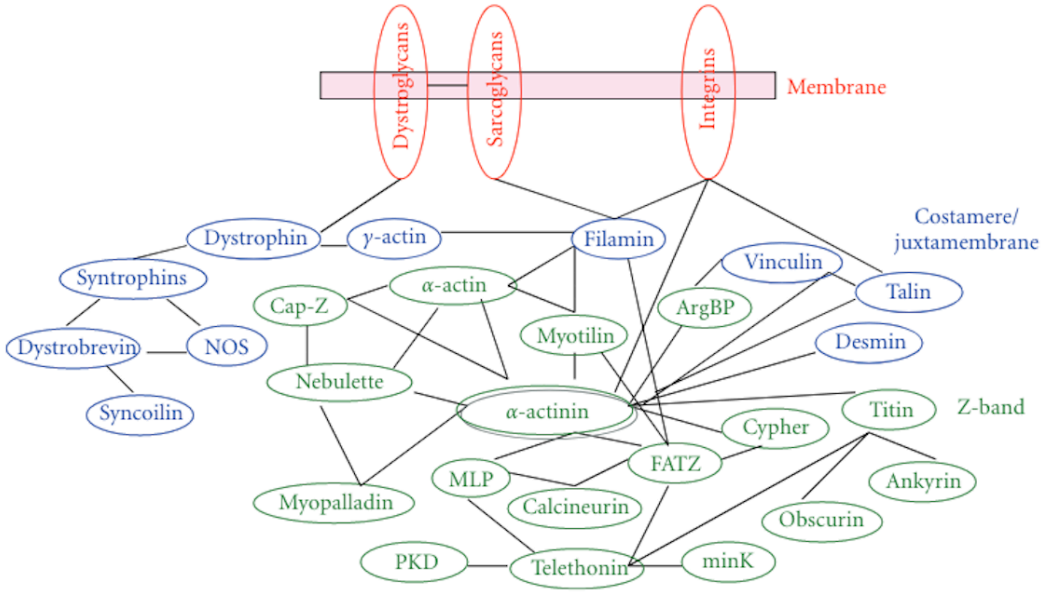

Figure 2: Schematic representation of proteins located in the Z-disc (Modified from Sanger et al., 2010). In mature myofibrils, costameric proteins attach the Z-disc to the muscle cells' sarcolemma (membrane in pink). The diversity of proteins in the Z-disc supports its role in maintaining the structural integrity of the sarcomere and as a signal transduction center.

Several Z-disc proteins involved in Z-disc signalling pathways bind α-actinin and bind to each other, creating an intricate protein network in which molecular organization and dynamics are challenging to understand (Faulkner et al., 2001a). However, the molecular architecture of some Z-disc proteins are known and have been used to create a model of the Z-disc (Gautel & Djinović-Carugo, 2016). **Figure 3** displays the proposed model where α-actinin-2 crosslinks actin filaments via its ABD domain and titin via the C-terminal calmodulin-like domain (Efhands). In addition, molecular details of the titin capping by telethonin and the actin filaments capping by CapZ are also depicted, where the nebulin is placed near the capping

complex as a cooperator in actin filament regulation, and the capZ is identified as a capping protein (Gautel & Djinović-Carugo, 2016).

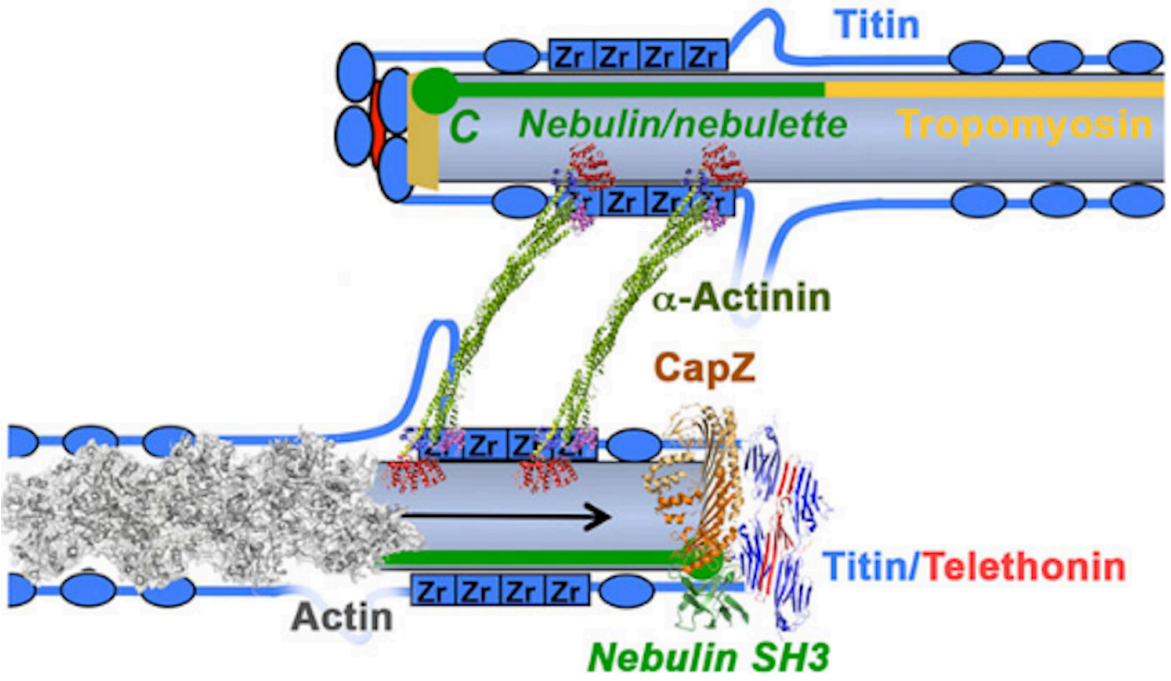

Figure 3: Structural model of the Z-disc proposed by Gautel & Djinović-Carugo in 2016. The structure of the leading players, such as α-actinin-2, α-actin, CapZ, Titin, Telethonin and Nebulin, are known and have been placed in the Z-disc structural model.

α-Actinin-2

α-Actinin is a highly conserved protein in many different organisms. It belongs to the spectrin superfamily of actin-binding proteins, including spectrin and dystrophin (Broderick & Winder, 2005; Sjöblom et al., 2008). Its principal function is to cross-link actin filaments and help maintain the structural integrity of cells (Masaki et al., 1967). In addition, α-actinin plays an essential role in cell adhesion and migration and in forming stress fibres and focal adhesions (Edlund et al., 2001).

α-Actinin isoforms can be classified into two main groups based on their sensitivity to calcium: muscle isoforms (which are calcium-insensitive) and non-muscle cytoskeletal isoforms (which are calcium-sensitive) (Burridge & Feramisco, 1981; Sjöblom et al., 2008). Non-muscle cytoskeletal α-actinin is

expressed in various cell types and regulates cytoskeletal dynamics, cell adhesion, and migration (Sjöblom et al., 2008). Skeletal, cardiac, and smooth muscle isoforms of α-actinin (isoforms 2 and 3) are primarily localized in the Z-disc, where they cross-link actin filaments from adjacent sarcomeres, forming a lattice-like structure that helps to stabilize the sarcomere (Luther, 2009; Squire, 1997). α-Actinin-2 is a major isoform in cardiac and oxidative skeletal muscle, while α-actinin-3 is primarily expressed in glycolytic skeletal muscle fibres (Mills et al., 2001).

The structure of α-actinin-2 has been studied in detail (Djinović-Carugo et al., 1999; Franzot et al., 2005; Ribeiro et al., 2014; Sjöblom et al., 2008; Ylänne et al., 2001). **Figure 4** shows the complete structure published by Ribeiro et al. in 2014, where it can be observed that α-actinin-2 is a functional anti-parallel dimer, with each monomer consisting of an ABD connected via a flexible neck region to four spectrin repeats that form the central rod and followed by a C-terminal calmodulin-like domain, which in the dimer are binding the neck region of the opposed monomeric chain. Such a molecular architecture results in the formation of a rod-shaped molecule with functional domains (ABD and EFhands) at both ends, allowing α-actinin-2 to cross-link actin filaments in bundles (Ribeiro et al., 2014; Sjöblom et al., 2008). The α-actinin-2 regulation model proposes that without Phosphatidylinositol 4,5-bisphosphate (PIP2), α-actinin-2 exists in two conformational states: a highly populated closed state and a lowly populated open and active state. Upon PIP2 binding to the ABD domain, EFhands(3-4) are released from the neck, increasing the open and active conformation of α-actinin-2 and allowing the titin to bind to the EFhands (Ribeiro et al., 2014). In this open conformation, ABD domains may undergo a rotation around the flexible neck region, allowing the ABDs of the same α-actinin-2 molecule to interact with actin filaments in an antiparallel manner (Ribeiro et al., 2014).

In addition to its well-established role in actin filaments cross-linking, α-actinin has also been recognized as a significant mediator of protein-protein interaction involving many cytoskeletal and regulatory proteins (Luther, 2009; Noureddine & Gehmlich, 2023; Ribeiro et al., 2014). In striated muscle, α-actinin interacts with various proteins, including contractile machinery and associated adaptor or signalling proteins, transmembrane receptors and channels, and metabolic proteins (Sjöblom et al., 2008). Among the proteins that interact with α-actinin are the molecular rulers'

titin and nebulin, the actin filament capping protein CapZ, telethonin as well as the paladin/myotilin/myopalladin family, the enigma/cypher family proteins, hCLIM1 Z-disk-associated protein (ZASP/cypher/oracle), and the actinin-associated LIM protein (ALP) (Faulkner et al., 2001b; Sjöblom et al., 2008).

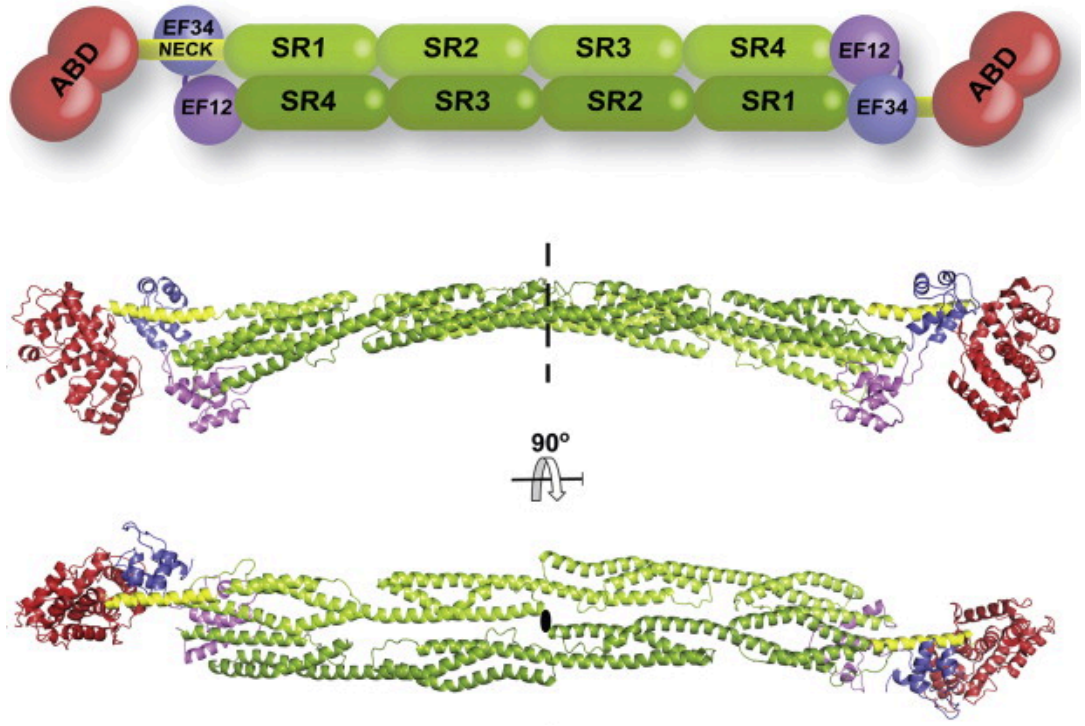

Figure 4: Structure of α-actinin-2 full-length (modified from Ribeiro et al., 2014). Top: Scheme of α-actinin-2 domains: ABD (red), neck(yellow), SR1-SR4 (green), EFhands 3-1 (violet), EFhands 3-4 (blue). Bottom: The dimeric structure of α-actinin-2 obtained by X-ray at 3.5 Å resolution with a symmetrical plane at the center of the rod domain and a rotated view at 90° (figure extracted from Ribeiro et al., 2014).

Additionally, α-actinin interacts with the FATZ protein family (myozenin, calsarcin family) (Faulkner et al., 2000), which binds to calcineurin, a Ca2+ CaM-dependent phosphatase (Frey et al., 2000; Frey & Olson, 2002). The interaction with FATZ proteins links α-actinin to the calcineurin/NFAT signalling pathway and modulates the muscle fibre type in skeletal muscle and the hypertrophic response in cardiac fibres (Frey et al., 2004, 2008).

The diversity of proteins interacting with the rod domain of α-actinin suggests a

highly complex and sophisticated interaction landscape. The exact mechanism by which α-actinin coordinates these interactions is not fully understood, raising the question of whether these interactions might coexist or exclude each other.

The FATZ protein family

The FATZs are a protein family, also known as calsarcins or myozenins (Faulkner et al., 2000; Frey et al., 2000; Takada et al., 2001) comprising three isoforms: FATZ-1, FATZ-2 and FATZ-3, whose expression in muscle fibres changes during the curse of embryonic development and has specificity to muscle fibre type (Frey et al., 2000; Frey & Olson, 2002). In early embryonic days, FATZ-1 is expressed in cardiac and skeletal muscle and as embryogenesis progresses, the FATZ-1 expression decreases in cardiac muscle and increases in skeletal muscle, where it is found in gastrocnemius muscle, composed mainly of fast-twitch fibres (Faulkner et al., 2000; Frey et al., 2000; Takada et al., 2001). In contrast, FATZ-2 expression is persistent in cardiac and skeletal muscle all over the embryonic development. In skeletal muscle, FATZ-2 is expressed in soleus and plantaris muscles, predominately composed of slow-twitch fibres (Frey et al., 2000). In addition, FATZ-3 is exclusively expressed in skeletal muscle and predominantly in fast-twitch fibres (Frey & Olson, 2002).

FATZ-1/ Myozenin-1/ calsarcin-2

FATZ-1 stands for Filamin-C, α-Actinin-2, and Telethonin Z-disc binding protein, which already informs about the multiple interactions of this protein in the Z-disc (Faulkner et al., 2000; Takada et al., 2001). In addition to those binding partners, FATZ-1 interacts with the phosphatase domain of calcineurin and the PDZ domain of Enigma proteins (Frey et al., 2000, 2008; von Nandelstadh et al., 2009). Research evidence suggested that FATZ-1 (also referred to as calsarcin-2 and myozenin-1) may facilitate the assembly of Z-disc during the initial stages of myofibrillogenesis (Faulkner et al., 2000; Frey et al., 2000; Wang et al., 2005). Moreover, previous studies have highlighted the significant role played by FATZ-1 in regulating muscle fibre composition and enhancing exercise performance *in vivo* (Frey et al., 2008).

The three FATZ isoforms have conserved sequence regions in their N and

C-terminal regions, with a glycine-rich region in the middle of their sequence displaying a notable variability (**Figure 5**). Based on this conservation profile, the FATZ-1 sequence was annotated as presented in **Figure 6**, like conserved domain 1 (CD1) from residues 1 through 75, the glycine-rich region (GRR) from residues 76 through 171, and conserved domain 2 (CD2) from residue 172 through 299 (Faulkner et al., 2000). This annotation obeys the conservation profile among the three isoforms and not any structural criteria since the search for structural homologs in public databases was unsuccessful in returning structural or functional domains (Faulkner et al., 2000; Takada et al., 2001).

While FATZ proteins have been identified in several vertebrate species, their expression has been primarily observed in striated muscle, suggesting that they are a unique set of proteins that have evolved to perform a specific role in the Z-disc (Takada et al., 2001). It is worth noting that the study of human FATZ protein homologs has been carried out in mice and zebrafish, which has provided valuable insights into their function in Z-disc signalling and assembly (Faulkner et al., 2000; Frey et al., 2000; Frey & Olson, 2002; Takada et al., 2001).

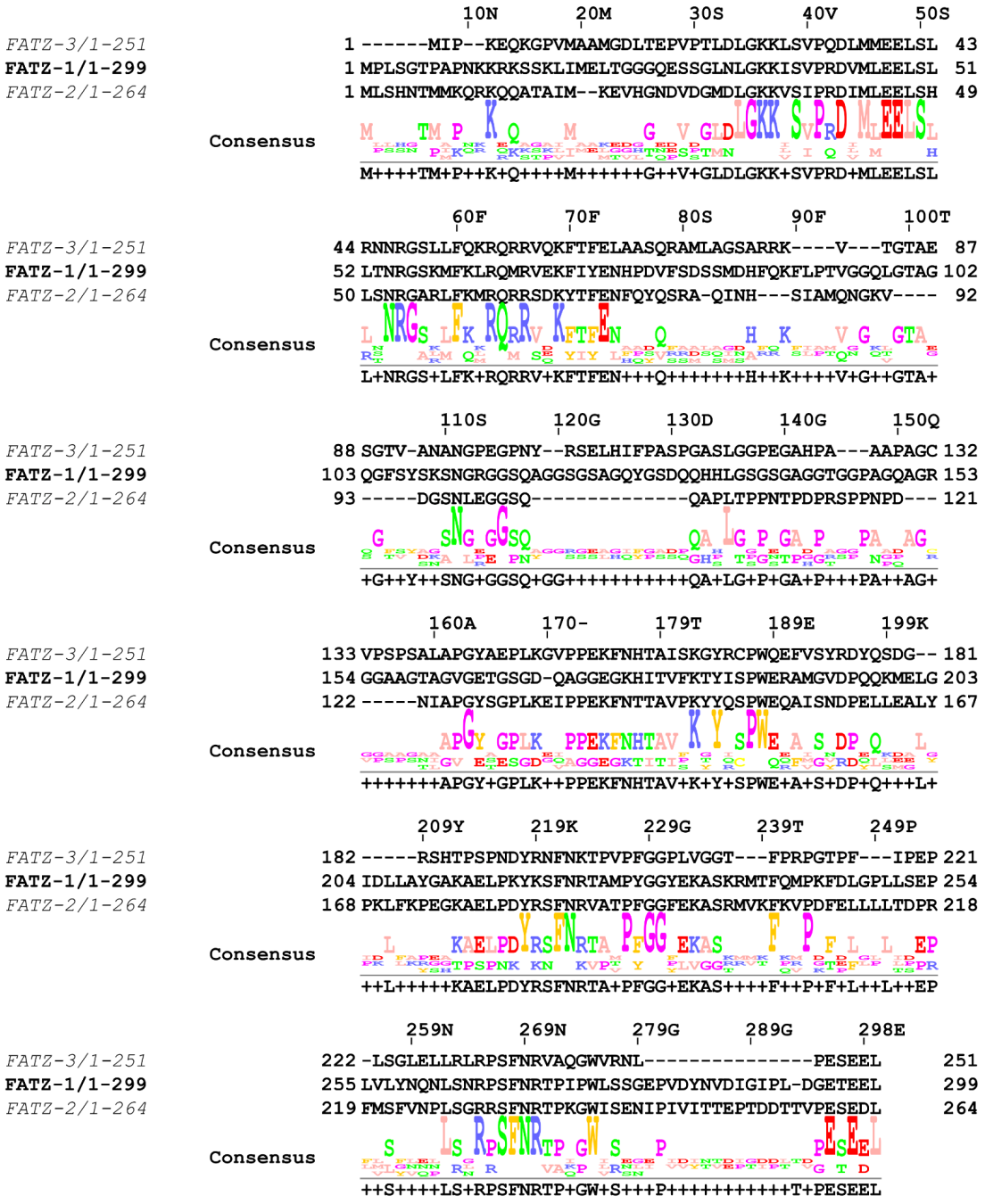

Figure 5. Sequence alignment of the FATZ human protein family. The three FATZ isoforms have conserved sequence regions in their N and C-terminal regions, with a glycine-rich region in the middle of their sequence displaying a notable variability. The residue positions are numbered after the FATZ-1 sequence.

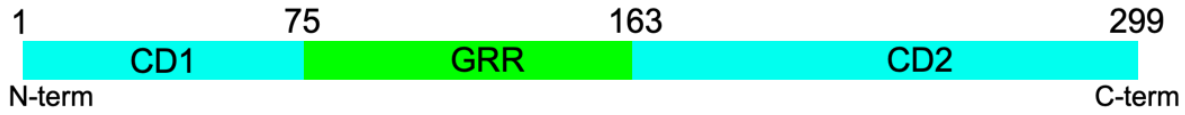

Figure 6. Annotation of FATZ-1 protein sequence. CD1 stands for conserved domain 1 (residues 1 through 75), GRR stands for glycine-rich region (residues 76 through 171), and CD2 stands for conserved domain 2 (residues 172 through 299) (Faulkner et al., 2000).

FATZ-1's role in Z-disc signalling pathways

FATZ-1 interaction with calcineurin has been proven essential in regulating muscle fibre composition and exercise performance *in vivo* (Frey et al., 2008). Calcineurin is a positive modulator of the NFAT (nuclear factor of activated T-cells) transcription factors, which activation leads to a muscle fibre type switch towards a slow-twitch and oxidative phenotype, enabling fatigue-resistant and sustained muscle activity. (Chin et al., 1998; Delling et al., 2000).

The genetic ablation of FATZ-1 resulted in a notable increase in calcineurin/NFAT activity and a fibre-type shift from glycolytic toward oxidative fibres with enhanced endurance (Frey et al., 2008), demonstrating that FATZ-1 negatively regulates calcineurin activity in fast-twitch fibers. Interestingly, the deletion of α-actinin-3 in mice, similar to FATZ-1 deletion, exhibits an increase in exercise endurance capacity, an increase in oxidative metabolism and a change toward oxidative fibres (MacArthur et al., 2007). The absence of α-actinin-3 is observed in around 18% of healthy humans and is associated with high athletic performance (Kn et al., 1999). Like FATZ-1, α-actinin-3 is confined to fast-twitch fibres (North & Beggs, 1996). Since FATZ-1 and α-actinin-3 are Z-disc interacting proteins (Frey et al., 2000; Takada et al., 2001), FATZ-1 may be a downplayer of α-actinin-3 modulating the fibre type phenotype by inhibiting calcineurin activity (Frey et al., 2008).

FATZ-1's role in the Z-disc assembly

FATZ-1 interaction with α-actinin-2, filamin-C and the Enigma proteins has been proposed to be relevant in the Z-disc assembly from the early stages of myofibrillogenesis (Faulkner et al., 2000; Takada et al., 2001; Wang et al., 2005). Previous research demonstrated that FATZ-1 expression is detected in the early

stages of skeletal myofibrillogenesis, and it is upregulated as myofibril development progresses (Faulkner et al., 2000; Frey et al., 2000). Additionally, FATZ-1 has been localized in Z-bodies (small amorphous aggregates precursors of the Z-disc during myofibrillogenesis) with α-actinin-2, filamin-C, cypher and myotilin (Sanger et al., 2010). It has been observed that FATZ-1 and α-actinin-2 undergo a dynamical protein exchange between the Z-bodies and the cytosol in the early stage of myofibrillogenesis. This exchange persists through the Z-discs of mature myofibrils, suggesting that the interaction between FATZ-1 and α-actinin-2 plays a significant role in Z-disc assembly and, later, in structure maintenance (Sanger et al., 2010; Wang et al., 2005, 2014).

FATZ-1 interacting partners

The interaction map of FATZ-1 with its Z-disc binding partners is complex and involves several proteins. FATZ-1 has been shown to interact with α-actinin-2, filamin-C, telethonin, calcineurin, myotilin, and ZASP/Cypher (Faulkner et al., 2000; Frey et al., 2000; Gontier et al., 2005; Takada et al., 2001; von Nandelstadh et al., 2009). All of them are Z-disc proteins involved in versatile tasks such as structural support, Z-disc assembly, or signalling pathways. Notably, their binding sites are concentrated in the conserved N- and C-terminal regions of FATZ-1.

Research has confirmed that FATZ-1 binds α-actinin-2, α-actinin-3, filamin-A, filamin-B and filamin-C (Faulkner et al., 2000; Frey & Olson, 2002; Gontier et al., 2005; Takada et al., 2001) with a binding region located in the CD-2 region (Takada et al., 2001). The binding of FATZ-1 on α-actinin-2 was observed in SR3-SR4 (Faulkner et al., 2000). However, it was reported that the SR4 was sufficient to promote binding (Takada et al., 2001). Similarly, the filamin-C binding region of FATZ-1 was identified between repeats 19-24 (Gontier et al., 2005), and repeat 23 was observed to be sufficient to promote binding (Takada et al., 2001). Furthermore, it was observed that α-actinin-2 and filamin-C binding to FATZ-1 was competitive, which could be explained by the fact that both proteins interact with the same region (Takada et al., 2001). Indeed, the high density of partners in the C-terminal has raised the question of whether they co-exist in ternary complexes or exclude each other.

In addition, several studies confirmed the binding of FATZ-1 to the calcineurin phosphatase domain (CnB) (Frey et al., 2000, 2008). Moreover, they indicated that the binding region for CnB spanned residues 214 to 240 of the FATZ-2 protein (Frey et al., 2000). Since FATZ-1 and FATZ-2 isoforms are highly conserved in this region, it has been suggested that the binding region in FATZ-1 is likely present in the same region.

Two independent studies have confirmed the binding of FATZ-1 to telethonin, but the binding region has yet to be mapped (Faulkner et al., 2000; Frey & Olson, 2002). However, one of the studies identified the binding region of FATZ-3 to telethonin in the CD-1 region, which spans residues 50 to 67 (Frey & Olson, 2002). This region is highly conserved in FATZ proteins, suggesting it may also be the binding region for FATZ-1.

The interaction between myotilin and FATZ-1 has been proved by biochemical assays (Gontier et al., 2005). Coexpression of both proteins in non-muscle cells has been shown to alter the subcellular distribution of FATZ-1 and lead to significant colocalization with myotilin. Moreover, FATZ-1 has been found to bind to GST-myotilin in vitro, indicating that they can form a complex. Finally, myotilin has been shown to bind directly to FATZ-1 in yeast two-hybrid assays. The CD2 C-terminal region of FATZ-1 is responsible for its association with myotilin, while the entire molecule of myotilin contributes to the interaction with FATZ-1 (Gontier et al., 2005).

It was reported that a class III PDZ binding peptide was found in the C-terminus of FATZ-1, which binds specifically with several Enigma proteins, including ZASP/Cypher, CLP-36, ALP, and RIL (von Nandelstadh et al., 2009). This peptide motif was also found in FATZ-2 and FATZ-3, as well as other Z-disc proteins like myotilin, palladin, and myopalladin. Interestingly, phosphorylation increased the binding between all FATZ family peptides and the PDZ domain of ZASP/Cypher, and PKA kinases were found to phosphorylate the C-terminus of FATZ-1 and 2 (von Nandelstadh et al., 2009). The implications of FATZ-1 phosphorylation by PKA for the Z-disc signalling pathways remain unclear. Still, it was suggested that ZASP/Cypher could link FATZ-1 to signalling events such as PKC phosphorylation,

as ZASP/Cypher is known to bind protein kinases via their LIM domains (von Nandelstadh et al., 2009).

Figure 7 summarises all the FATZ-1 interacting partners, such as α-actinin-2, filamin-C, myotilin, telethonin, calcineurin and ZASP/Cypher. The figure highlights the intricate interactions between these proteins. The possibility of ternary complexes has been envisaged in some interactions such as the FATZ, α-actinin-2 and calcineurin (Frey et al., 2000) and the FATZ, α-actinin-2, Filamin-C (Takada et al., 2001). However, the molecular mechanism FATZ employs to interact with α-actinin-2 and other Z-disc proteins remains yet to be unravelled.

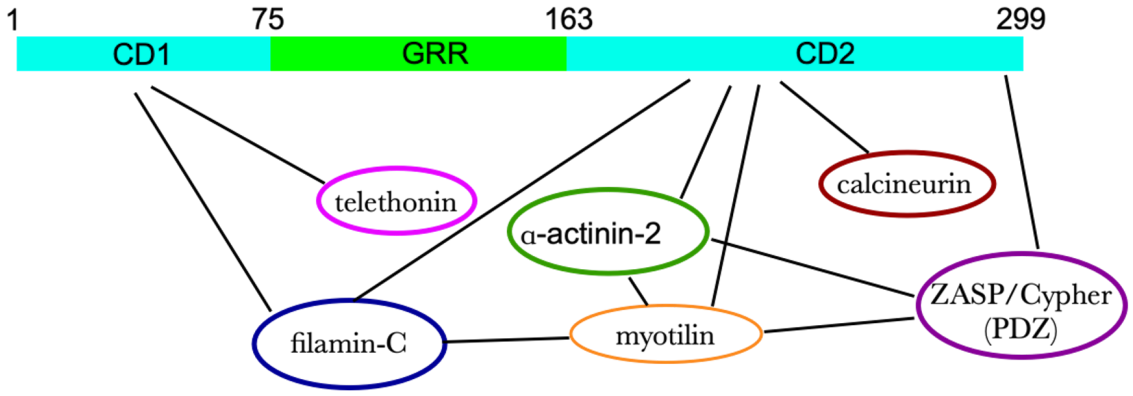

Figure 7: FATZ-1 interaction map. Interacting partners described in the literature include α-actinin-2, filamin-C, myotilin, telethonin, calcineurin, and ZASP/Cypher. The map illustrates the multiple interactions among FATZ-1 and its partners.

AIM OF THE THESIS

Cellular and biochemical approaches have described the FATZ-1 interaction with α-actinin-2. In addition to binding α-actinin-2, FATZ-1 binds to other Z-disc proteins like Filamin-C, telethonin, mytolilin, calcineurin and ZASP/Cypher via its CD2 region. These interactions are highly conserved among the skeletal and cardiac isoforms. In fast-twitch fibers, FATZ-1 may recruit other proteins to the Z-disc during myofibrillogenesis by providing an anchoring point to α-actinin-2. Whether those interactions are competitive or cooperative and what the molecular mechanism FATZ-1 employs to interact with α-actinin-2 and other Z-disc proteins is not entirely well understood.

This project proposes a biophysical and structural characterization of FATZ-1 alone and in complex with α-actinin-2 to understand its contribution to the Z-disc structure and assembly.

We aim to answer the following questions:

a) What is the molecular architecture of FATZ-1?

b) How can the molecular architecture of FATZ-1 support its function?

c) What is the binding affinity of the complex FATZ-1/α-actinin-2?

d) What are the molecular bases of the complex FATZ-1/α-actinin-2?

e) How does the molecular architecture of the complex FATZ-1/α-actinin-2 contribute to the Z-disc structure?

RESULTS

Part I: FATZ-1 structural characterization

FATZ-1 predictions of secondary structure and disordered regions

FATZ-1 has 299 residues and a calculated molecular mass of 31.74 kDa. The FATZ-1 sequence was annotated according to the conservation profile of the FATZ protein family (Faulkner et al., 2000). As **Figure 1.1** shows, the N-terminal (residues 1 to 75) was identified as the conserved domain 1 (CD1), the central region (residues 76 to 163) as the glycine-rich region (GRR), and the C-terminal (residues 164 to 299) as the conserved domain 2 (CD2).

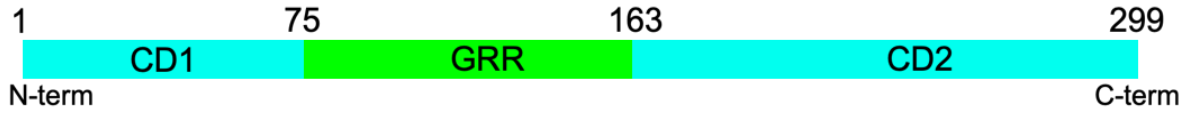

Figure 1.1: FATZ-1 schematic representation (Faulkner et al., 2000). The N-terminal is shown as CD1 (cyan), the central region as GRR (green) and the C-terminal as CD2 (cyan)

Since no structural homologs or canonical domains were reported in the literature, structural predictions were made to identify secondary structure elements in FATZ-1 with the Jpred server (Drozdetskiy et al., 2015). According to the prediction, FATZ-1 might bear a few α-helix in CD1 (9-22 aa, 42-49 aa, 56-66 aa) and CD2 (188-192 aa, 196-201 aa). In addition, there are predicted β-sheets in CD1 (70-74 aa) and in CD2 (177-181 aa) (**Figure 1.2A**). MetaPrDos (Ishida & Kinoshita, 2007) was used to predict intrinsically disordered regions of FATZ-1. The prediction showed three disordered regions: the first in the CD1 (1-34 aa), the second in the GRR (94-174 aa), and the third in the CD2 (293-299 aa) (**Figure 1.2B**). Both predictions agreed that there may be some structured elements in CD1 (residues 44 to 66) and CD2 (residues 177 to 201).

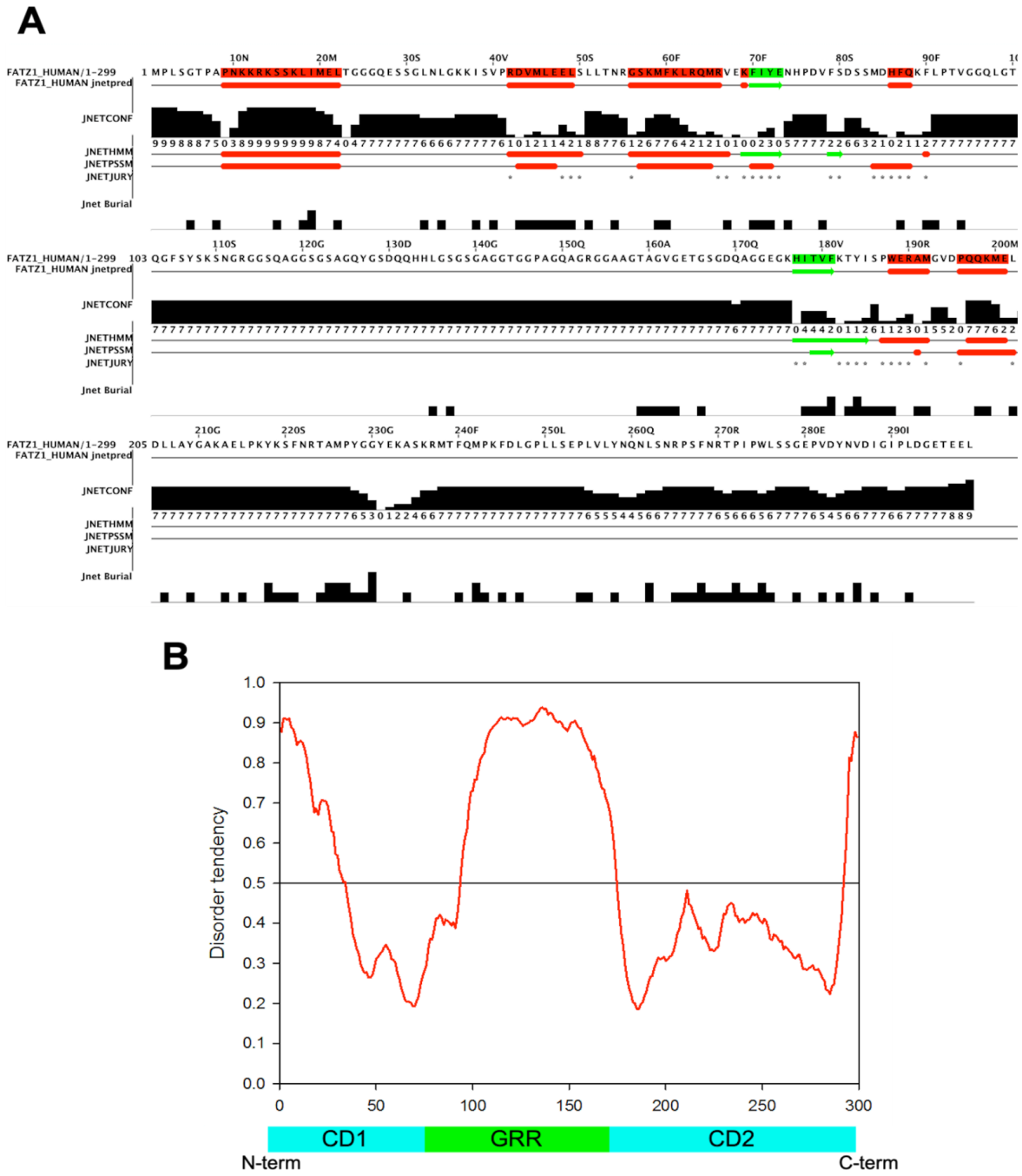

Figure 1.2: FATZ-1 secondary structural predictions. A) JPred (Drozdetskiy et al., 2015) predictions of FATZ-1, α-helix are represented as red tubes and β-sheets as green strands. **B)** Disorder plot of FATZ-1 (top panel) predicted by metaPrDos (Ishida & Kinoshita, 2007) and FATZ-1 schematic representation (bottom panel). Residues with a disorder tendency higher than 0.5 are located in the CD1 (1-34 aa), the GRR (94-174 aa), and the CD2 (293-299 aa).

FATZ1Δ184 purification

The construct FATZ1Δ184 was designed based on the structural predictions of FATZ-1 by a project collaborator (COSS at the MFPL, Vienna). The construct FATZ1Δ184 spanned residues 185 to 299 with a His6 tag in the N-term and a precision protease cleavage site (**Figure 1.3**). The resulting protein had an expected molecular mass of 15.36 kDa.

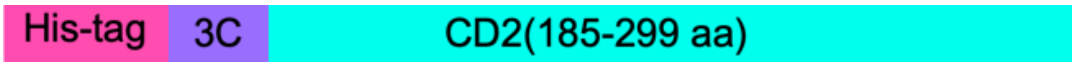

Figure 1.3: FATZ1Δ184 schematic representation. Construct with a His-tag at the N-terminal position, followed by a 3C protease cleavage site and the residues 185 to 299 of FATZ-1. The resulting protein had an expected molecular mass of 15.36 kDa.

FATZ1Δ184 was expressed in *E. coli* Bl21(DE3) cells and purified following the protocol described in the chapter **Material and Methods.** Although several experimental conditions were tried to improve the protein solubility and the purification yield, the outcomes were not improved. After the SEC (**Figure 1.4A**), a small amount of protein was obtained to perform SDS-PAGE (**Figure 1.4B**) and SEC-MALS (**Figure 1.4C**). In SDS-PAGE and CBB staining, bands with molecular weight lower than 15 kDa were observed (**Figure 1.4B, lanes 1 and 3)**. Since the predicted molecular weight of FATZ1Δ184 was 15.36 kDa, some degradation was suspected. The SEC-MALS of the purified product indicated a protein fragment of 6 kDa (**Figure 1.4C**), confirmed by mass spectrometry as a 6.41 kDa fragment corresponding to the first 57 residues of FATZ1Δ184.

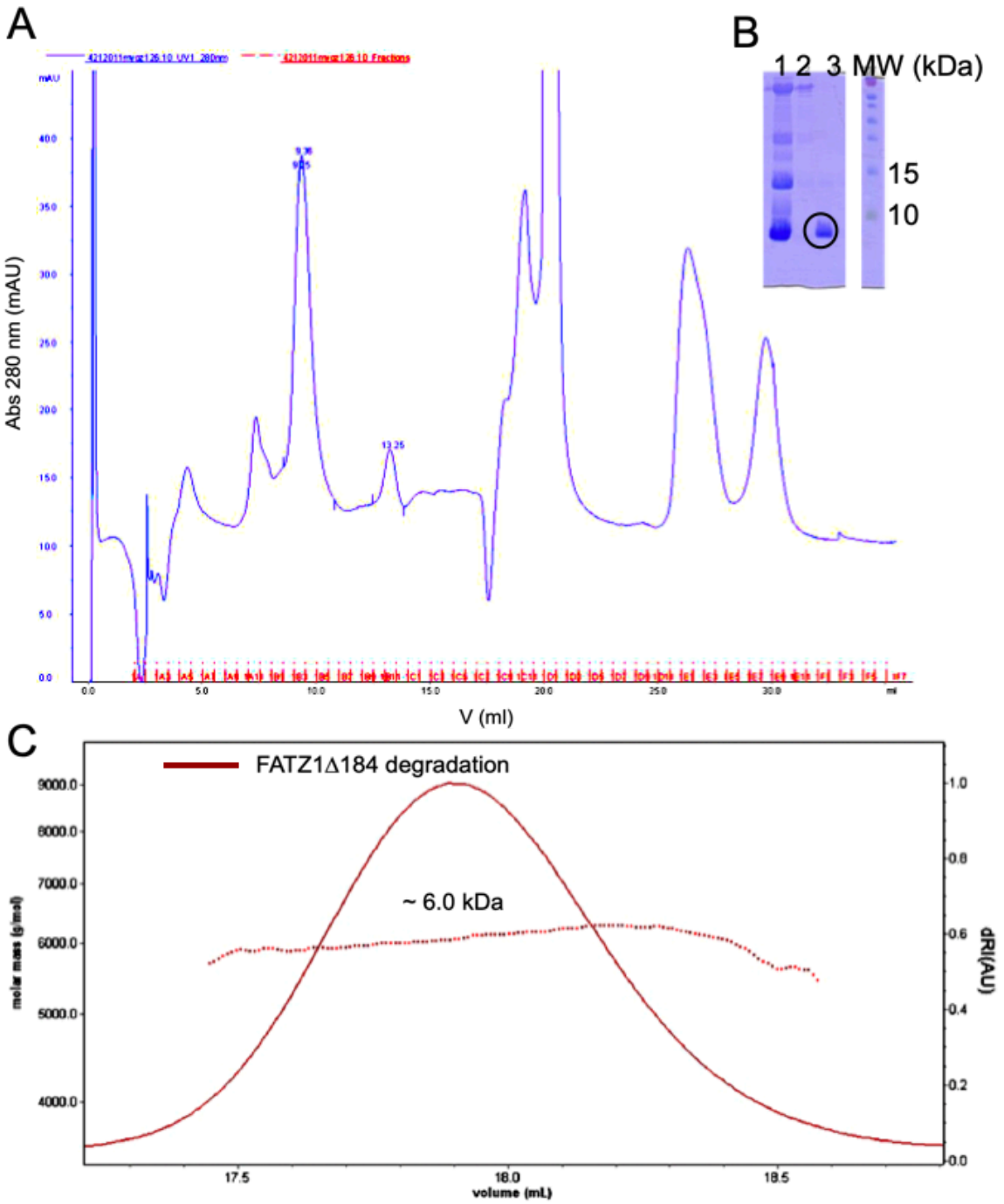

Figure 1.4: FATZ1Δ184 purification product after SEC. A) FATZ1Δ184 final purification step using SEC in an S75-10/300 column (GE Healthcare). **B)** SDS-PAGE 18% of purified products; lane 1: product after affinity purification (Histrap); lane 2: product eluted at 9.9 ml in SEC; lane 3: sample eluted at 13.26 ml in SEC. **C)** SEC-MALS of the final purified product indicated a molar mass of ~ 6.0 kDa. SEC-MALS was performed in an HPLC (Agilent) with a S200-10/300 column (GE Healthcare) in line with a miniDAWN™ TREOS detector (Wyatt Technology) and a Shodex Refractive Index detector.

Significant improvement was observed in the FATZ1Δ184 stability when arginine and glutamine were added to the purification buffers at 50 mM each. After adding those additives, protein yields were increased to purify using SEC preparative grade columns **(Figure 1.5A),** and there was no degradation in the sample (**Figure 1.5B).** However, the protein precipitated over time and after each thawing step.

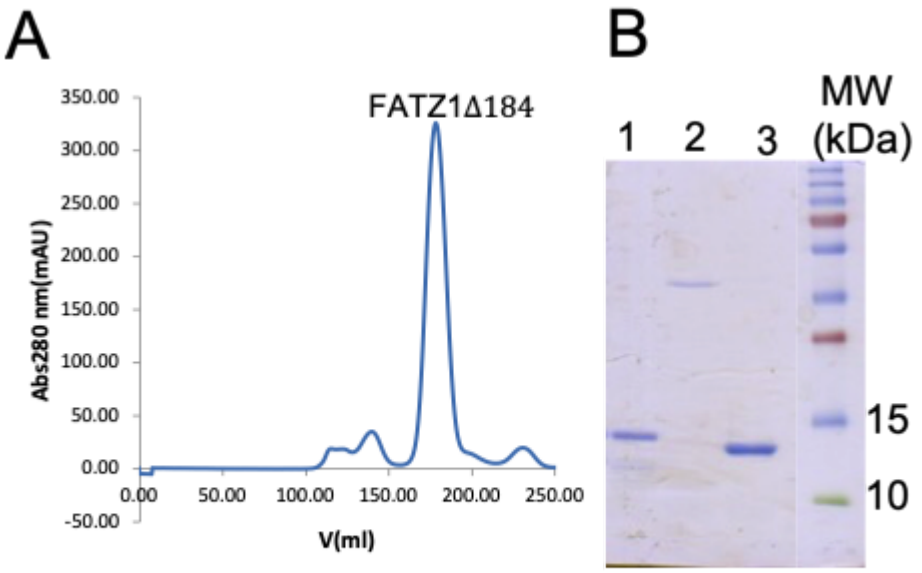

Figure 1.5: FATZ1Δ184 purification after adding additives arginine and glutamine to buffers. A) FATZ1Δ184 final purification step using SEC in an S750-26/60 prep grade column (GE Healthcare). The protein was eluted in 20 mM Tris pH 8, 100 mM NaCl, glycerol 5%, 50 mM Glu, and 50 mM Arg. **B)** SDS-PAGE 18% of FATZ1Δ184, lane 1: sample after affinity purification (Histrap), lane 2: by-products collected in first peak (Ve=130 ml), lane 3: FATZ1Δ184 collected below the highest peak (Ve=175 ml).

FATZ1Δ184 oligomerization assessed by SEC-MALS

SEC-MALS was performed to determine the oligomerization state of FATZ1Δ184 at concentrations 1 to 5.7 mg/ml. BSA was used as an oligomerization control at 2 mg/ml. As shown in **Figure 1.6**, the BSA molar mass was 132.3 kDa for peak 1 (dimer) and 63.69 kDa for peak 2 (monomer), which agrees with the expected values. As summarized in **Table 1.1,** the FATZ1Δ184 average molar mass was ~13.21 kDa for all concentrations, in agreement with the expected molar mass of a monomer (15.36 kDa). These results indicated that FATZ1Δ184 is a monomer in solution.

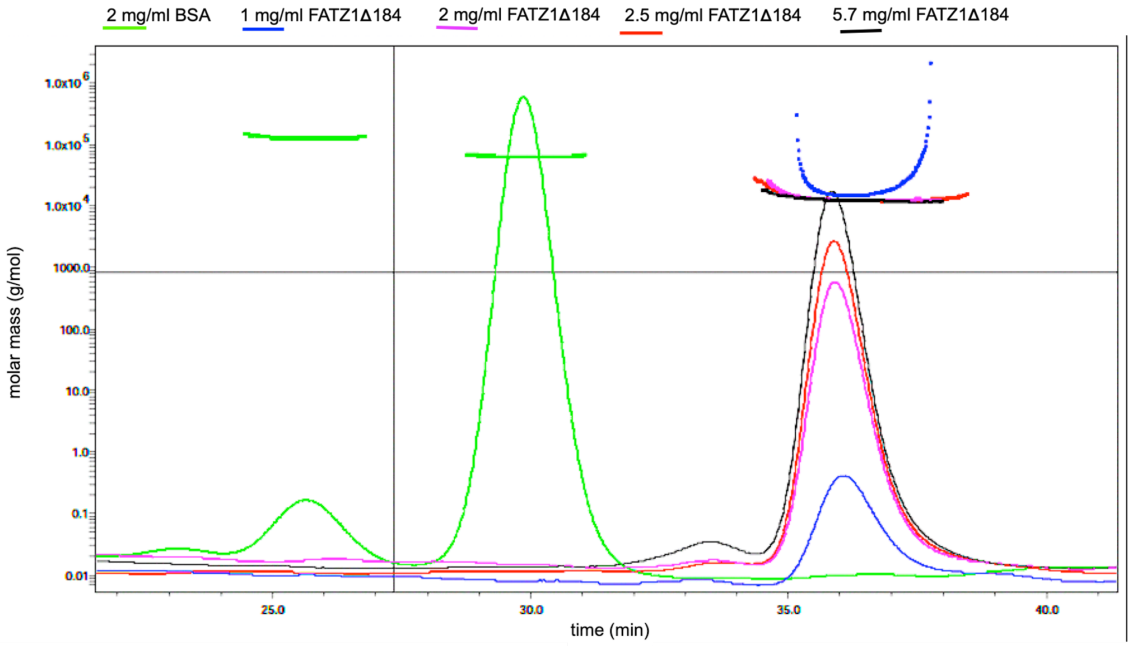

Figure 1.6: FATZ1Δ184 oligomerization assessed by SEC-MALS. FATZ1Δ184 was analysed at 1.0 mg/ml (bleu), 2.0 mg/ml (magenta), 2.5 mg/ml (red), and 5.7 mg/ml (black). BSA (green) was used as control at 2.0 mg/ml. All samples were eluted in 20 mM Tris pH8, 250 mM NaCl, 5% glycerol, and 0.5 mM EDTA. The average calculated molar mass of FATZ1Δ184 was ~13.21 kDa for the four concentrations, indicating a monomer. As expected, the BSA molar mass was 132.3 kDa for peak 1 (dimer) and 63.69 kDa for peak 2 (monomer). The SEC-MALS was performed in an HPLC (Agilent) with an S200-10/300 column (GE Healthcare) in line with a miniDAWN™ TREOS detector (Wyatt Technology) and a Shodex Refractive Index detector.

Table 1.1: FATZ-1Δ184 molar mass at different concentrations

[FATZ1Δ184] (mg/ml)	**[FATZ1Δ184] (µM)**	**MM_{SLS} (kDa)**
1.0	65.10	14.0
2.0	130.20	12.15
2.5	162.76	13.12
5.7	371.09	13.30
	MEDIAN MM_{SLS}	13.21

FATZ1∆91 purification

The construct FATZ1∆91 was obtained from a project collaborator (Evitra at the Karolinska Institute, Sweden). Their method allowed screening multiple combinations of ORF to select the best soluble constructs (Cornvik et al., 2006). This approach yielded a library of 14 soluble constructs, from which the construct FATZ1∆91 was selected, covering residues 92 to 299 with an N-terminal His-tag and an Enterokinase cleavage site. The resulting protein had 224 residues and an expected molecular weight of 23.37 kDa (**Figure 1.7**). FATZ1∆91 spaned part of the GRR, which MetaPrdos predict to be disordered. In addition, the entire CD2 region contains predicted secondary structure elements and binding sites for several partners, including α-actinin-2.

Figure 1.7: FATZ1Δ91 schematic representation. Construct with a His-tag at the N-terminal position, followed by an Enterokinase (EK) cleavage site and the residues 92 to 299 of FATZ1 covering the GRR (green) and the CD2 regions (cyan). The resulting protein had 224 residues and an expected molecular weight of 23.37 kDa.

FATZ1∆91 was expressed in *E. coli* Bl21(DE3) cells and purified following the protocol described in the chapter **Material and Methods.** Several experimental conditions were tried to improve the protein solubility and the purification yield. **Figure 1.8A** displays the final purification step by SEC. The fractions below the peak with Ve=150 ml were collected and concentrated to 2 mg/ml for further experiments. Protein quality was assessed by SDS-PAGE, where a single band at 25 kDa was observed using CBB staining (**Figure 1.8B**). In addition, SEC-MALS analysis showed a single peak with a molar mass of 25.53 kDa (**Figure 1.8C**), which agrees with the expected value for a monomer (23.37 kDa).

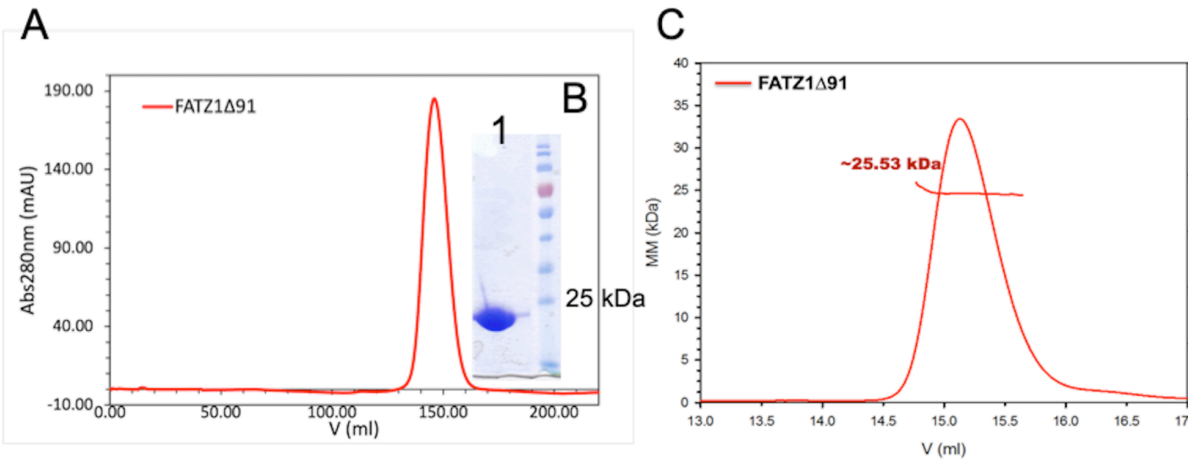

Figure 1.8: FATZ1Δ91 purification after SEC. A) Last purification step by SEC in an S75-26/60 prep grade column(GE Healthcare). The protein was eluted in 50 mM Sodium Phosphate pH 7, 100 mM NaCl, 50 mM Glu, 50 mM Arg, 0.5 mM PMSF and 1 mM EDTA. **B)** SDS-PAGE 15% of the fractions collected below the peak (Ve=150 ml). A single band at ~25 kDa was observed with CBB staining. **C)** SEC-MALS of FATZ1Δ91 indicated a single peak with a molar mass of 25.53 kDa. The SEC-MALS was performed in an HPLC (Agilent) with an S200-10/300 column (GE Healthcare) in line with a miniDAWN™ TREOS detector (Wyatt Technology) and a Shodex Refractive Index detector.

The NMR spectra of FATZ1Δ91

Given that FATZ1Δ91 comprised the GRR, predicted by the MetaPrdos as disordered, NMR experiments were done to investigate its folding state in solution. A sample of FATZ1Δ91 labelled with ^{15}N was purified from the soluble fraction (**Figure 1.9A**) and used to collect HSQC spectra at pH 7.8 (**Figure 1.9**). The NMR spectra were recorded at 25 ℃ using Varian Inova 800 MHz in collaboration with Prof. Robert Konrat's group (MFPL, Vienna). FATZ1Δ9 spectra showed a few peaks with several overlapping and a narrow distribution (**Figure 1.9B**).

To confirm the NMR result of FATZ1Δ91, the experiment was repeated with a sample at a higher concentration and pH 6. This time, FATZ1Δ91 was purified from the inclusion bodies with GuHCl to obtain higher yields, and the protein was returned to native conditions during the affinity step. The quality of the NMR spectra increased significantly, showing more peaks and higher intensities **(Figure 1.9B)**. Signals from

polar amino acids like Ser, Thr and the Gly peaks were better defined, and no spectra distortion was observed. The peak distribution remained narrow and in the same region as the previous experiment with protein purified from the soluble fraction **(Figure 1.9B)**. The 2D-HSQC spectra of FATZ1Δ91 indicated a lack of defined tertiary structure with narrow and overlapping peaks.

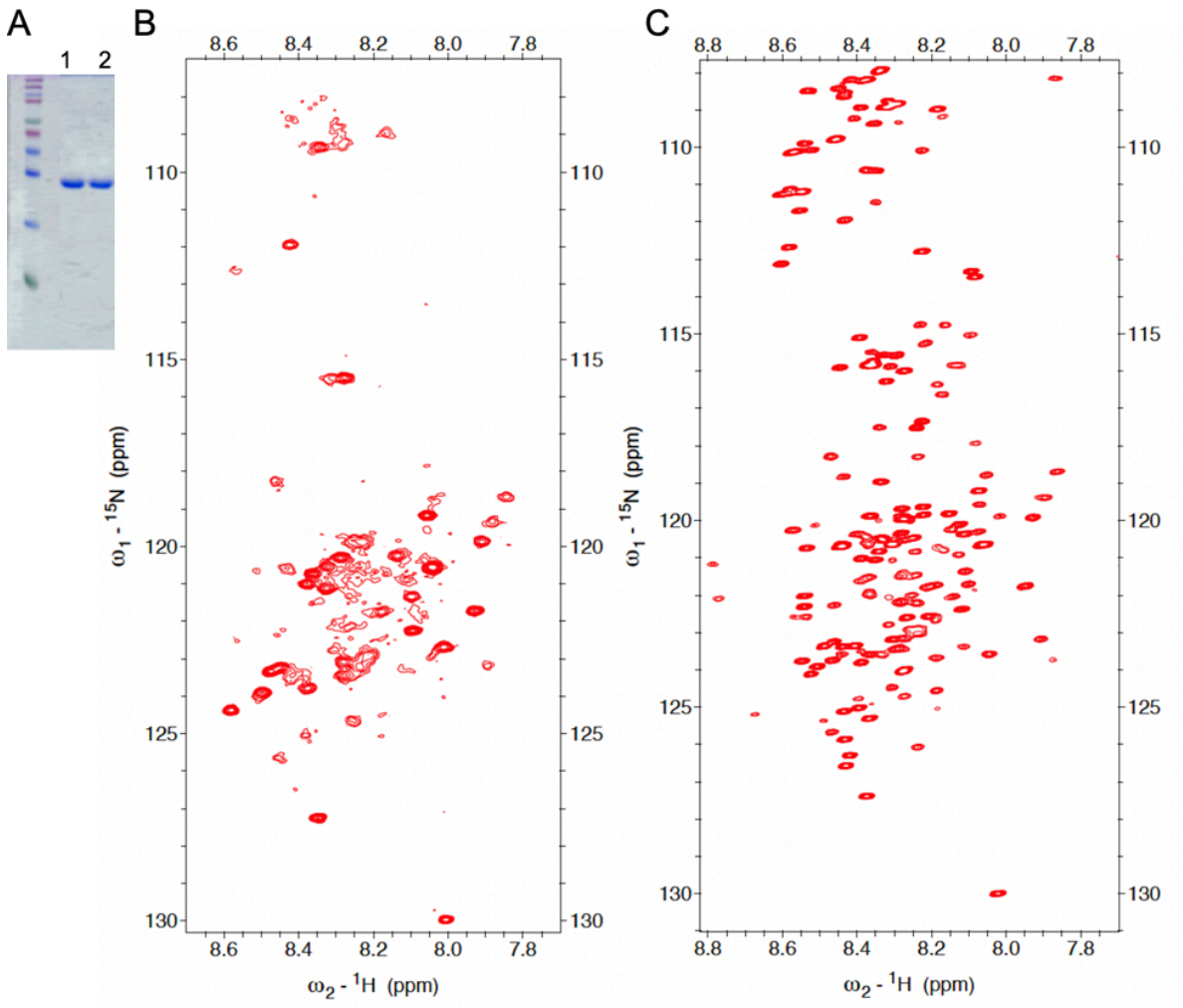

Figure 1.9: 2D-HSQC spectra of FATZ1Δ91 at 100 uM. **A)** SDS-PAGE 15% of FATZ1Δ91 purified from the soluble fraction (lane 1) and from the insoluble fraction (lane 2). A single band at ~25 kDa was observed with CBB staining. **B)** 2D-HSQC of FATZ1Δ91 purified from the soluble fraction in 50 mM Sodium Phosphate pH 7.8, 100 mM NaCl, 50 mM ER, 1 mM EDTA, and 0.5 mM PMSF. **C)** 2D-HSQC of FATZ1Δ91 purified from the insoluble fraction. NMR spectra were recorded in 50 mM Sodium Phosphate pH 6, 100 mM NaCl, 50 mM ER,1 mM EDTA, and 0.5 mM PMSF. The narrow peak distribution indicates the lack of a defined tertiary structure.

Circular dichroism of FATZ1Δ91

CD spectroscopy was used to investigate the presence of secondary structure elements in FATZ1Δ91. The measurement was performed at 0.15 mg/ml concentration in the far-UV region: 260 to 180 nm (**Figure 1.10A**).

The ellipticity signal was converted to mean residue molar ellipticity ($[\theta]_{MR}$, degrees cm^2 $dmol^{-1}$) to assess the secondary structure content (**Figure 1.9B**). The CD spectra of FATZ1Δ91 displayed a minimum near 200 nm and a relatively low ellipticity at 220 nm (**Figure 1.9B**), typical characteristics of intrinsically disordered proteins (Uversky, 2002).

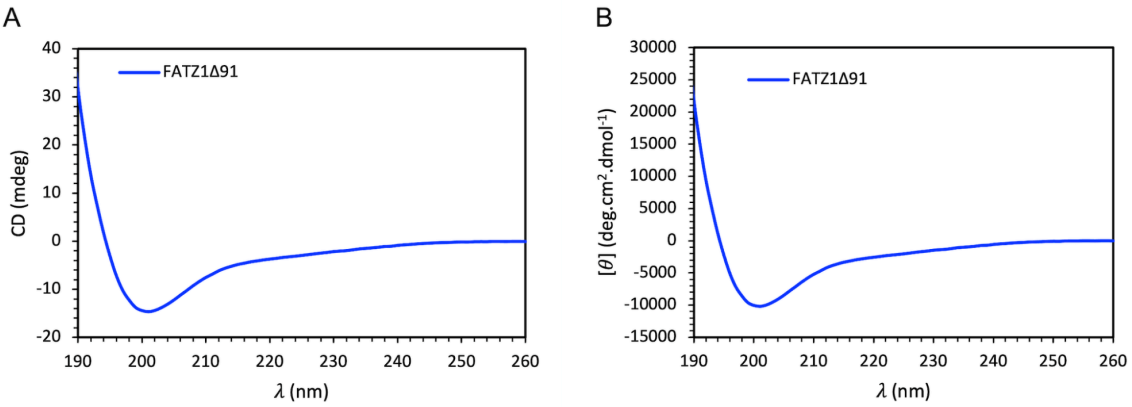

Figure 1.10: FATZ1Δ91 CD spectra. A) CD spectra of FATZ1Δ91 at 0.15 mg/ml in 10 mM Sodium Phosphate pH 7. Measurement was performed in a Chirascan spectrophotometer (Applied Photophysics) in a 0.1 cm path-length cell. **B)** CD signal converted into mean residue molar ellipticity showing a minimum near 200 nm and a relatively low ellipticity at 220 nm.

Since there was some residual ellipticity at 208 and 222 nm, indicative of some α-helical content, a secondary structure prediction was made with DichroWeb using the CDSSTR method and the Set175 (Miles et al., 2022). The FATZ1Δ91 estimated secondary structure content was 47% unordered, 28% strands, 18% turns and 6% helix. The fit of predicted to experimental data had an NRMSD=0.013 (**Figure 1.11**).

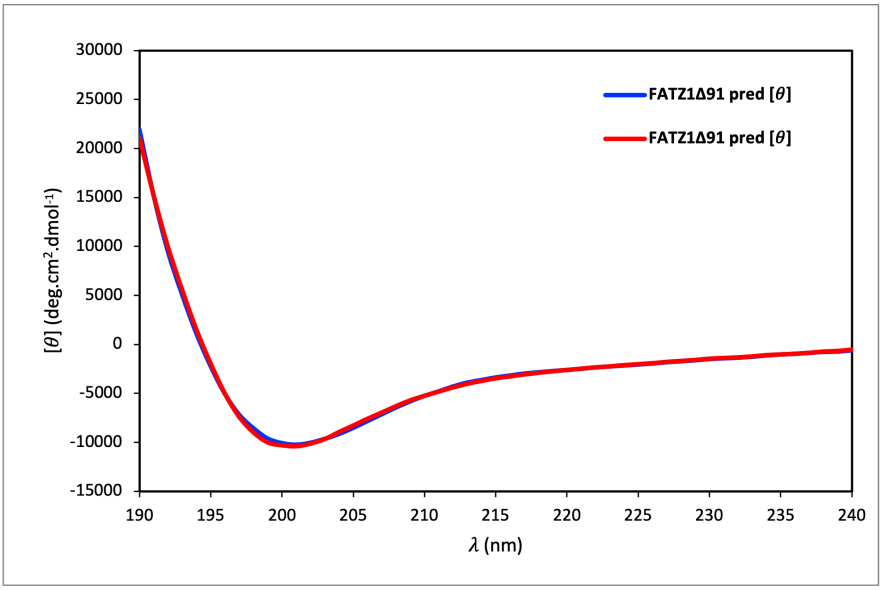

Figure 1.11: Fit of FATZ1∆91 predicted vs experimental CD spectra used to estimate secondary structure. The predictions were made with the CDSSTR model and the reference dataset SP175 (Miles et al., 2022). The predicted FATZ1∆91 spectra (red) fit the experimental data (bleu) with an NRMSD = 0.013. The estimated FATZ1∆91 secondary structure from the predicted data was 47% unordered, 28% strands, 18% turns and 6% helix.

Small-angle X-ray scattering of FATZ1∆91

Small-angle X-ray scattering (SAXS) was conducted to study the structure of FATZ1Δ91 in solution in the SWING BEAMLINE at Synchrotron Soleil, France. The data collection was performed in an HPL-SAXS due to the polydispersity of FATZ1Δ91. Data processing was done following standard procedures using the software FOXTROT (provided by SWING BEAMLINE).

Figure 1.12 displays the I(0) and Rg values per collected frame. The Guinier region was determined based on the highest intensity frame corresponding to the highest protein concentration. The same Guinier region (0.738 <SRg>1.2) was used for the rest of the data set. Rg and I(0) were determined for every frame across the peak (**Figure 1.12**). According to the I(0) plot (**Figure 1.12A**), frames 75 to 165 contained protein scattering concurrent with the region where Rg (green curve) had a narrow oscillation**.** The Rg values for frames 94 to 140, where the scattering signal was most potent, showed that Rg values oscillate between 47 to 25 Å **(Figure**

1.12B). From frames 110 to 120 (**Figure 1.12B**, red circles), where I(0) values were the highest, Rg values were 37.9 ±3.67 Å.

A

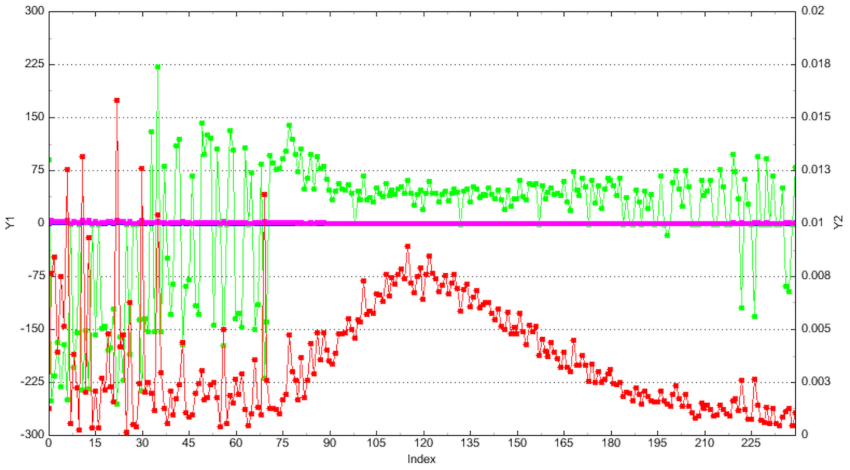

B

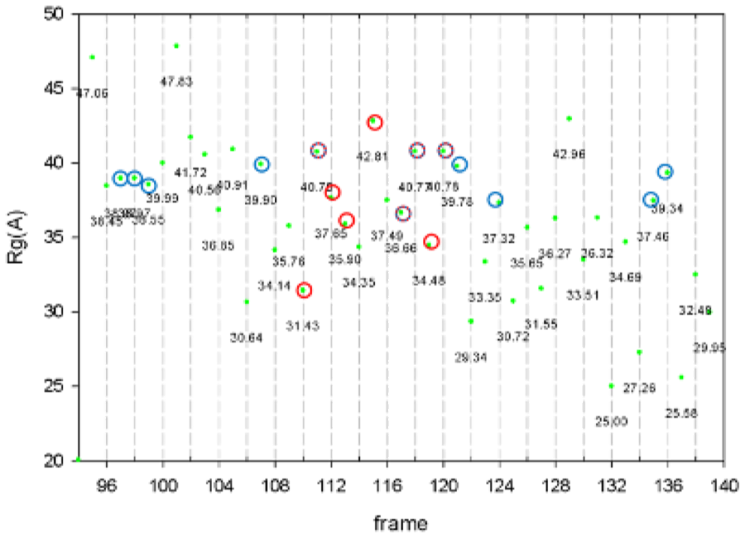

Figure 1.12: FATZ1Δ91 scattering data collected in HPL-SAXS mode. A sample of 6.0 mg/ml FATZ1Δ91 was run in a Superdex 75-10/300 column (GE Healthcare). The sample was prepared in 20 mM Tris pH 7.5, 100 mM NaCl, 50 mM Glu, 50 mM Arg, 1 mM EDTA, 0.5 mM PMSF, and 0.5 mM βME. **A)** Plots of Rg (green) and I(0) (red) per collected frames of the FATZ1Δ91 protein eluted from the column. **B)** Zoom of the Rg plot from frames 94 to 140. Frames with similar Rg values (red circles) were scaled and further processed in primus (Manalastas-Cantos et al., 2021).

After selecting a subset of frames with the lowest variation in Rg and I(0) values, the software primus (Manalastas-Cantos et al., 2021) was used to scale and average the data, resulting in two SAXS curves of FATZ1Δ91 (**Figure 1.13A**). The Guinier analysis of the SAXS data showed that the scattering of average-1 had Rg and I(0) values of 4.48 nm and 0.007, respectively. In addition, the average-2 scattering curve had Rg and I(0) values of 4.32 nm and 0.0069, respectively (**Figure 1.13B**). The Pr function of the two curves indicated similar Rg values (4.02 and 4.62 nm). However, average-2 showed a more extended Dmax (20 nm) than average-1 (15 nm, **Figure 1.13C**). **Table 1.2** summarizes the structural parameters calculated from the scattering of FATZ1Δ91.

Table 1.2: Structural parameters of FATZ1Δ91

	Rg(nm), Guinier	I(0)	Dmax (nm)	Rg (nm), Pr	Rg (nm), Flory*
FATZ1Δ91 average-1	4.49	$0.70*10^{-2}$	15	4.02	4.28
FATZ1Δ91 average-2	4.32	$0.69*10^{-2}$	20	4.62	4.28

*using the parameters for intrinsically disordered proteins by (Kikhney & Svergun, 2015)

The dimensionless Kratky plot shown in **Figure 1.13D** displayed a rising curve from low sRg values, which reached a plateau at $(sRg)^2*I/I(0)=2$ and was followed by a monotonous increase at higher sRg values. Such a Kratky plot indicates the absence of a compact core and has already been observed in other intrinsically disordered proteins (Kikhney & Svergun, 2015; Receveur-Brechot & Durand, 2012; Uversky, 2002).

According to Flory's equation for random coil (Fitzkee & Rose, 2004), $Rg = Ro \times N^v$, where Ro is 1.33 ± 0.076, and v is 0.598 ± 0.028, the expected Rg value for FATZ1Δ91 is 3.38 nm, which is smaller than the Rg obtained from the SAXS data (4.02 and 4.62 nm). However, using the modified Flory's equation for intrinsically disordered proteins (Kikhney & Svergun, 2015), where Ro is 2.54 ± 0.001, and v is 0.522 ± 0.001, the expected Rg value is 4.28 nm, which agrees with the Rg

determined from the SAXS data. Therefore, FATZ1Δ91's Rg can be described with Flory's equation for IDPs.

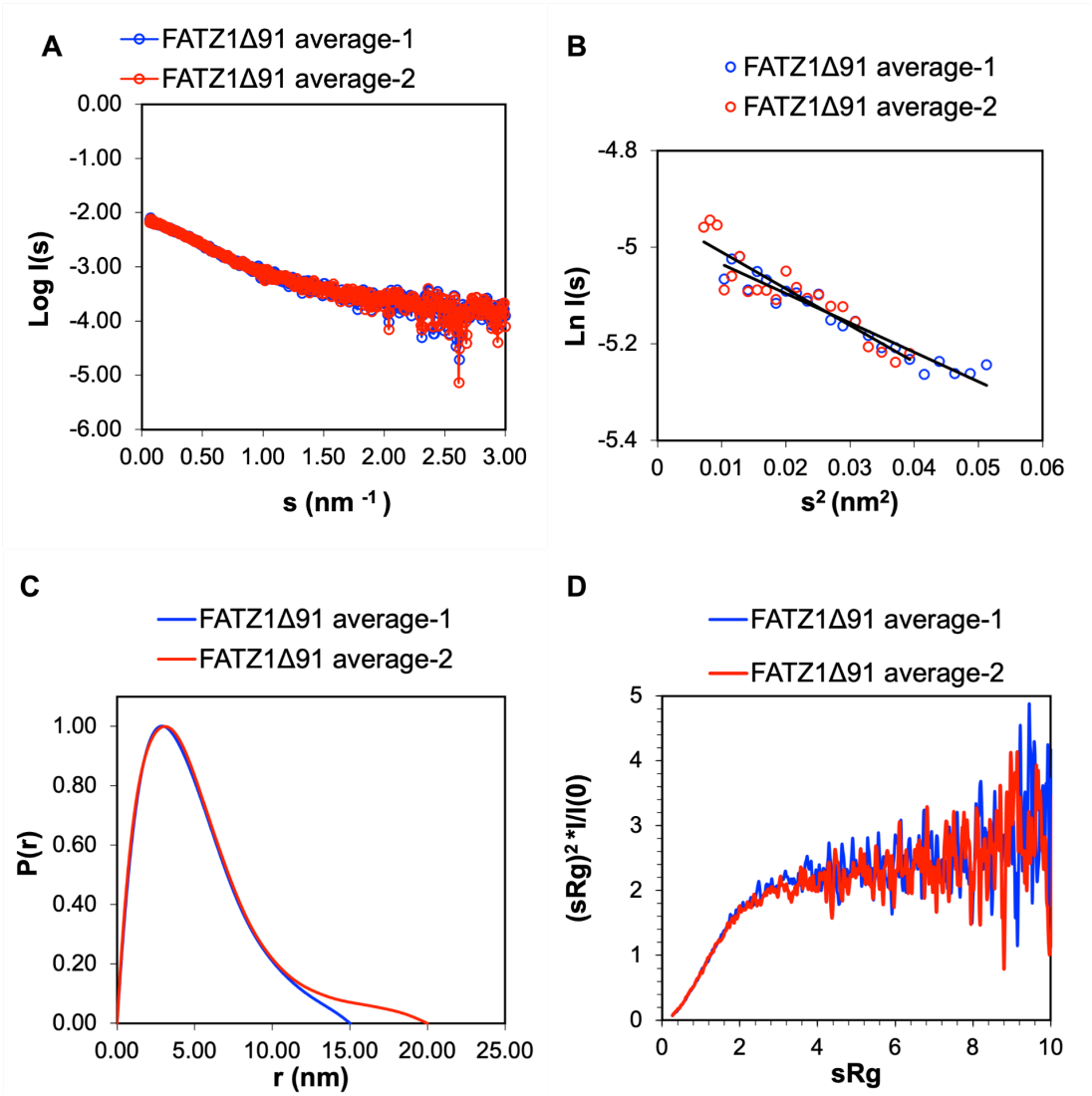

Figure 1.13: FATZ1Δ91 scattering data collected in HPL-SAXS mode. A) SAXS curves of FATZ1Δ91 obtained from two datasets with Rg of 3.7 ± 0.37 nm, average-1 in blue and average-2 in red. **B)** Guinier plots of the average-1 and average-2. The Guinier analysis indicated Rg and I(0) values of 4.48 nm and 0.007 for the average-1 and 4.32 nm and 0.0069 for the curve average-2**. C)** Pr functions of average-1 and average-2. **D)** Dimensionless Kratky plots of FATZ1Δ91 display a rising curve and a monotonous increase at high sRg.

The ensemble optimization method (EOM) (Bernadó & Svergun, 2012) was used to explore the flexibility of FATZ1Δ91. EOM generated a pool of 10,000 random conformations of FATZ1Δ91, from which an optimized ensemble was selected to fit the scattering data with a χ=0.66. The Rg and Dmax distributions of the FATZ1Δ91

optimized ensemble showed different populations with a wide range of Rg and Dmax values spanning compact and extended conformations. The average Rg and Dmax of the ensemble were 4.62 nm and 14.93 nm, respectively. The final ensemble comprised a conformation ensemble composed of 7 conformations with Rg from 3.00 to 7.58 nm and Dmax from 8.36 to 23.36 nm, which are shown in **Figure 1.14A** and **B**.

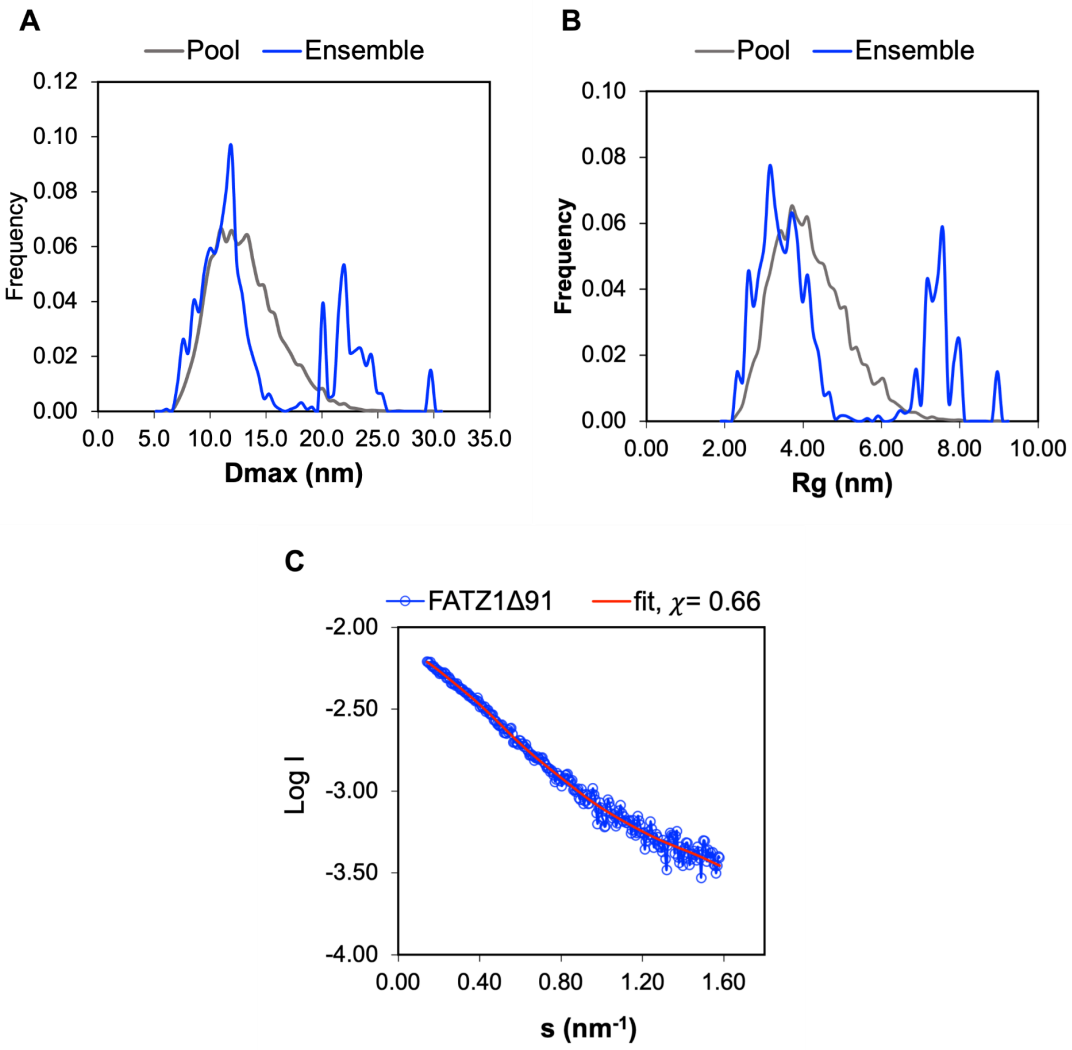

Figure 1.14: EOM analysis of FATZ1Δ91 scattering data. A) Rg distribution of FATZ1Δ91, where the conformational pool is gray and the optimized ensemble is bleu. The average Rg of the optimized ensemble was 4.62 nm. **B)** Dmax distribution of FATZ1Δ91, where the conformational pool is gray, and the optimized ensemble is bleu. The average Dmax of the optimized ensemble was 14.49 nm. **C)** Fit of the optimized ensemble (red) to the experimental scattering data (blue), with χ= 0.66.

Part II: The FATZ-1 and α-actinin-2 interaction

Purification of α-actinin-2 constructs for the binding studies

Two α-actinin-2 constructs were prepared for the binding studies: ACTN2 (α-actinin-2 full-length) and ACTN2hd (α-actinin-2 half-dimer). The ACTN2 construct comprises the α-actinin-2 homodimer of 206 kDa. This construct was previously used to obtain the complete X-ray structure of the α-actinin-2 (Ribeiro et al., 2014). The ACTN2hd construct comprises the half-dimer of α-actinin-2 truncated at the symmetrical plane in the center of the ROD domain, forming a heterodimer of 110 kDa, where Chain A with 60 kDa comprises ABD-neck-SR1-SR2 and Chain B with 40 kDa comprises SR3-SR4-EFhands. **Figure 2.1** presents a scheme of both constructs.

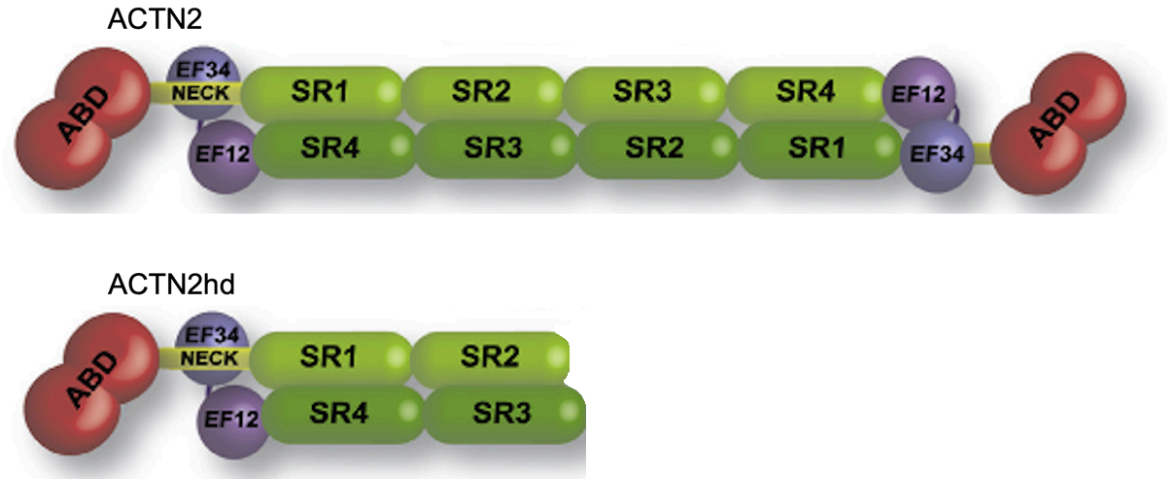

Figure 2.1: Scheme of α-actinin-2 constructs used for the binding studies with FATZ1Δ91. Figure adapted from (Ribeiro et al., 2014). Top: ACTN2 comprises the α-actinin-2 homodimer of 206 kDa. Bottom: ACTN2hd comprises the half-dimer of α-actinin-2 truncated at the symmetrical plane in the center of the ROD domain, forming a heterodimer of 110 kDa.

The α-actinin-2 constructs were expressed in *E. coli* Bl21(DE3) cells and purified following the protocol described in the chapter **Material and Methods.** SEC was done as the final step of purification. The ACTN2 was collected from a peak eluting at 335 ml from the HiLoad 26/600 Superdex 200 pg column (**Figure 2.2A**), and the ACTN2hd was collected from a peak eluting at 776 ml from a Superdex 200 Increase 10/300 GL column (**Figure 2.2B**). The protein purity was assessed by

SDS-PAGE 15% with CBB staining, where ACTN2 was observed as a protein band of ~100 kDa, and ACTN2hd was seen as two protein bands of ~60 and ~40 kDa (**Figure 2.2C**).

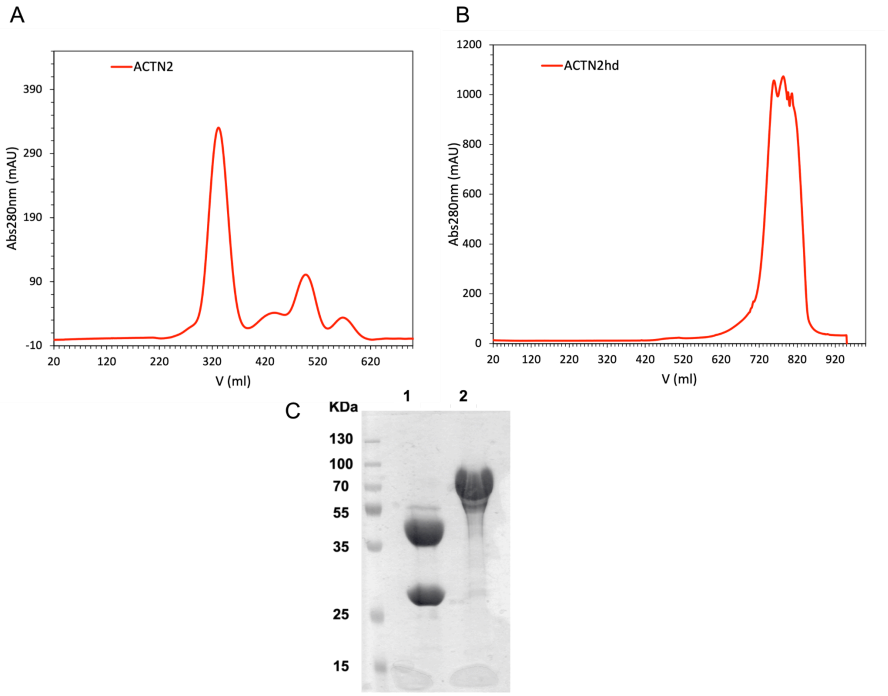

Figure 2.2. Purification of α-actinin-2 constructs. The proteins were eluted in 50 mM Sodium Phosphate pH 7, 100 mM NaCl, 50 mM Glu: Arg, 0.5 mM PMSF, and 1 mM EDTA. **A)** SEC of ACTN2 in HiLoad 26/600 Superdex 200 pg column (GE Healthcare); ACTN2 eluted at 335 ml. **B)** SEC of ACTN2hd in Superdex 200 Increase 10/300 GL column (GE Healthcare); the ACTN2hd eluted at 776 ml. **C)** SDS-PAGE 15% of the purified products stained with CBB. **Line 1:** ACTN2hd is observed as two bands corresponding to chain-A (60 kDa) and chain-B (40 kDa). **Line 2**: ACTN2 is observed as one band (110 kDa).

SEC-MALS of FATZ1Δ91 and α-actinin-2

SEC-MALS was conducted to determine if FATZ1Δ91 could bind to α-actinin-2 in solution and to determine the complex stoichiometry. Three α-actinin-2 constructs were used for the test, namely ACTN2, ACTN2hd, and Efhands. **Table 2.1** presents the expected molar mass for each protein and the expected complex. During the experiment, FATZ1Δ91 was first injected alone, followed by the α-actinin-2 construct, and then both proteins together. The samples were prepared at 175 uM of FATZ1Δ91 and 35 uM of α-actinin-2 in 50 mM Sodium Phosphate pH 7, 100 mM NaCl, 50 mM ER, 1 mM EDTA, 0.5 mM PMSF.

Table 2.1: Molar mass of FATZ1Δ91, the α-actinin-2 constructs and their complexes.

Sample	MM, expected (kDa)	MM, calculated(kDa)
FATZ1Δ91	23.37	26.0
ACTN2	206.0	199.0
ACTN2hd	106.0	110.0
EFhands	17.7	18.0
FATZ1Δ91/ACTN2	253.0	257.0
FATZ1Δ91/ACTN2hd	129.3	~131.0
FATZ1Δ91 + EFhands	23.37⏎ 17.7	25.95 17.97

The SEC-MALS revealed that FATZ1Δ91 forms a complex with ACTN2 and ACTN2hd (**Figure 2.3A and B**). The sample containing FATZ1Δ91 and ACTN2 showed a peak eluting earlier than ACTN2 alone (**Figure 2.3A).** The calculated molar mass of the early peak was 257 kDa, in agreement with the expected molar mass of the complex FATZ1Δ91/ACTN2, formed by two FATZ1Δ91 molecules per ACTN2 dimer (**Table 2.1**). The calculated molar mass of the ACTN2 peak was 199 kDa, as expected for the dimer of 206 kDa. The analysis of the sample containing FATZ1Δ91 and ACTN2hd, also showed a peak eluting earlier than ACTN2hd alone (**Figure 2.3B**). The molar mass of the early peak was determined to be approximately 131 kDa, which was 22 kDa higher than the molar mass of ACTN2hd (110 kDa), indicating a complex of FATZ1Δ91/ACTN2hd with a stoichiometry of one FATZ1Δ91 molecule per ACTN2hd molecule (as depicted in **Figure 2.3B** and listed in **Table 2.1**). As anticipated, the SEC-MALS analysis of FATZ1Δ91 and EFhands did not reveal a peak corresponding to a complex. The mixture of these two proteins showed peaks eluting at the same positions as the proteins alone, with similar molar mass (as shown in **Figure 2.3C** and listed in **Table 2.1**). This observation confirmed that EFhands do not interact with FATZ1Δ91 (Faulkner et al., 2000).

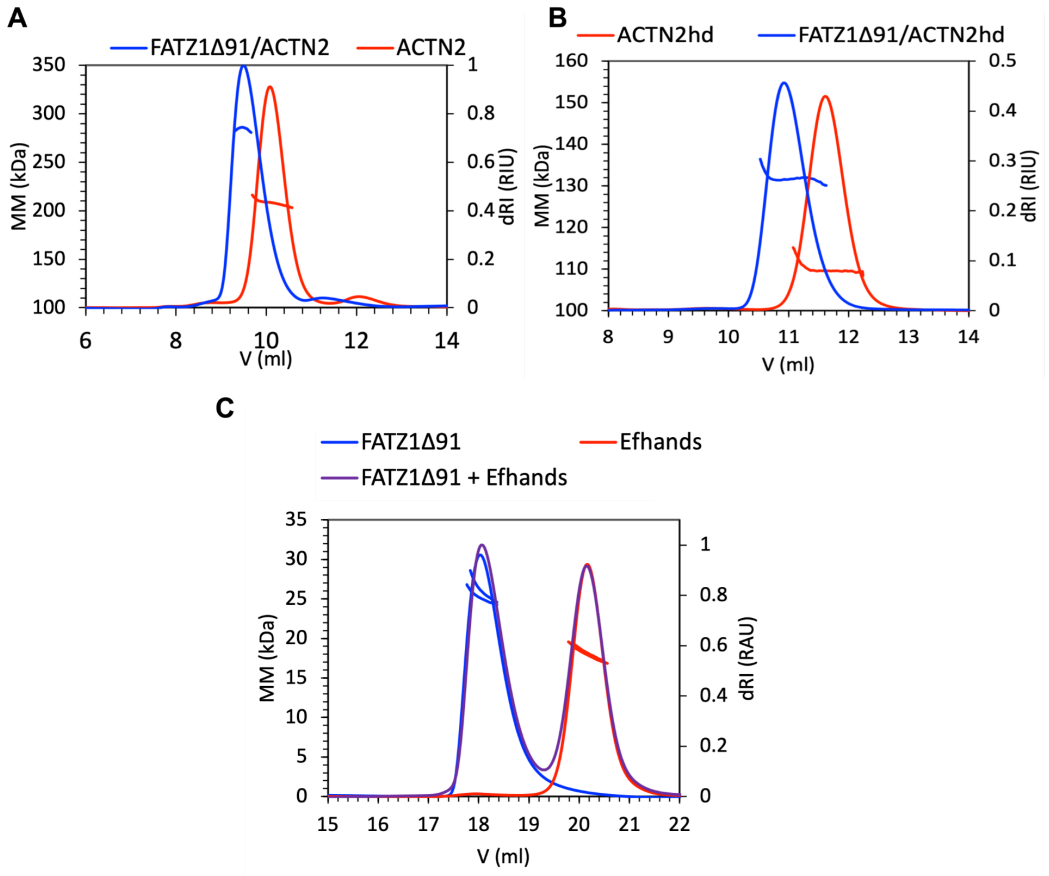

Figure 2.3: SEC-MALS of the interaction between FATZ-1 and α-actinin-2. A) SEC-MALS of FATZ1Δ91/ACTN2: complex (blue), and ACTN2 (red). The molar mass of the blue peak was determined to be 257 kDa, corresponding to the expected molar mass of the complex. The calculated molar mass of the red peak was 199 kDa, as expected for the α-actinin-2 dimer. **B)** SEC-MALS of FATZ1Δ91/ACTN2hd: complex (blue), and ACTN2hd (red). The molar mass of the blue peak was determined to be 131 kDa, corresponding to the expected molar mass of the complex. The calculated molar mass of the red peak was 106 kDa, as expected for the α-actinin-2 half-dimer. **C)** SEC-MALS of FATZ1Δ91 and EFhands: FATZ1Δ91 (blue), EF-hands (red), and the sample with both proteins (violet). The molar mass of the blue peak was determined to be 25.95 kDa for FATZ1Δ91 and 17.7 kDa for EFhands, corresponding to the expected molar mass of the individual proteins alone. All SEC-MALS experiments were performed using an HPLC system (Agilent) with a Superdex 200 10/300 column (GE Healthcare) in line with a miniDAWN™ TREOS detector and a Shodex Refractive Index detector.

ITC of the complex FATZ1Δ91/α-actinin-2

ITC was used to determine the binding affinity (Kd) of the complex FATZ1Δ91/ACTN2 and FATZ1Δ91/ACTN2hd and to corroborate the stoichiometry suggested by the SEC-MALS analysis (**Figure 2.4**).

A double sigmoidal thermogram with two binding events was observed during the titration of FATZ1Δ91 into ACTN2. The first binding event was exothermic (ΔH1 = -26.66 kcal/Mol) with a Kd1 = 3.18 nM. The second event was also exothermic (ΔH2 = -10.26 kcal/Mol) with Kd2 = 227.65 nM. These results indicated a strong interaction with a stoichiometry of 2 FATZ1Δ91 per ACTN2 dimer (**Figure 2.4A**). When titrating FATZ1Δ91 into ACTN2hd, a sigmoidal thermogram with one binding event (ΔH ~ -23.58 kcal/Mol) and a Kd = 188 nM was observed, confirming a stoichiometry of 1 FATZ1Δ91 per ACTN2hd (**Figure 2.4B**).

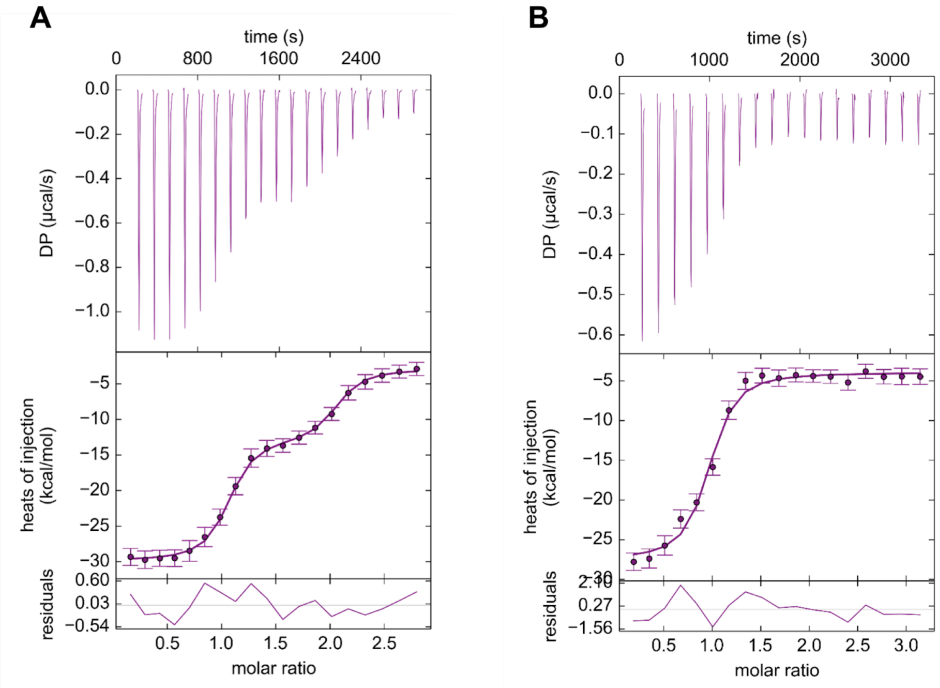

Figure 2.4: ITC of FATZ1Δ91 binding to ACTN2 and ACTN2hd. **A)** Titration of 206.8 µM FATZ1Δ91 into 20.5 µM of ACTN2 showing a double sigmoidal thermogram with two binding events, Kd1 = 3.18 nM, ΔH1 = -26.66 kcal/Mol and Kd2 = 227.65 nM, ΔH2 = -10.26kcal/Mol. **B)** Titration of 149 uM of FATZ1Δ91 into 9.4 uM of ACTN2hd showing a sigmoidal thermogram with one binding event, Kd = 188 nM, ΔH = -23.58 kcal/Mol. The proteins were in 50 mM NaPO4 pH 7.5, 100 mM NaCl, 50 mM Glu, 50 mM Arg, 1

mM EDTA,1mM βME and 0.5 mM PMSF. Titrations were done in 20 injections with a MicroCal iTC200 (Malvern Panalytical). The top panel shows the power versus molar ratio curve, while the bottom panel shows the thermogram of the integrated peak intensities plotted against the molar ratio. The fit global reduced chi-square values were 3.35e-02 (n=19) and 4.34e-02 (n=19) for the FATZ1Δ91/ACTN2 and FATZ1Δ91/ACTN2hd respectively.

XL-MS of the complex FATZ1Δ91/α-actinin-2

Cross-linking and mass spectrometry (XL-MS) was employed to identify the contact residues of the complex FATZ1Δ91/α-actinin-2, in collaboration with Dr. Friedel Drepper and Prof. Bettina Warsheid at the University of Freiburg, Germany. To simplify the analysis, we performed cross-linking of the complex FATZ1Δ91/ACTN2hd, which had only one binding site.

EDC/sulfo-NHS were tested as a zero-length cross-linker and performed cross-linking using one- and two-step methods. The one-step reaction led to the observation of cross-linked products for the complex (**Figure 2.5, lane 1**) and ACTN2hd alone (**Figure 2.5, lane 2**). The gel bands were digested using trypsin to identify these products and analyzed further using high-resolution LC-MS.

After analyzing the gel bands using high-resolution LC-MS, it was found that bands 4 and 5 (**Figure 2.5, lane 1**) were specific products of the complex FATZ1Δ91/ACTN2-hd. Band 5 corresponded to a cross-linked product of FATZ1Δ91/SR3-SR4-Ef with K176-E658 and K233-E567 as contact residues. (**Table 2.2**, contact residues in bold). Band 4 corresponded to a cross-linked product of FATZ1Δ91/ABD-SR1-SR2, with the contact residues D205-K383 (**Table 2.2**, contact residues in bold).

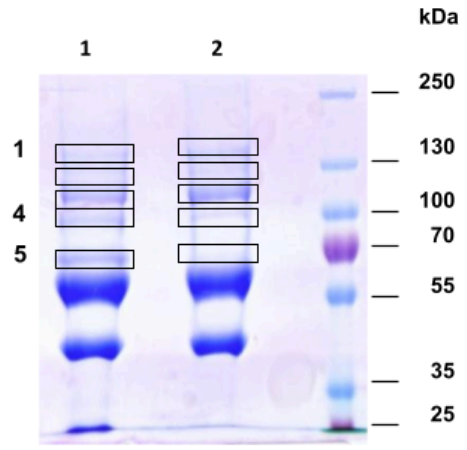

Figure 2.5: Cross-linking results of the complex FATZ1Δ91/ACTN2hd. The XL was done using EDC in a one-step reaction in 50 mM Sodium Phosphate pH 7, 150 mM NaCl, one mM EDTA, and 0.5 mM TCEP. SDS-PAGE 7.5% and CBB staining were used to visualize the cross-linked products. Lane 1 shows the products of 20 µM of complex FATZ-1Δ91/ACTN2hd. MS analysis revealed specific products of the complex FATZ1Δ91/ACTN2-hd with ~100 kDa (band 4) and ~70 kDa (band 5). Lane 2 shows the products of 20 µM ACTN2hd alone.

Table 2.2: The MS results of the complex FATZ1Δ91/ACTN2hd. (Results provided by Dr. Friedel Drepper)

m/z	charge	FATZ1Δ91		SR3-SR4-Ef (ACTN2hd)		P-value[3]
		sequence[1]	P-value[2]	sequence[1]	P-value[2]	
841.1565	4	R.GGAAGTAGVGETGSGDQAGGEG**K**HITVFK.T	1.1E-12	M**E**EIAR	2.8E-01	2.3E-12
1121.206	3	R.GGAAGTAGVGETGSGDQAGGEG**K**HITVFK.T	1.8E-08	M**E**EIAR	6.7E-02	1.1E-08
872.0889	3	R.TAMPYGGYE**K**ASKR.M	8.9E-06	ATLP**E**ADGER	2.5E-03	1.2E-07
820.0561	3	R.TAMPYGGYE**K**ASK.R	2.5E-03	ATLP**E**ADGER	2.5E-03	6.6E-06
		FATZ1Δ91		**ABD-SR1-SR2 (ACTN2hd)**		
		sequence[1]	P-value[2]	sequence[1]	P-value[2]	
878.4517	4	K.MELGI**D**LLAYGAK.A	9.7E-06	LEQAE**K**GYEEWLLNEIR	1.1E-09	9.2E-14

917.4806	4	K.MELGI**D**LLAYG AK.A	5.5E-05	LEQAE**K**G YEEWLLN EIRR	1.8E-03	8.3E-07

[1)] D, E, K signifies site of cross-linker, M: oxidized Met, [2)] Subscores per peptide, [3)] P-value for cross-link peptide

Figure 2.6 summarizes the proposed contact residues of the complex based on the XL-MS assay. For FATZ1Δ91, K176, D205, and K233, located in the CD2 domain and for ACTN2hd, K383, E567, and E658, located in SR1, SR3 and SR4, respectively.

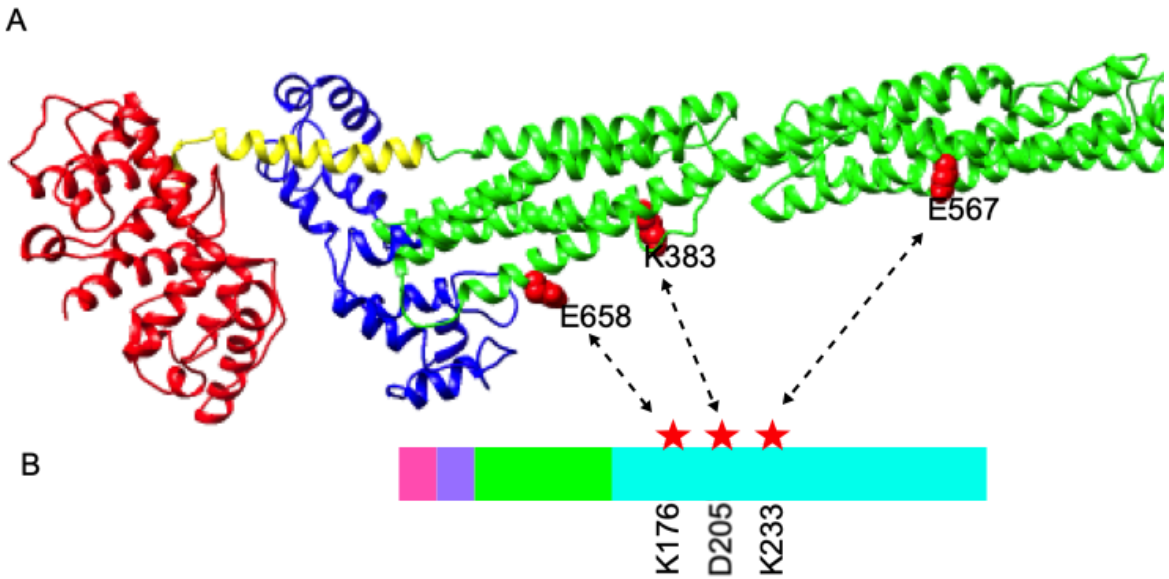

Figure 2.6: Schematic representation of the complex FATZ1Δ91/ACTN2hd contact residues proposed by XL-MS. A) The structure of ACTN2hd, where SR1, SR2, SR3, and SR4 are depicted in green; Efhands in blue, neck in yellow and ABD in red. The contact residues are highlighted as red dummy residues, K383 (SR1), E567 (SR3), and E658 (SR4). **B)** The scheme of the FATZ1Δ91 construct is shown, where the Glycine reach region (GRR) is highlighted in green, and the CD2 domain is in cyan. The contact residues are represented as red stars, with K176, D205, and K233 being the proposed contact residues.

The interaction of FATZ1Δ91 mutant with α-actinin-2

FATZ1Δ91 mutants were developed to test the contact residues revealed by XL-MS data. The mutations were designed to break down the electrostatic interaction of the contact residues in a conserved region shared by the three FATZ isoforms (see **Figure 2.7**). Two mutants were created: KK_FATZ1Δ91, which had

mutations K176A and K233A, and KDK_FATZ1Δ91, which had mutations K176A, D205A, and K233A.

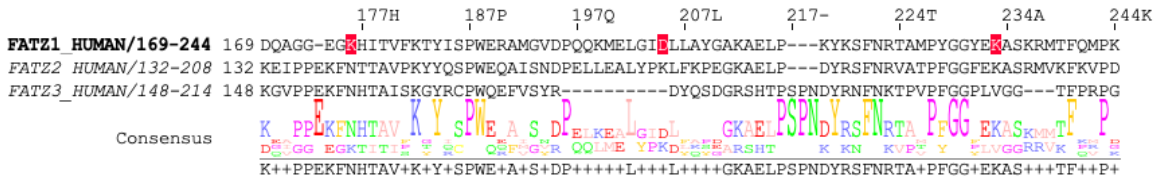

Figure 2.7: Sequence alignment of the three FATZ human isoforms in the region containing the contact residues. The contact residues K176, D205, and K233 are highlighted in red. Conserved motifs around the K176 and the K233 are indicated in the consensus view at the bottom. KK_FATZ1Δ91 mutant had mutations K176A and K233A, while KDK_FATZ1Δ91 mutant had mutations K176A, D205A, and K233A.

Mutants were obtained by site direct mutagenesis, expressed and purified as previously the wild-type FATZ1Δ91. **Figure 2.8A and B** shows the purification result for the mutant KK_FATZ1Δ91. The KDK_FATZ1Δ91 mutant precipitated after the affinity step. SEC-MALS analysis of FATZ1Δ91 wild-type and mutants revealed that KDK_FATZ1Δ91 with 23.99 kDa eluted earlier than FATZ1Δ91 (**Figure 2.8C**). In contrast, KK_FATZ1Δ91 with 24.84 kDa eluted similarly to FATZ1Δ91 with 24.69 kDa (**Figure 2.8C)**. This indicated that KDK_FATZ1Δ91 had a higher R_h than the wild-type. Due to the challenges faced while handling the KDK_FATZ1Δ91 mutant without precipitation and little yield being recovered from its purification, we decided not to pursue further experiments with this construct.

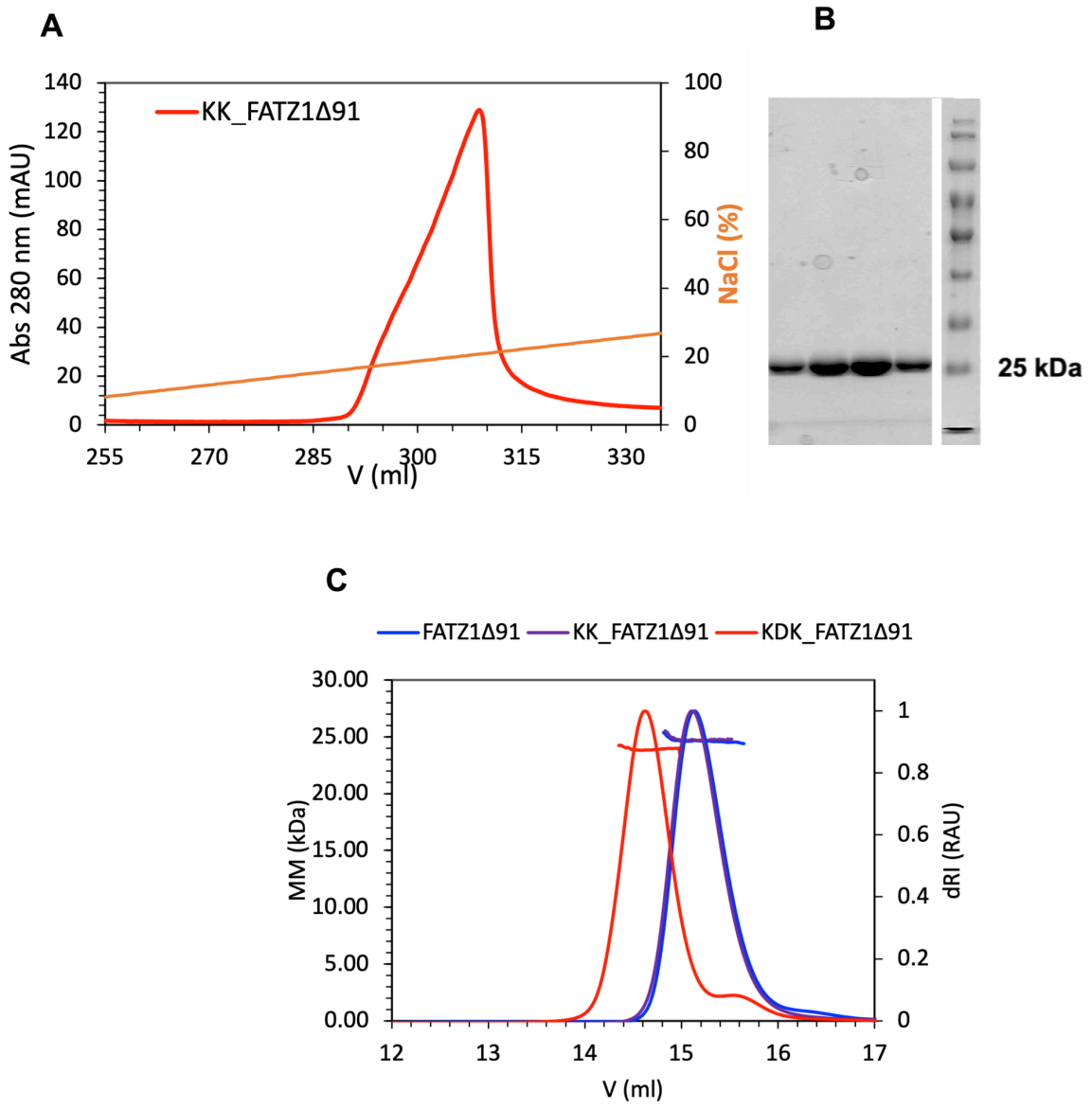

Figure 2.8: Purification of the mutant KK_FATZ1Δ91 and SEC-MALS of FATZ1Δ91 mutants and wild-type. A) Elution profile of KK_FATZ1Δ91 from a Resource Q (Sigma Aldrich). **B)** SDS-PAGE 12.5 % of fractions collected below the peak eluting at 30% NaCl. The single band at 25 kDa corresponded to the expected size of the mutant KK_FATZ1Δ91. **C)** SEC-MALS of FATZ-1Δ91, where wild-type is blue, KK_FATZ1Δ91 is violet, and KDK_FATZ1Δ91 is red. The mutant KDK_FATZ1Δ91 eluted earlier than the wild-type, while the mutant KK_FATZ1Δ91 eluted similarly to the wild-type. As expected, the determined molar masses were 23.99 kDa for KDK_FATZ1Δ91, 24.84 kDa for KK_FATZ1Δ91, and 24.69 kDa for FATZ1Δ91 wild-type. The proteins were in 50 mM Sodium Phosphate pH 7, 100 mM NaCl, 50 mM Arg, 50 mM Glu, 1 mM EDTA, and 0.5 mM PMSF. SEC-MALS experiments were performed using an HPLC system (Agilent) with a Superdex

200 10/300 column (GE Healthcare) in line with a miniDAWN™ TREOS detector and a Shodex Refractive Index detector.

SEC-MALS was conducted to determine whether KK_FATZ1Δ91 could still bind to α-actinin-2 following the same procedure used in the section “SEC-MALS of FATZ1Δ91 and α-actinin-2”. The SEC of the mixture KK_FATZ1Δ91/ACTN2 showed a peak eluting earlier than ACTN2 alone. The molar mass of the peak KK_FATZ1Δ91/ACTN2 was approximately 283.21 kDa, while for ACTN2 alone, it was 206.88 kDa. The increased molar mass indicated the formation of a complex of KK_FATZ1Δ91/ACTN2 with two molecules of KK_FATZ1Δ91 per ACTN2 dimer (as shown in **Figure 2.9**).

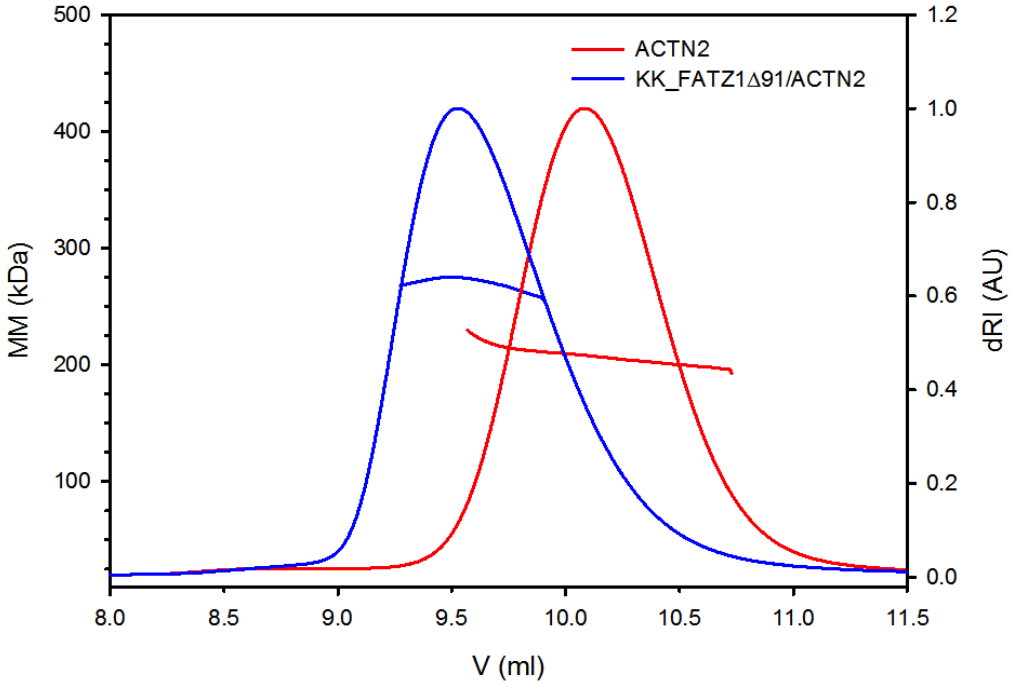

Figure 2.9: **SEC-MALS of the complex KK_FATZ1Δ91/α-actinin-2**. The KK_FATZ1Δ91/ACTN2 peak (in blue) eluted earlier than ACTN2 alone (in red). The molar mass of the peak for KK_FATZ1Δ91/ACTN2 is approximately 283.21 kDa, while for ACTN2 alone is 206.88 kDa. The increment of molar mass indicated the formation of a complex of KK_FATZ1Δ91/ACTN2 with two molecules of KK_FATZ1Δ91 per ACTN2 dimer. The samples were prepared at 175 uM of FATZ1Δ91 and 35 uM of ACTN2 in a solution containing 50 mM Sodium Phosphate pH 7, 100 mM NaCl, 50 mM Arg, 50 mM Glu, 1 mM EDTA, and 0.5 mM PMSF. SEC-MALS experiments were performed using an HPLC system (Agilent)

with a Superdex 200 10/300 column (GE Healthcare) in line with a miniDAWN™ TREOS detector and a Shodex Refractive Index detector.

ITC was performed to determine the influence of the two mutations (K176A and K233A) in the complex KK_FATZ1Δ91/ACTN2 binding parameters. The titration of 217.12 μM KK_FATZ1Δ91 into 20.0 μM ACTN2 showed a double sigmoidal thermogram with two exothermic binding events. The first binding event had a ΔH1 = -20.61 kcal/Mol with a Kd1 = 9.1 nM, and the second one had a ΔH2 = -7.53 kcal/Mol with a Kd2 = 383.4 nM (**Figure 2.10**).

The data obtained from the ITC analysis indicated that the mutant had an interaction with ACTN2 similar to the wild-type FATZ-1Δ91. However, there were some differences in the binding parameters of the two complexes. The Kd values for both binding sites in the mutant complex were relatively higher than those of the wild-type complex, and the exothermic release was also relatively smaller. To further illustrate these differences, **Table 2.3** compares the binding parameters of the wild-type and mutant complexes, providing a clear view of their respective properties.

Table 2.3: FATZ1Δ91/ACTN2 binding parameters comparison between wild type and mutant.

	KK_FATZ1Δ91/ACTN2	**FATZ1Δ91/ACTN2 (wild-type)**
Kd1 (nM)	9.1	3.18
ΔH1 (kcal/Mol)	-20.61	-26.66
Kd2 (nM)	383.4	227.65
ΔH2 (kcal/Mol)	-7.53	-10.26

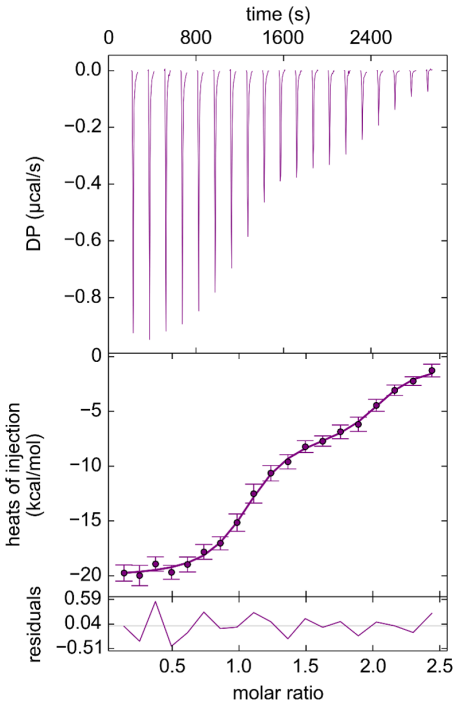

Figure 2.10: ITC data of KK_FATZ1Δ91 binding to α-actinin-2. The determined binding parameters were Kd1=9.7 nM, ΔH1=-20.61 kcal/Mol, Kd2=383.4 nM, and ΔH2=-7.53 kcal/Mol. The global reduced chi-square value was 1.22e-01 (n=19). The assay was done with a titration of 217.12 µM FATZ1Δ91 into 20 µM of ACTN2 in 20 injections with a MicroCal iTC200 (Malvernpanalytical). The proteins were in 50 mM NaPO4 pH 7.5, 100 mM NaCl, 50 mM Glu, 50 mM Arg, 1 mM EDTA,1mM βME, and 0.5 mM PMSF. The top panel shows the power versus molar ratio curve, while the bottom panel shows the thermogram of the integrated peak intensities plotted against the molar ratio.

CD of the complex FATZ1Δ91/α-actinin-2

Circular dichroism spectroscopy was employed to study the changes in the secondary structure of FATZ1Δ91 upon binding to α-actinin-2. The CD spectra of FATZ1Δ91 and ACTN2 were measured independently and together in the complex FATZ1Δ91/ACTN2. The CD signal was then converted from ellipticity (θ, millidegree) to mean residue molar ellipticity($[\theta]_{MR}$, degrees cm^2 $dmol^{-1}$) to assess the presence of a secondary structure, specifically α-helices and unordered regions.

Consistent with the α-actinin-2 structure detailed in Ribeiro et al. (2014), the full-length ACTN2 dimer displayed α-helical content in its CD spectra, supported by two negative minima at 208 and 222 nm and a positive maximum at 198 nm (**Figure 2.11A and B**). FATZ1∆91 had a minimum near 200 nm and a relatively low ellipticity at 220 nm (**Figure 2.11A and B**), indicating unordered regions. The complex FATZ1Δ91/ACTN2 exhibited negative minima at 208 and 222 nm and a positive maximum at 198 nm, indicating the presence of α-helices. However, compared to ACTN2 alone, the complex displayed an increase in ellipticity values at 208 and 222 nm and a reduction at 198 nm, suggesting a lower helical content than in ACTN2 alone (**Figure 2.11A and B**).

In order to assess the secondary structure of the complex FATZ1Δ91/ACTN2 from the CD data, the CDSSTR method was employed using Set4 as a reference dataset (Miles et al., 2022). **Table 2.3** shows that the estimated secondary structure content of ACTN2 alone has 59% helix and 15% unordered regions (as shown in **Table 2.3** and **Figure 2.10C**), which is in agreement with the helix and unordered percentages obtained from analyzing the X-ray structure of α-actinin-2 (Ribeiro et al., 2014) using the DSSP classes. The FATZ1∆91 secondary structure prediction resulted in 6% helix and 47% unordered, while the complex FATZ1Δ91/ACTN2 prediction resulted in 42% helix and 27% unordered regions. The secondary structure predictions indicated a decrease of 17% in helical content and an increase of 12% in unordered regions of the complex FATZ1Δ91/ACTN2 compared to ACTN2 alone, suggesting that FATZΔ91 remains relatively flexible after binding to α-actinin-2.

Table 2.3: Secondary structure prediction from CD data using the CDSSTR algorithm and Set4 as reference dataset (Miles et al., 2022)

Protein	**helix (%)**	**unordered (%)**	**NRMSD**
α-actinin-2	59	15	0.005
α-actinin-2 (DSSP classes from pdb 4D1E)	69	15	NA
FATZ1Δ91	6	47	0.013
FATZ1Δ91/α-actinin-2	42	27	0.014

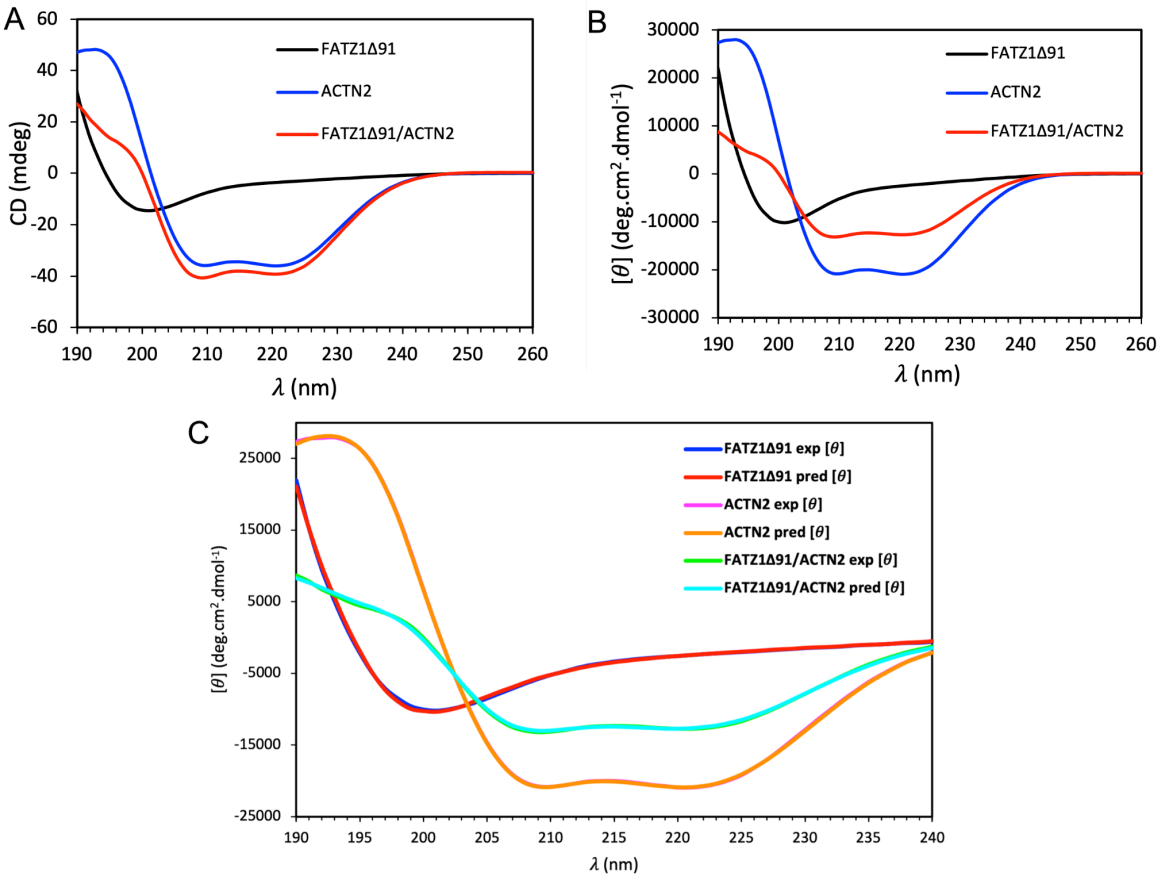

Figure 2.11. CD spectroscopy of FATZ1Δ91, α-actinin-2 and the complex FATZ1Δ91/α-actinin-2. A) CD spectra of FATZ1Δ91(black), ACTN2 alone (blue), and the complex FATZ1Δ91/ACTN2 (red). Samples were measured as 6.42 μM FATZ1Δ91, 0.99 μM ACTN2 and 1.36 μM FATZ1Δ91/ACTN2 in 10 mM Sodium Phosphate pH 7 after extensive dialysis. CD spectrum was collected from 260 to 180 nm in a Chirascan CD spectrophotometer (Applied Photophysics) with a 0.1 cm path-length quartz Suprasil cuvette. **B)** Mean residue molar ellipticity of FATZ1Δ91(black), ACTN2 (blue) and the complex FATZ1Δ91/ACTN2 (red). **C)** Fit of the predicted vs experimental CD data used by the CDSSTR method with the Set4 reference dataset (Miles et al., 2022) for the secondary structure predictions. Predictions were evaluated by the NRMSD of the experimental vs the predicted data. Only predictions with minimum residuals between experimental and predicted CD data (NRMSD < 0.02) were retained. Spectra are labelled as FATZ1Δ91 predicted (red) and experimental (blue), ACTN2 predicted (orange) and experimental (magenta), and FATZ1Δ91/ACTN2 predicted (cyan) and experimental (green).

SAXS of the complex FATZ1Δ91/α-actinin-2

SAXS experiments were performed to assess the flexibility of FATZ1Δ91 after binding to α-actinin-2. For this experiment, α-actinin-2 half-dimer (ACTNhd) and

α-actinin-2 full-length (ACTN2) were employed. The ACTN2hd and ACTN2 were prepared without histags to eliminate flexibility, as previously described in the section "Purification of α-actinin-2 constructs for the binding studies." The complexes FATZ1Δ91/ACTNhd and FATZ1Δ91/ACTN2 were copurified by SEC, as shown in **Figure 2.12**.

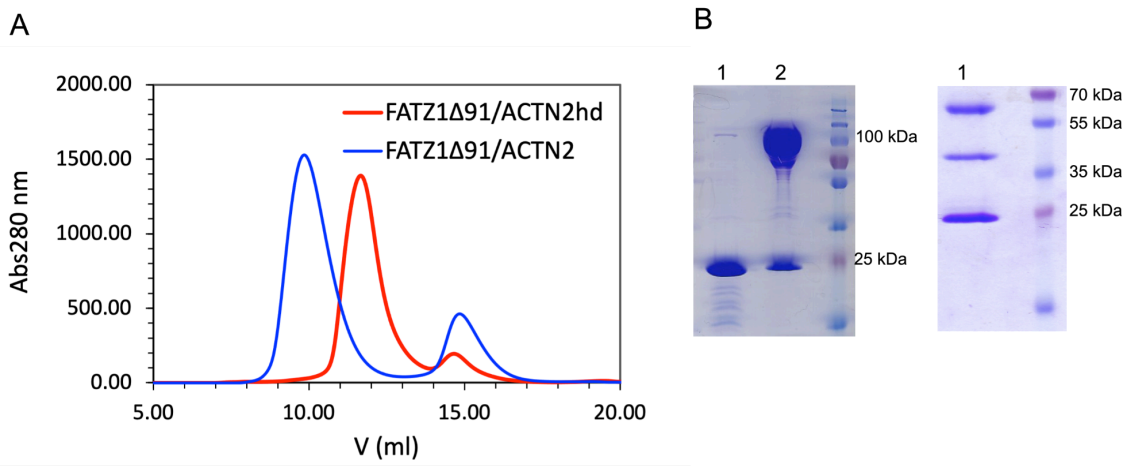

Figure 2.12: Copurification of the complexes FATZ1Δ91/ACTN2hd and FATZ1Δ91/ACTN2. **A)** SEC of the complex FATZ1Δ91/ACTN2hd (red) and FATZ1Δ91/ACTN2 (bleu). The complex FATZ1Δ91/ACTN2hd eluted at 12 ml, the complex FATZ1Δ91/ACTN2 eluted at 10 ml, and the unbound FATZ1Δ91 at 15 ml. **B)** SDS-PAGE 15 % with CBB staining of copurifications. **Left panel:** FATZ1Δ91/ACTN2 copurification; lane 1 shows FATZ1Δ91 eluted at 15 ml, and lane 2 shows the complex FATZ1Δ91/ACTN2 eluted at 10 ml. **Right panel:** FATZ1Δ91/ACTN2hd copurification; lane 1 shows the complex FATZ1Δ91/ACTN2hd eluted at 12 ml. SEC copurifications were done in a S200 10/300 column (GE Healthcare) in 50 mM Tris HCl pH 7.5, 100 mM NaCl, 50 mM Glu, 50 mM Arg, and 1mM βME.

For the SAXS experiment, three concentrations were prepared for each protein or complex. Polydispersity and Rs were measured for each concentration to ensure sample quality, as shown in **Table 2.4**.

The SAXS measurements were conducted at the BioSAXS beamline at ESRF, Grenoble, following the experimental procedure described in **Material and Methods**. **Table 2.5** summarizes the Guinier analysis of the SAXS dataset, and **Table 2.6** summarizes the structural parameters extracted from the data.

Table 2.4: Quality check of samples prepared for SAXS experiments

Protein	C (mg/ml)	Polydispersity (%)	Rs (nm)
ACTN2hd			
	6.22	14.8	5.6
	3.26	13.2	5.3
	1.05	18.6	4.9
FATZ1Δ91/ACTN2hd			
	6.70	5.0	6.3
	3.00	5.6	5.9
	1.10	12.1	5.5
ACTN2			
	1.89	8.8	7.3
	1.49	6.1	7.2
	4.12	6.1	7.5
FATZ1Δ91/ACTN2			
	2.63	8.5	8.7
	3.99	9.6	8.9
	7.78	14.9	9.8

The SAXS data of ACTN2hd is depicted in **Figure 2.13A**, and the Guinier analysis is in **Figure 2.13B**. The Guinier plot indicated that an increase in particle concentration led to a leger decrease in Rg (**Table 2.5**). The I(0) values remained constant for the lower and middle concentrations but increased for the higher concentration, indicating non-specific aggregation (Jacques & Trewhella, 2010). The lower and medium concentrations were combined into a new curve shown in **Figure 2.13E** to eliminate the impact of the aggregation. This new curve's calculated Rg value from the Guinier region was 6.07 nm (**Figure 2.13F**). The Pr function calculated for a Dmax of 23 nm also indicated an Rg value of 6.19 nm (**Figure 2.15**).

The SAXS data of FATZ1Δ91/ACTN2hd is shown in **Figure 2.13C,** and the Guinier analysis is shown in **Figure 2.13D**. The Guinier plot revealed that the Rg

was consistent for the three concentrations (**Table 2.5**). The I(0) values remained similar for the lower and middle concentrations but increased for the higher concentration, suggesting non-specific aggregation (Jacques & Trewhella, 2010). The lower and higher concentrations were merged into a new saxs curve (**Figure 2.13F**). In the new curve, the Rg determined from the Guinier region was 6.28 nm (**Figure 2.13E**). The Pr function calculated for a Dmax of 25 nm indicated an Rg value of 6.55 nm (**Figure 2.15**).

Table 2.5: Guinier parameters of the SAXS data

Dataset	**Rg(nm)**	**I(0)**	**sRg limits**
ACTN2hd			
1.05 mg/ml	6.18	92.5	0.39-1.02
3.26 mg/ml	6.13	90.76	0.40-0.86
6.20 mg/ml	6.11	101.73	0.41-0.95
FATZ1Δ91/ACTN2hd			
1.10 mg/ml	6.28	118.83	0.41-0.95
3.0 mg/ml	6.29	118.83	0.41-0.8
6.7 mg/ml	6.28	124.1	0.41-1.09
ACTN2			
1.49 mg/ml	11.03	163.46	0.56-1.08
1.89 mg/ml	11.29	171.76	0.57-1.05
4.12 mg/ml	11.32	183.1	0.57-1.16
FATZ1Δ91/ACTN2			
2.63 mg/ml	11.57	269.67	0.48-1.13
3.99 mg/ml	11.86	272.65	0.54-1.11
7.78 mg/ml	12.71	307.98	0.52-1.06

The SAXS data of ACTN2 is depicted in **Figure 2.14A,** and the Guinier analysis is in **Figure 2.14B**. It was observed from the Guinier plot that the Rg values for the three concentrations were similar, as shown in **Table 2.5**. In contrast, the I(0)

values increased with the concentration, indicating non-specific aggregation in the samples (Jacques & Trewhella, 2010). To mitigate the effects of aggregation, only the curve at 1.49 mg/ml was selected for further analysis (**Figure 2.14E**). The Rg determined from the Guinier region was 11.03 nm in this curve (**Figure 2.14F**), and the calculated Pr function at a Dmax of 40 nm indicated an Rg of 11.59 nm, as shown in **Figure 2.15**.

The SAXS data of the complex FATZ1Δ91/ACTN2 is illustrated in **Figure 2.14C**, and the Guinier analysis is in **Figure 2.14D**. The three FATZ1Δ91/ACTN2 concentrations showed similar Rg and I(0) values for low and medium concentrations (**Table 2.5**). However, the higher concentration exhibited increased Rg and I(0) values compared to the others, indicating non-specific aggregation (Jacques & Trewhella, 2010). Examining the Pr functions of the three concentrations at extended Dmax showed a negative Pr function for the lower concentration, indicating interparticle interference in this sample (Jacques & Trewhella, 2010). This phenomenon was not observed in the medium concentration, and the higher concentrations merged into a new curve used for the rest of the analysis (**Figure 2.14E**). The Rg value obtained from the Guinier region (**Figure 2.14F**) was 11.86 nm. Additionally, the calculated Pr function for a Dmax of 48 nm indicated an Rg value of 12.46 nm, as shown in **Figure 2.15**.

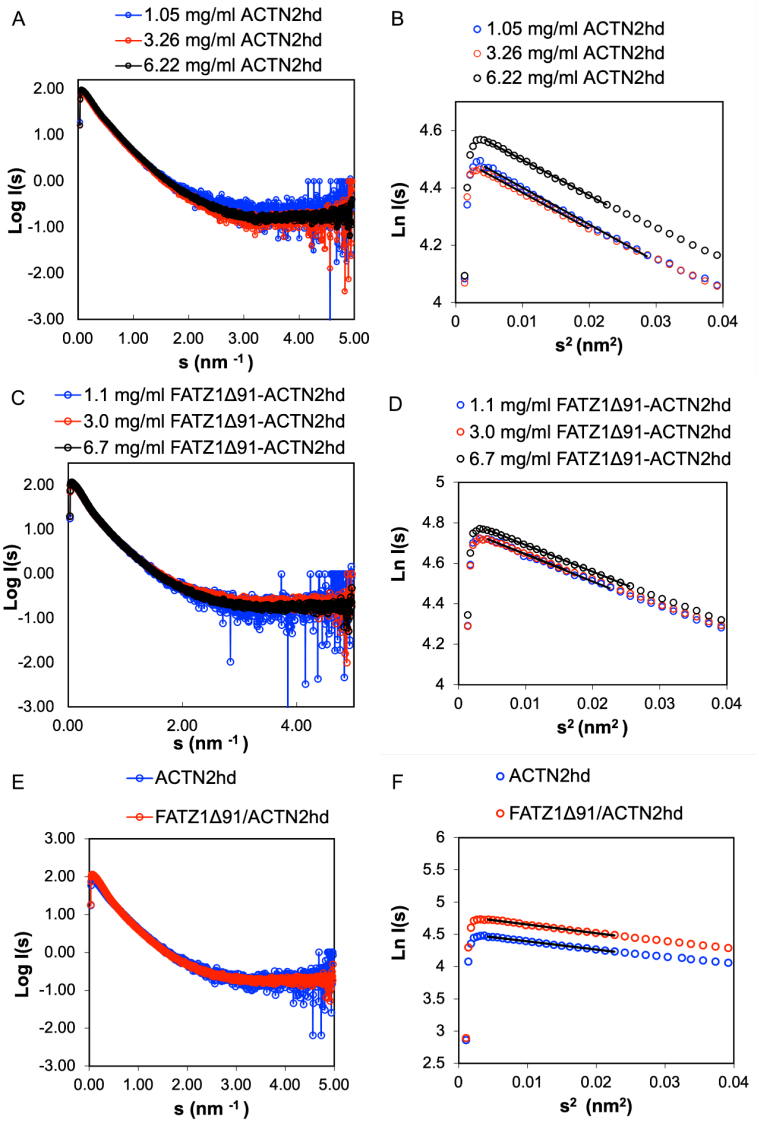

Figure 2.13. SAXS of the complex FATZ1Δ91/α-actinin-2 half-dimer. A) Scattering plot of ACTN2hd at concentrations 1.05 (bleu), 3.26 (red) and 6.2 mg/ml(black). **B)** Guinier plot of ACTN2hd at the three concentrations. **C)** Scattering plot of the complex FATZ1Δ91/ACTN2hd at concentrations: 1.10 (bleu), 3.00 (red), and 6.70 mg/ml (black). **D)** Guinier plot of complex FATZ1Δ91/ACTN2hd at three concentrations. **E)** Scattering plot of ACTN2hd and the complex FATZ1Δ91/ACTN2hd after merge. **F)** Guinier plot of ACTN2hd and FATZ1Δ91/ACTN2hd after the merge. All samples were in 50 mM Tris HCl pH 7.5, 100 mM NaCl, 50 mM Glu, 50 mM Arg, 1mM βME. The buffer scattering was subtracted from the sample, and intensities were normalized by concentration.

Table 2.6: Structural parameters extracted from the SAXS data				
Sample	**Rg(nm), Guinier**	**I(0)**	**Dmax (nm)**	**Rg (nm), Pr**
ACTN2hd	6.07	91.28	23	6.19
FATZ1Δ91/ACTN2hd	6.28	119.58	25	6.55
ACTN2	11.03	163.46	40	11.59
FATZ1Δ91/ACTN2	11.86	275.41	48	12.46

The Pr functions of ACTN2hd, ACTN2, and the complexes FATZ1Δ91/ACTN2hd and FATZ1Δ91/ACTN2 showed distinct shapes, reflecting the structural differences of each protein or protein complex in solution (**Figure 2.15**). The ACTN2 Pr function was similar to the previously reported Pr function by Ribeiro et al. (2014), presenting a Dmax of 40 nm. The complex FATZ1Δ91/ACTN2 Dmax was 48 nm, indicating the presence of a larger particle compared to ACTN2 alone. The increase in particle size was less significant in the Pr function of the complex FATZ1Δ91/ACTN2hd compared to ACTN2hd alone since the Dmax was only 2 nm higher for the complex (**Figure 2.15**).

Figure 2.16 revealed distinct shapes in the dimensionless Kratky plots of the proteins. The ACTN2hd and the complex FATZ1Δ91/ACTN2hd curves exhibited a bell-shaped curve with a tail, indicating compacted domains with loops (Receveur-Brechot & Durand, 2012). The ACTN2 plot showed a less pronounced bell shape, suggesting a compact structure with flexible loops. The complex FATZ1Δ91/ACTN2 Kratky plot showed a curve that increased at lower sRg values before reaching a plateau, indicating the presence of flexibility. The FATZ1Δ91 curve displayed a similar shape, suggesting it is an Intrinsically Disordered Protein (IDP), which aligns with the CD and NMR results previously obtained.

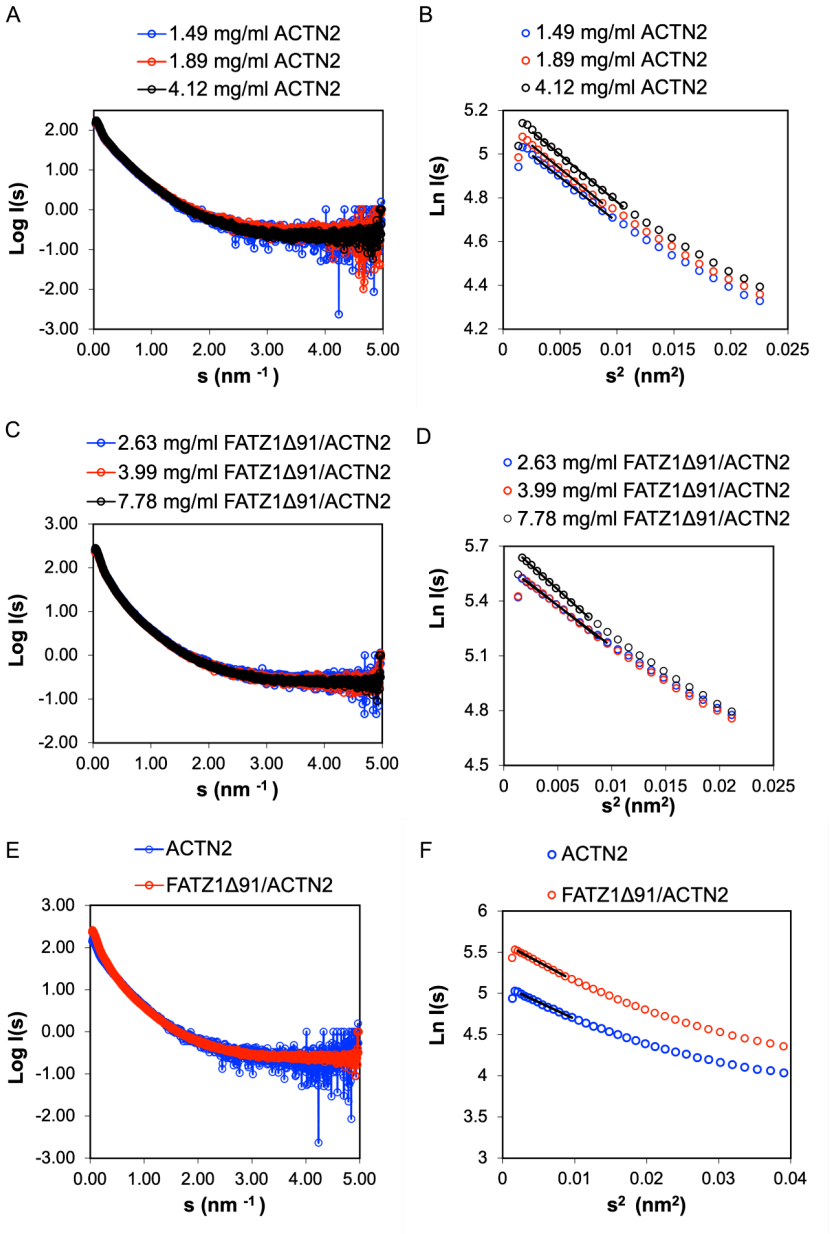

Figure 2.14. SAXS of the complex FATZ1Δ91/α-actinin-2 full-length. A) Scattering plot of ACTN2 at concentrations: 1.49 (bleu), 1.89 (red), and 4.12 mg/ml (black). **B)** Guinier plot of ACTN2 at three concentrations. **C)** Scattering plot of the complex FATZ1Δ91/ACTN2 at concentrations 2.63 (bleu), 3.99 (red), and 7.78 mg/ml (black). **D)** Guinier plot of the complex FATZ1Δ91/ACTN2 at three concentrations. **E)** Scattering plot of ACTN2 and FATZ1Δ91/ACTN2 after merge. **D)** Guinier plot of the ACTN2 and FATZ1Δ91/ACTN2 after merge. All samples were in 50 mM Tris HCl pH 7.5, 100 mM NaCl, 50 mM Glu, 50 mM Arg, 1mM βME. The buffer scattering was subtracted from the sample, and intensities were normalized by concentration.

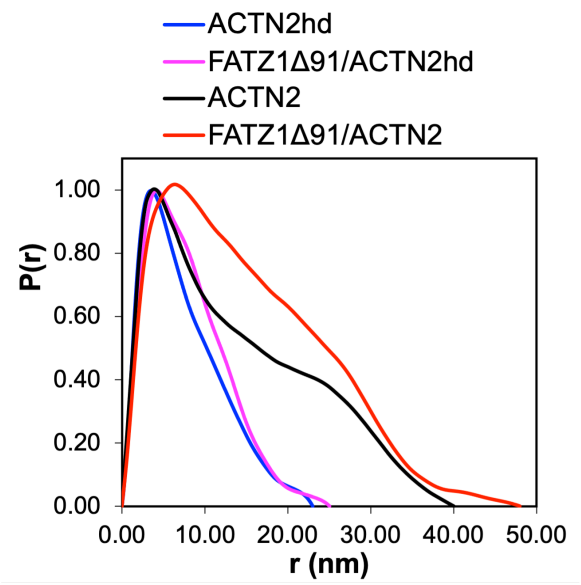

Figure 2.15: Pr functions of the complexes FATZ1Δ91/α-actinin-2. The P(r) function of ACTN2hd with a Dmax = 23 nm is shown in blue. The FATZ1Δ91/ACTN2hd with a Dmax = 25 nm function is shown in magenta. The ACTN2 function with a Dmax = 40 nm is shown in black. The FATZ1Δ91/ACTN2 function at a Dmax = 48 nm is shown in red. The Pr functions showed different shapes reflecting the structural differences among the proteins and complex in solution.

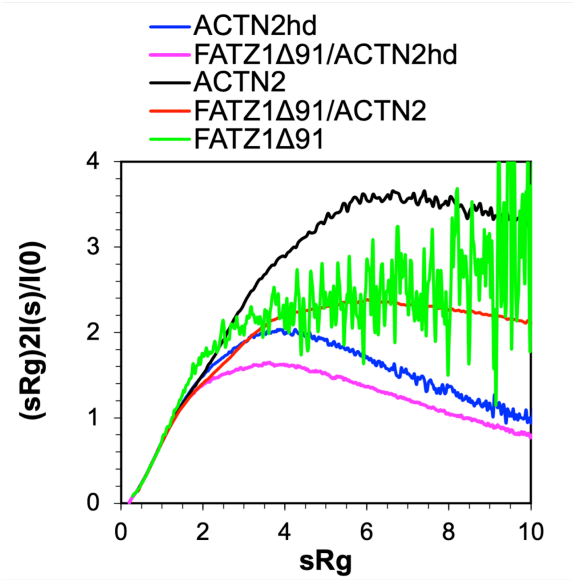

Figure 2.16: Dimensionless Kratky plots of FATZ1Δ91 alone and in complex with α-actinin-2. Dimensionless Kratky plot depicted as follows: FATZ1Δ91 is shown in vert, ACTN2hd is shown in blue, FATZ1Δ91/ACTN2hd is shown in magenta, ACTN2 is shown in black, and FATZ1Δ91/ACTN2 is shown in red. The ACTN2hd, FATZ1Δ91/ACTN2hd, and ACTN2 had curves of proteins consisting of several domains with loops in compact conformations. The FATZ1Δ91/ACTN2 (red) had a curve characteristic of a protein consisting of folded domains with loops in extended conformations. The FATZ1Δ91 curve (green) displays a rising curve and a monotonous increase at high sRg, indicating an extended conformation with flexible loops.

DISCUSSION

When FATZ-1 was discovered (Faulkner et al., 2000), database searches indicated no structural homologs or canonical domains. However, it was found that FATZ-1 had two isoforms sharing conserved regions in the N-terminal and C-terminal, named conserved domain 1 (CD1) and conserved domain 2 (CD2) as depicted in **Figure 1.1** (Faulkner et al., 2000). In addition, the FATZ-1 sequence showed a central region enriched in glycines named after the glycine-rich region (GRR).

Given the lack of defined structural domains, working with FATZ-1 full length was very difficult. Protein expression yields were low, and the protein tended to precipitate at concentrations higher than 1 mg/ml, which are required for most structural studies. To address this challenge, optimized constructs were developed, such as FATZ1Δ184. This construct includes only the CD2 region, as shown in **Figure 1.3**. The FATZ1Δ184 construct learned us that its apparent higher molecular weight in size exclusion chromatography was not due to a dimer since the SEC-MALS experiments confirmed that FATZ1Δ184 was a monomer in solution with a molar mass corresponding to a monomer at 13.21 kDa (**Figure 1.6**), but suggested that FATZ1Δ184 was not in a globular form either. Although FATZ1Δ184 was expected to be soluble and stable in solution, degradation was observed during the purification. A degradation product of ~6 kDa was confirmed by SEC-MALS (**Figure 1.4C**), and mass spectrometry identified a fragment corresponding to the first 57 residues of FATZ1Δ184, implying from residue 185 to 241 of the FATZ-1 full-length. The stability of the construct was improved by adding arginine and glutamine to the purification buffers (**Figure 1.5B**). However, the protein precipitated over time and after each thawing step. Therefore, the work in this construct was not promising and we focused on a longer construct containing the GRR and the entire CD2. The new construct was named FATZ1Δ91 (**Figure 1.7**) since it had a deletion of the 91 residues at the N-terminal, and it was provided by a collaborator from Evitra at the Karolinska Institute. According to Evitra's methodology, this construct was scored as soluble in *E. coli* expression and yields were promising.

FATZ-1 displays characteristics of an IDP with residual secondary structure

Predictions of FATZ-1 secondary structure with JPred server (Drozdetskiy et al., 2015) indicated helical content in the CD2 (188 - 192 aa, 196 - 201 aa) and β-sheets (177-181 aa) (**Figure 1.2A**). In addition, the metaPrDos prediction (Ishida & Kinoshita, 2007) indicated disordered regions in the GRR (94 - 174 aa) and the C-terminal of CD2 (293 - 299 aa) (**Figure 1.2B**). The analysis of predictions suggests the existence of ordered regions with secondary structure elements in the CD2 region between residues 177 and 201. This region was entirely covered by the construct FATZ1∆91 (**Figure 1.2**).

NMR and CD spectroscopy of FATZ1Δ91 were done to investigate its folding state in solution. The FATZ1Δ91 HSQC spectra (**Figure 1.9**) showed a narrow peak distribution, indicating a lack of a defined tertiary structure (Kosol et al., 2013). In addition, the CD spectra depicted a band with a minimum of around 200 nm and a relatively low ellipticity at 220 nm (**Figure 1.10**), characteristics of intrinsically disordered proteins (Uversky, 2002b). Nevertheless, the signal at 208 and 222 nm, indicative of some α-helical content, was higher than expected for a completely random coil (Uversky, 2002). Therefore, a secondary structure estimation was performed using the CDSSTR method and the Set175 (Miles et al., 2022). This secondary structure analysis indicated that FATZ1Δ91 was 47% unordered, 18% turns, and 6% helix. Moreover, the estimation indicated 28% strands, higher than expected for FATZ1Δ91. This result may be due to the limitations of the CDSSTR method since estimations are made using datasets of folded proteins whose structures are already available; therefore, predictions may be biased toward structured regions (Miles et al., 2023).

More evidence supporting that FATZ1Δ91 is an intrinsically disordered protein was obtained by analyzing its small-scale X-ray scattering curve (**Figure 1.12**). The SAXS analysis showed that FATZ1Δ91 lacks features typically present in native state proteins. For instance, the Kratky plot of a globular native state protein displays a bell shape with a maximum value at sRg=$\sqrt{3}$ (Receveur-Brechot & Durand, 2012). In contrast, the Kratky plot of an intrinsically disordered protein shows a rising curve at low sRg, which flattens out at higher sRg values (Kikhney & Svergun, 2015; Receveur-Brechot & Durand, 2012). The Kratky plot of FATZ1Δ91 displayed the

latter characteristics, indicating that it lacks a packed core as other well-known intrinsically disordered proteins such as α-synuclein and prothymosin-α (Uversky, 2002b).

Moreover, according to the EOM analysis of the scattering curve, FATZ1Δ91 comprises a conformational ensemble with Rg ranging from 3.00 to 7.58 nm and Dmax ranging from 8.36 to 23.36 nm (**Figure 1.13**). Therefore, the experimental evidence collected here indicates that FATZ1Δ91 is intrinsically disordered with a residual secondary structure content and can be better described as a conformational ensemble.

Many intrinsically disordered proteins have been recognized as essential in signalling pathways and protein interaction networks (Wright & Dyson, 2015). Some of these IDPs fulfil their multiple protein interactions by providing linear motifs that can be bound by more than one binding partner with different affinities (Wright & Dyson, 2015). The intrinsically disorder characteristics of FATZ-1 are compatible with being part of a signalling pathway and recruiting protein partners into the Z-disc during assembly (Frey et al., 2000, 2008; Sanger et al., 2010). Since FATZ-1 has multiple binding partners with their binding sites in the CD2 region (Faulkner et al., 2000; Frey et al., 2000; Gontier et al., 2005; Takada et al., 2001; von Nandelstadh et al., 2009), it is possible that providing linear binding motifs and small secondary structure elements rather than compact globular domains may represent an advantage to perform multiple interactions. In this sence, a linear motif was identified in the FATZ-1 C-terminus binding to the PDZ domain of the ZASP and Enigma families (von Nandelstadh et al., 2009). It may be possible that other binding partners bind to linear motifs as well.

Although we did not address the effect of post-translational modifications on the FATZ-1 structure, experimental data show that FATZ-1 and other family members undergo phosphorylation in the PDZ binding motif ETEEL (von Nandelstadh et al., 2009). In addition, FATZ-1's phosphoproteomic data (Uniprot entry Q9NP98) shows evidence of phosphorylation sites in the GRR. Investigating whether phosphorylation can modulate the intrinsic disorder features of FATZ-1 and its interaction with binding partners would be an exciting avenue to explore.

FATZ-1 and α-actinin-2 form a complex of high affinity

Here, we presented the binding parameters of the interaction between the CD2 region of FATZ-1 and its binding partner α-actinin-2. Our experimental data revealed that FATZ1Δ91 interaction with α-actinin-2 is stable in the low nanomolar range. SEC-MALS experiments supported this, where the complex FATZ-1/α-actinin-2 was observed with α-actinin-2 full-length and half-dimer constructs (**Figure 2.3**). The complex FATZ-1/α-actinin-2 full-length displayed a molar mass corresponding to two molecules of FATZ1Δ91 per ACTN2 dimer, and the complex FATZ-1/α-actinin-2 half-dimer displayed the molar mass of one molecule of FATZ1∆91 per ACTN2hd (**Figure 2.3**, **Table 2.1**). It is worth noticing that the size-exclusion chromatography diluted the samples from the micromolar range to the nanomolar range. Still, a stable molecular mass distribution was observed for the corresponding peaks of FATZ1∆91/ACTN2hd and FATZ1∆91/ACTN2. In contrast, no complex was observed between FATZ1Δ91 and the Efhands, in agreement with the biochemical data previously reported in (Faulkner et al., 2000), which indicated that the binding sites of FATZ1Δ91 were located in the rod domain of α-actinin-2.

The ITC data corroborated that the interaction happens with high affinity in the nanomolar range (**Figure 2.4**). The interaction between FATZ1Δ91 and α-actinin-2 occurs with a stochiometry of 2:1 in two binding events. During the first binding event, the FATZ1Δ91 molecules occupy one of the two binding sites of α-actinin-2 with high affinity (Kd1=3.18 nM) and a strong enthalpy release (ΔH1 = -26.66 kcal/Mol), indicating a strong interaction (Leavitt & Freire, 2001). In a later stage, a second binding event takes place where FATZ1Δ91 binds the other α-actinin-2 site with lower affinity (Kd2 = 227.65 nM) and enthalpy (ΔH2 = -10.26 kcal/Mol), implying that the second binding event is less favourable than the first one. It may be possible that the first FATZ1Δ91 molecule blocks partially the second binding site due to the flexible loops not implicated in the binding region. Therefore, the second FATZ1Δ91 molecule may need a higher concentration to gain the binding site. This hypothesis, was later corroborated by coworkers, which found detailed structural evidence of a fuzzy complex between FATZ-1 and α-actinin-2 (Sponga et al., 2021).

Contact residues at the binding interface

The MS analysis of the crosslinked complex found three crosslinked pairs of residues between FATZ1Δ91 and ACTN2hd (**Figure 2.5** and **Table 2.2**). Based on this data, we proposed three contact points for the complex FATZ1Δ91/ACTN2hd comprising the residues K176-E658, D205-K383, and K233-E567 (**Figure 2.6**). The FATZ1Δ91 contact residues are located in the CD2, in agreement with previously reported data (Faulkner et al., 2000; Frey et al., 2000; Takada et al., 2001), while the ACTN2hd contact residues are located on SR1(K383), SR3(E657), and SR4(E658). The binding to SR3 and SR4 was already reported in (Faulkner et al., 2000; Frey et al., 2000; Takada et al., 2001); however, the binding to SR1 was for the first time observed. Since the contact residues have side chains with electric charges, there may be an electrostatic interaction at the binding interface.

We created a mutant called KK_FATZ1Δ91 to test the relevance of the contact residues for the interaction with α-actinin-2 half-dimer. The mutations K176A and K233A aimed to abolish the electrostatic interactions between the pairs K176-E658 and K233-E567. We observed that the mutant KK_FATZ1Δ91 could still bind α-actinin-2 full-length, forming a stable complex observed in SEC-MALS with a molar mass corresponding to two molecules of FATZ1Δ91 per α-actinin-2 dimer as the wild-type FATZ1Δ91 (**Figure 2.9**). Intresting, the ITC data indicated that the mutant KK_FATZ1Δ91 binds α-actinin-2 with a slightly lower affinity for ACTN2 than the wild-type and a stochiometry of 2:1 (**Figure 2.10**).

It is worth noticing that the affinities of the mutant were relatively lower (Kd1=9.7 nM and Kd2=383.4 nM) than those of the wild-type (Kd1=3.18 nM and Kd2=227.65 nM). Moreover, the exothermic release was also relatively reduced for the mutant (ΔH1=-20.61 kcal/Mol and ΔH2=-7.53 kcal/Mol) than for the wild-type (ΔH1=-26.66 kcal/Mol and ΔH2=-10.26 kcal/Mol). This observation suggested that the mutant interaction with α-actinin-2 is less favoured thermodynamically than the wild-type interaction.

A triple mutant named KDK_FATZ1Δ91, which had a third mutation (D205A), was also created. Interestingly, this mutation caused an unstable version of FATZ1Δ91 that precipitated and degraded very quickly during purification. In SEC-MALS, KDK_FATZ1Δ91 eluted earlier than the wild-type FATZ1Δ91 and the

KK_FATZ1Δ91 mutant, indicating a more elongated conformation due to the mutation (D205A). Because this construct was highly unstable, we decided not to pursue further experiments under the experimental conditions we had at that time.

Our data suggested that the crosslinked residues were not the only residues involved in the binding interface. The failed attempt to disrupt the binding with two point mutations suggests that more contact residues are implicated in the binding interface between FATZ-1/α-actinin-2. This agrees with the obtained ITC data for the wild-type complex, which indicated a strong affinity between these two binding partners. Other co-workers later corroborated these findings (Sponga et al., 2021). In the X-ray structure of the complex FATZ-1/α-actinin-2, they found two linear motifs (LM) of FATZ1Δ91, called LM1 and LM2, as responsible for the binding. In particular, residues Y218 to Y228, located in the LM2 (CD2), were identified as the primary binding site for α-actinin-2 (Sponga et al., 2021). The LM1 is located inside the region delimited by the contact residues (K176 to K233) we found here, while the LM2 goes farther until the residue F240 (Sponga et al., 2021).

Other Z-disc protein-protein interactions have been characterized at the physico-chemical level with reported binding parameters. These studies have provided one step closer to understanding how multiple protein-protein interactions can support the Z-disc assembly. Among them are myotilin/α-actinin-2 (Kostan et al., 2021), titin/α-actinin-2 (Young & Gautel, 2000), and ZAPS/α-actinin-2 (Au et al., 2004). The present study was part of this endeavour since it provided valuable details of the interaction FATZ-1/α-actinin-2 at the physicochemical level, which were further used by Sponga and collaborators to pursue the study of the complex FATZ-1/α-actinin-2 structure (Sponga et al., 2021).

FATZ-1 remains flexible after binding to α-actinin-2

Circular dichroism spectroscopy and small-angle X-ray scattering were employed to explore the structure of the complex FATZ-1/α-actinin-2. We chose those biophysical techniques, considering that our construct FATZ1Δ91 displayed characteristics of an IDP with residual secondary structure, and those techniques could give us information about the structure of the complex, whether its is well defined or not (Bernadó & Svergun, 2012; Dyson & Wright, 2005; Receveur-Brechot & Durand, 2012; Uversky, 2002a). Although CD and SAXS gave us an overall view

of FATZ-1/α-actinin-2 structural properties, these techniques did not provide molecular details of the binding interface. Other structural techniques, such as X-ray crystallography, may had provided more details but needed to use smaller constructs of FATZ-1, bearing only well-defined structured elements to obtain crystals and observe their electrodensity maps (Uversky, 2002a). Early attempts to purify the construct FATZ1Δ184 (**Figure 1.5**) showed that shorter versions of FATZ-1 were not necessarily more stable than larger versions such as FATZ1Δ91. Therefore, we chose the challenge of studying the complex FATZ-1/α-actinin-2 with a more flexible construct and appreciated the beauty of FATZ-1 intrinsic disorder nature.

The CD data of FATZ1Δ91 and α-actinin-2 alone and in the complex revealed that the complex FATZ1Δ91/α-actinin-2 conserves the α-helical blueprint of α-actinin-2 alone. However, there was an increase in molar ellipticity values at 208 and 222 nm and a reduction at 198 nm, suggesting a lower helical content in the complex than in α-actinin-2 (**Figure 2.11B**). The assessment of the complex FATZ1Δ91/α-actinin-2 secondary structure from the CD data suggested that FATZΔ91 remains relatively flexible after binding to α-actinin-2. Moreover, the estimations of the secondary structure from the CD data employing the CDSSTR method (Miles et al., 2022) indicated a decrease of 17% in helical content and an increase of 12% in unordered regions of the complex FATZ1Δ91/α-actinin-2 compared to α-actinin-2 alone (**Table 2.3**).

SAXS experiments were performed to assess the flexibility of FATZ1Δ91 after binding to α-actinin-2. The α-actinin-2 full-length and half-dimer were used to obtain data on the complex with two and one binding sites, aiming to understand if the flexibility of the complex with one and two binding sites differed. The SAXS data of the complexes FATZ1Δ91/α-actinin-2 half-dimer and FATZ1Δ91/α-actinin-2 full-length showed distinct shapes, reflecting the structural differences of the complexes (**Figure 2.15**). The Dmax values obtained for the complex FATZ1Δ91/α-actinin-2 suggest a larger particle since the Dmax of the complex was approximately 8 nm larger than the Dmax of α-actinin-2 alone. However, the increase in Dmax was less significant for the complex FATZ1Δ91/α-actinin-2 half-dimer, as the Dmax was only 2 nm higher for the complex than for the α-actinin-2 half-dimer. The higher Dmax of the complex with two binding sites vs one binding site also confirms the difference in the overall shape observed in the Pr function (**Figure 2.15**).

The dimensionless Kratky plot analysis was employed to assess the degree of flexibility of FATZ1Δ91 after binding to α-actinin-2. This information is extracted from the scattering data analysis in the form of a Kratky plot, whose shape is sensitive to the conformational state of the scattering proteins (Uversky, 2002a). The Kratky plots of α-actinin-2 half-dimer and the complex with FATZ1Δ91 (**Figure 2.16**) exhibit a bell-shaped curve with a tail, indicating scattering proteins with compacted domains and flexible loops (Kikhney & Svergun, 2015; Receveur-Brechot & Durand, 2012). In contrast, the α-actinin-2 full-length displayed the shape of a modular rod-like particle (Jeffries & Svergun, 2015), and the complex with FATZ1Δ91 exhibits an increasing curve until reaching a plateau, similar to FATZ1Δ91 alone. This analysis suggested that the complex FATZ1Δ91/α-actinin-2 full-length is more flexible than the complex FATZ1Δ91/α-actinin-2 half-dimer. Moreover, they suggest that FATZ1Δ91 remains flexible after binding to α-actinin-2. This findings were later corroborated by Sponga et al. (2021), their structural analysis showed that the complex FATZ1Δ91/α-actinin-2 full-length was fuzzy and could be better represented as a conformational ensemble (Sponga et al., 2021).

The implications of the complex FATZ-1/α-actinin-2 affinity and flexibility for the Z-disc

In the early stages of myofibrillogenesis, the complex FATZ-1/α-actinin-2 appears in the Z-bodies, condensates of biomolecules that will evolve into the Z-disc (Sanger et al., 2009). Other FATZ-1 binding partners will be recruited from this stage until the mature Z-disc is assembled (Sanger et al., 2010). Since FATZ-1 has multiple binding partners with their binding sites in the CD2 region, providing small binding motifs displayed in small secondary structure elements rather than in compact globular domains could represent an advantage in performing multiple interactions. Such a mechanism has been proven effective for other disordered proteins whose interactions reside in linear motifs separated by disordered regions (Wright & Dyson, 2015). In a further study, coworkers reported that two linear motifs were responsible for binding to α-actinin-2 (Sponga et al., 2021), suggesting that FATZ-1, like other IDPs, combines flexible regions with linear motifs to bind its partners.

Biochemical and genetic assays have discovered most Z-disc protein-protein interactions (Faulkner et al., 2001a; Sanger et al., 2010). In these approaches, one gets binary answers (binding or non-binding), while the physicochemical binding parameters supporting the interaction are ignored. The binding parameters give us information about the strength of those interactions and can allow us to understand whether multiple interactions can co-exist or are competitive in supramolecular assemblies. Since the Z-disc is supported by a supramolecular structure of multiple protein-protein interactions, knowing their binding parameters is essential to understanding its assembly and function.

The high affinity of the complex FATZ-1/α-actinin-2 may play a crucial role for its function, allowing α-actinin-2 maintain FATZ-1 tighlty anchored to the Z-disc while interacting with other binding partners that would exchange with lower affinities. Since the Z-disc comprises proteins with multiple interactions, some interactions may be competitive, while others may be cooperative. Determining the binding parameters of these interactions would provide another piece of the puzzle to understand how those proteins may interact to assemble the Z-disc. This may be the case for the interaction between α-actinin-2, FATZ-1, and myotilin. Myotilin and α-actinin-2 interact through the myotilin N-terminus and the Efhands 3-4 of α-actinin-2 with a Kd of 5.4 μM (Kostan et al., 2021). FATZ-1 does not bind to Efhands. However, the interaction myotilin/FATZ-1 has been mapped to the CD2 domain (Gontier et al., 2005), where α-actinin-2 binds. Would it be possible for FATZ-1, myotilin and α-actinin-2 to form a ternary complex via the CD2 region of FATZ-1? Or, are these interactions competitive? FATZ-1 remains flexible after binding to α-actinin-2 suggesting that myotilin could find a binding site in the CD2 region not involved in the interaction with α-actinin-2. Therefore, the binding parameters of the interaction FATZ-1/myotilin and the structural information about their complex are needed to understand if a ternary complex may exist between these three Z-disc proteins.

One of the possible interactions that may co-exist is the FATZ-1, α-actinin-2 and ZASP (von Nandelstadh et al., 2009). The interaction between PDZ and α-actinin-2 occurs in the C-terminal motif (Efhands 3-4), and the interaction between PDZ and FATZ-1 happens in the C-terminus motif ETEEL (von Nandelstadh et al., 2009), which is not involved in the binding to α-actinin-2 (Frey et al., 2000) and may

be exposed in the flexible region of FATZ-1 upon binding to α-actinin-2. Whether the PDZ domain may bind exclusively α-actinin-2 or FATZ-1 in a ternary complex is difficult to say. We know the binding affinity of the PDZ/α-actinin-2 interaction is in the micromolar range (Au et al., 2004); however, the binding constant of the interaction between FATZ-1 and the PDZ domain is unknown. Obtaining this information and performing a competing binding assay between FATZ-1 and α-actinin-2 for the PDZ domain may allow an understanding of whether a ternary complex exists.

Another possible binding partner that might take advantage of FATZ-1 flexibility in the Z-disc is the filamin-C. Filamin-C is associated with costameric proteins and the β1A integrin subunit in the sarcolema (Gontier et al., 2005). In addition, filamin-C is a binding partner of FATZ-1 and myotilin, which in turn are binding partners of α-actinin-2 (Faulkner et al., 2000; Gontier et al., 2005; Takada et al., 2001). Therefore, the interactions among these proteins may provide a protein network linking the sarcolema and the Z-disc (Gontier et al., 2005). Whether these interactions are competitive or cooperative is not entirely understood. As per existing research, it has been established that filamin-C and α-actinin-2 both have a binding affinity towards the CD2 region of FATZ-1(Takada et al., 2001). Furthermore, a binding assay has indicated that these two proteins compete for binding to FATZ-1. Interestingly, α-actinin-2 can displace filamin-C from the complex (Takada et al., 2001). It can be hypothesized that the binding affinity of the interaction FATZ-1/filamin-C is weaker than that of FATZ-1/α-actinin-2. It would be interesting to conduct additional studies on the FATZ-1/filamin-C complex. This could help determine if there is a weaker interaction compared to α-actinin-2 and assess the binding affinities of the ternary complex. It would also be important to investigate whether FATZ-1 remains flexible upon binding to filamin-C.

FATZ-1 interaction with the phosphatase calcineurin has been proven essential in regulating muscle fibre composition and exercise performance via the calcineurin/NFAT signalling pathway (Frey et al., 2008). It has been observed that FATZ-1 inhibits calcineurin activity, leading to NFAT phosphorylated molecules remaining in the cytoplasm and impeding its translocation to the nucleus (Frey et al., 2008). Currently, no structural or binding parameters of the FATZ-1/calcineurin complex are available. However, calcineurin's binding region is known to reside in the CD2 domain of FATZ-1 (Frey et al., 2000). As for the other partners, it might be a

competitive interaction between calcineurin and α-actinin-2 for the FATZ-1 CD2 region or a cooperative interaction. Since the interaction FATZ-1/calcineurin may be modulable in response to the biomechanical forces transduced through the Z-disc (Frank & Frey, 2011), it is expected to find some signals activating FATZ-1 interaction with calcineurin. Interestingly, calcineurin is a phosphatase, and the binding of FATZ-1 was mapped to its catalytic domain (Frey et al., 2000). Phosphorylation sites have been reported for FATZ-1 in the UniProt database (Q9NP98); however, no dephosphorization of FATZ-1 by calcineurin has been reported in the literature. Would FATZ-1 be an antagonist of phosphorylated substracts by competing for the catalytic unit with a strong affinity? Would FATZ-1 remain flexible upon binding to calcineurin, as in the case of α-actinin-2?

There are still numerous questions that need to be addressed to gain a better understanding of the role of FATZ-1 in the Z-disc. Our study has contributed one step closer to this understanding by providing the binding parameters between FATZ-1 and α-actinin-2. Furthermore, it has provided insights into the intrinsic disorder nature of FATZ-1, its remaining flexibility after binding to α-actinin-2 and how this flexibility may contribute to its role in the Z-disc.

MATERIALS AND METHODS

Constructs

FATZ1Δ184

The FATZ1Δ184 was provided by the Centre of Optimization for Structural Studies (project COSS, MFPL). They designed constructs using a bioinformatics approach that combined disordered and secondary structure predictions to create potentially soluble constructs. The fatz1 cDNA was amplified by PCR from 552 to 900 nt and cloned into the pETM14 vector, with a His6 tag in the N-term and a precision protease cleavage site. The resulting protein had FATZ-1's residues 185 to 299 and an expected molecular mass of 15.36 kDa.

FATZ1Δ91

The FATZ1Δ91 construct was provided by a project collaborator (Evitra at the Karolinska Institute, Sweden). They combined erase a base with colony filtration blot to screen multiple combinations of ORF and select the best soluble constructs (Cornvik et al., 2006). The *fatz1* cDNA was amplified by PCR from 274 to 900 nt and cloned into the vector pET-46 Ek/LICvector (Novagen). The resulting construct had an N-terminal His6-tag followed by a cleavage site for the protease Enterokinase and FATZ1's residues 92 through 299 with a calculated molecular mass of 23.37 kDa.

FATZ1Δ91 mutants

FATZ1Δ91 mutants were obtained by site-directed mutagenesis of the fatz1Δ91 construct. Mutagenic primers were designed to have a melting temperature of approximately 61 ºC. Phusion Flash proofreading polymerase was used for PCR amplification with a two-step protocol using construct FATZ1Δ91. The PCR reaction was treated with DpnI and transformed into *E. coli*. Two clones were picked and sent for sequencing. The presence of the mutation(s) was confirmed via Sanger sequencing. The confirmed clones were named KK_FATZ1Δ91, bearing mutations K176A and K233A, and KDK_FATZ1Δ91, bearing mutations K176A, D205A, and K233A. The resulting construct had an N-terminal His6-tag followed by a cleavage site for the protease Enterokinase and FATZ1's residues 92 through 299 with a calculated molecular mass of 23.37 kDa.

α-actinin-2

The lab plasmid bank provided the α-actinin-2 constructs. The ACTN2 was cloned in pET3d with a His6-tag and a TEV cleavage site at the C-terminal extremity. The ACTN2 construct had an expected molecular weight of 206 kDa, corresponding to the full-length dimer of α-actinin-2 with a deletion of the first 18 residues.

The ACTN2hd was cloned into pET8c with a His6-tag and a TEV cleavage site at the C-terminal. The ACTN2hd construct is the half-dimer of α-actinin-2 truncated at the symmetrical plane in the center of the ROD domain. This construct comprised two chains, Chain-A: ABD-neck-SR1-SR2 with an expected molecular weight of 60 kDa and Chain-B: SR3-SR4-EFhands with 40 kDa.

Protein Expression

Proteins were expressed using autoinduction media following the protocol described by Studier (Studier, 2005). The plasmid was transfected into *E. coli* strain *BL21(DE3)*. Cells were grown in 400 ml of autoinduction media ZYP5052 containing 50 µg/mL carbenicillin at 28°C for 15 hrs at 180 rpm. The final OD_{600}nm was ~5.5 per flask.

In addition, the expression was done in a BioFlo 110 fermentor. Here, cells were grown in 1.5 L of ZYP5052 media at 30 degrees for 13 hrs. The culture started with 100% dO_2 at 120 rpm and finished with 1 % dO_2 at 350 rpm. The final OD_{600nm} was 5.55, and the pH was ~ 6.75. The dry biomass was ~ 22 g (14 g/L).

Expression with N-5052 autoinduction medium for ^{15}N labelling

FATZ1Δ91 was labelled using N-5052 media for ^{15}N labelling following the protocol described by Studier (Studier, 2005). Fresh N-5052 media was inoculated with 5 ml of an ON culture of *E. coli BL21(DE3)* transformed with pET46_*fatz*1Δ91. Cells were grown in 400 ml of N-5052 media containing 50 µg/mL carbenicillin at 28°C for 15 hrs at 180 rpm. The final OD_{600}nm was ~5.5 per flask.

Protein purification

FATZ-1 constructs

After expression with autoinduction media, cells were harvested by centrifugation. They were resuspended (10 mL/gr of dry biomass pellet) in 20 mM

Tris-HCl pH 8, 20 mM imidazole, and 6M Gu-HCl (Buffer A2). The cells were disrupted by Sonication, 5 cycles, 5 min, 60% Power (3X). The extract was centrifuged at 18,000xg for 20 min at 4°C.

The supernatant was loaded onto a Ni+2-resin column (Histrap FF 5ml, GE Healthcare) and pre-equilibrated with Buffer A2. The resin was washed with three-column volumes of Buffer A2, then with five-column volumes of 20 mM Tris-HCl pH 8, 20 mM imidazole, 100 mM NaCl, 50 mM Glu, 50 mM Arg, 0.5 mM PMSF (Buffer A1). The protein was eluted in two steps. 1) a five-column volume of Buffer A1 supplemented with 250 mM imidazole and 2) a five-column volume of Buffer A1 supplemented with 500 mM imidazole. The protein was eluted in step 1; therefore, fractions from this step were pooled to continue to the next step.

To start the next step, the protein sample was diluted 1:5 in buffer 20 mM Tris-HCl pH 8 and 1 mM EDTA to obtain a final concentration of 20 mM NaCl (Buffer B1). Later, the sample was loaded on Resource Q (6 mL column) at a constant flow rate of 4-6 ml/min, previously equilibrated in 20 mM Tris-HCl pH 7.5, 20 mM NaCl, and 1 mM EDTA. The protein was eluted using a gradient step (20 CV – gradient slope) in 20 mM Tris-HCl pH 7.5, 1 M NaCl, and 1 mM EDTA (Buffer C). The FATZ1E1 protein was eluted in 10-40% of Buffer C.

The purified protein was loaded onto a size exclusion chromatography column (HiLoad 26/60 Superdex 75 prep grade, GE Healthcare) pre-equilibrated in 50 mM Sodium Phosphate pH 7, 100 mM NaCl, 50 mM Glu, 50 mM Arg, 0.5 mM PMSF, 1mM EDTA. Separations were performed at a flow rate of 2.0 mL/min. The final product was concentrated (Vivaspin - 10,000 MWCO) up to 6 mg/ml, flash-frozen in liquid nitrogen and stored at -20 °C.

SDS-PAGE and SEC-MALS assessed the purity and quality of the protein samples. Protein concentration was measured by absorbance at 280 nm, using the extinction coefficient 24,410 $M^{-1}.cm^{-1}$ in water (calculated by Expasy ProtParam tool).

α-actinin-2 constructs

After expression with autoinduction media, cells were harvested by centrifugation and resuspended in 10 mL of 20 mM Tris-HCl, 150 mM NaCl, 10 mM imidazole, 0.5 mM BME pH 7.5 (Buffer A) supplemented with anti-proteases

(Complete™ Protease Inhibitor Cocktail Tablets, Roche), lysozyme, DNAse I and cells were disrupted by French Press®. The extract was centrifuged at 18,000xg for 30 min at 4°C.

The supernatant was filtered (0.45 µm) and loaded onto a Ni^{+2}-resin column (1 mL), pre-equilibrated with Buffer A. The resin was washed with three-column volumes of Buffer A, then with three-column volumes of 20 mM Tris-HCl, 1 M NaCl, and 10 mM Imidazole at pH 7.5 (optional step to remove excess nucleic acid), and the protein was eluted in Buffer A supplemented with 500 mM imidazole.

The protein sample was dialyzed in 50 mM Tris-HCl, 50 mM NaCl, 0.5 mM BME, and 5 mM EDTA containing 0.1 mM anti-protease (PMSF) pH 7.5 (Buffer B). Alternatively, to dialysis, the protein sample was diluted to reduce the salt concentration by a factor of 3. Then, it was loaded on Resource Q (6 mL column) at a constant flow rate of 4-6 ml/min, previously equilibrated in Buffer B. The protein was eluted using a gradient step (20 CV – gradient slope) in 50 mM Tris-HCl, 2 M NaCl, 0.5 mM BME, 5 mM EDTA containing 0.1 mM PMSF, pH 7.5 (Buffer C). All ACTN2 sample was eluted in the range of 10-40% of Buffer C.

The recombinant protein was loaded onto a size exclusion chromatography column (HiLoad 16/60 Superdex 200 prep grade, GE Healthcare) pre-equilibrated in 20 mM Tris-HCl, 150 mM NaCl, 5 mM EDTA, 0.5 mM BME, 0.1 mM PMSF pH 7.5. Separations were performed at a flow rate of 0.5 mL/min. The purified protein was concentrated (Vivaspin - 50,000 MWCO) up to 5 mg/ml, flash-frozen in liquid nitrogen and stored at -20 °C.

SDS-PAGE and SEC-MALS assessed the purity and quality of the protein samples. Protein concentration was measured by absorbance at 280 nm, using an extinction coefficient of 127,365 $M^{-1}.cm^{-1}$ of ACTN2 in water (calculated by Expasy ProtParam tool).

Size exclusion chromatography combined with multi-angle light scattering (SEC-MALS)

SEC-MALS was performed in an Agilent HPLC system coupled with a miniDAWN® TREOS detector (Wyatt Technology) and a Shodex Refractive Index detector. The size exclusion chromatography was done in an analytical Superdex

200 10/300 column (GE Healthcare) at 0.5 ml/min, previously equilibrated with the sample buffer. The protein concentration was determined using the Shodex Refractive Index detector. The molar mass of eluting proteins was calculated using the ASTRA® software.

Circular Dichroism

CD spectroscopy was performed in the Chirascan CD spectrophotometer (Applied Photophysics) at the Leeds University CD facility. Protein samples were collected in 10 mM Sodium Phosphate pH 7 at two concentrations. Each sample was loaded into a 0.1 cm path length quartz Suprasil cuvette (Hellma Ltd), and two spectra were collected at 21 °C, over the wavelength range from 260nm to 180nm, with a 1nm step size and a 1 s dwell time.

The CD signal was converted from ellipticity (θ, millidegree) to mean residue molar ellipticity ($[\theta]_{MR}$, degrees cm^2 $dmol^{-1}$). Data analysis was done with the software SigmaPlot Version 12.5 in the following manner. Replicates of the CD signal were averaged, and the buffer signal was subtracted from the averaged spectra to obtain the protein spectra. The protein spectra were converted to mean residue molar ellipticity $[\theta]_{MR,}$ degrees cm^2 $dmol^{-1}$ using the following formula:

$$[\theta]_{\lambda MR} = \frac{\theta_{\lambda}}{p \star C \star (Nres - 1)}$$

Where: $\theta_{\lambda:}$ ellipticity in milidegrees, p: cuvette pathlength in mm (1 mm), C: molar concentration of protein in $mol*L^{-1}$, *Nres*: number of residues.

Isothermal titration calorimetry

ITC was performed in a MicroCal iTC200 (Malvern Panalytical). The measurements were done in 20 injections of 7.52 s, 180 s of spacing time between injections, 5 s as filter period, agitation of 750 rpm, at 25°C and DP=11 microcal/s. Proteins were prepared ON by dialysis in 50 mM NaPO4 pH 7.5, 100 mM NaCl, 50 mM Glu, 50 mM Arg, 1 mM EDTA,1mM βME, and 0.5 mM PMSF. The dialysis buffer was used as a buffer blank.

In the measurements, FATZ1Δ91 was in the syringe, and the α-actinin-2 was in the cell. FATZ1Δ91 was titrated into the buffer to determine the heat release of

protein dilution. Later, FATZ1Δ91 was titrated into the α-actinin-2 sample. Triplicate measurements of the interactions were done for each protein sample (FATZ1Δ91/ACTN2hd and FATZ1Δ91/ACTN2). Data were analyzed using the integrated public-domain package NITPIC (Scheuermann & Brautigam, 2015).

Cross-linking combined with MS

Proteins were prepared in 50 mM Sodium Phosphate pH 7, 150 mM NaCl, 1 mM EDTA, and 0.5 mM TCEP by extensive dialysis, placing both dialysis bags in the same beaker, with two buffer exchanges every two hours and a last step of ON, to remove Arg and Glu from the buffer.

Cross-linking was done using the 1-step method by adding 2 mM of EDC to 20 uM of the complex FATZ1Δ91/ACTN2hd. The reaction was incubated for 2 hours at RT. Proteins were prepared in 50 mM Sodium Phosphate pH 7, 150 mM NaCl, 1 mM EDTA, and 0.5 mM TCEP by extensive dialysis, placing both dialysis bags in the same beaker, with two buffer exchanges every two hours and a last step of ON. In addition, it was done the 2 steps method. In the first step, one protein was activated by adding 2mM EDC and 5mM NHS, and quenched by 20 mM TCE before adding the second protein.

Reaction products were run in SDS-PAGE 7.5 %. Bands of suspected cross-linked products were sliced, subjected to in-gel digestion using trypsin and analyzed by nano-HPLC-ESI-MS/MS at the University of Freiburg, Germany, by Dr. Friedel Drepper.

Dynamic light scattering (DLS)

DLS measurements were made in a DynaPro instrument (Wyatt Technologies) at 22° C with 100 acquisitions taken at 1 s intervals each. DLS was used to evaluate the polydispersity of samples before the SAXS measurements. The hydrodynamic diameter of particles in solution was measured under a monochromatic light (laser) beam. Data analysis was performed using the DYNAMICS® software.

Small-angle X-ray scattering

DATA were done in the BioSAXS beamline at ESRF with λ = 0.9919 Å and a Pilatus detector placed at 2.867 m. It was collected 20 frames per sample. First, 20 frames of buffer were collected, then 20 frames of protein sample, and finally, 20 frames of buffer again. The data was processed at the beamline, those frames with radiation damage were discarded, and the rest were averaged, obtaining one curve for protein and two for buffers. Buffer scattering was subtracted from the sample scattering to obtain the protein scattering. The final scattering curve was scaled by concentration, meaning that the intensity values of the *.dat files were divided by the protein concentration.

HPLC-SAXS

HPLC-SAXS was performed in the SWING BEAMLINE, at the Synchrotron Soleil, France, using the parameters shown in **Table 3.1**. A sample of 0.5 ml FATZ1Δ91 at 6.0 mg/ml was injected into a Superdex 75 10/300 column (GE Healthcare) at a flow rate of 0.2 ml/min. The protein was in 20 mM Tris pH 7.5, 100 mM NaCl, 50 mM Glu, 50 mM Arg, 1 mM EDTA, 0.5 mM PMSF, and 0.5 mM βME.

Data processing was done using standard procedures with the software FOXTROT provided by the SWIN BEAMLINE. The I(0) and Rg profiles per collected frame were obtained to detect the frames with protein scattering. The Guinier region was determined based on the highest intensity frame corresponding to the highest protein concentration. The same Guinier region (0.738 <SRg>1.2) was used for the rest of the data set, and Rg and I(0) were determined for every frame across the peak.

Table 3.1: DATA COLLECTION PARAMETERS		
	BioSAXS beamline at ESRF	**SWING beamline at the synchrotron SOLEIL**
Sample to detector distance (m)	2.867	1.8
Wavelength (Å)	0.9919	1.03
S range (nm^{-1})	0.032-4.967	0.04-3.8
Exposure time (sec)	1s/frame	500
Temperature (K)	283	283

NMR spectroscopy

Two samples of 100 µM FATZ1Δ1-91 were recorded at pH 7.8 and 6 in 50 mM Sodium Phosphate, 100 mM NaCl, 50 mM Glu, 50 mM Arg, 1 mM EDTA, and 0.5 mM PMSF. NMR spectra were recorded at 25 °C using a Varian Inova 800 mHz spectrometer. Spectra were recorded using standard procedures to obtain a PFG sensitivity-enhanced 2D ^{1}H-^{15}N HSQC spectrum.

ANNEXE

List of constructs used in the study

Name	**Protein of origin**	**Residues**	**MW (kDa)**	**Extinction Coefficient (280 nm, $M^{-1}cm^{-1}$)**
ACTN2hd	α-actinin-2 half-dimer **Chain A**: ABD-neck-SR1-SR2 **Chain B**: SR3-SR4-EFhands	Chain A: 1-514 Chain B: 515-894	Chain A: ~60 Chain B: ~40	126 740
ACTN2	α-actinin-2 dimer	19-894	~ 206	126 740
ACTN2-Pip2	α-actinin-2 dimer	19-894	~ 206	126 740
Efhands	α-actinin-2 Calmodulin domain	751-894	~17.7	8 940
FATZ1Δ184	FATZ-1	185-299	15.36	19 940
FATZ1Δ91	FATZ-1	92-299	~23.37	24 410
KK_FATZ1Δ91	FATZ-1, mutations K176A/K233A	92-299	~23.37	24 410
KDK_FATZ1Δ91	FATZ-1, mutations K176A/D205A/K233A	92-299	~23.37	24 410

REFERENCES

Broderick, M. J. F., & Winder, S. J. (2005). Spectrin, alpha-actinin, and dystrophin. *Advances in Protein Chemistry*, *70*, 203–246. https://doi.org/10.1016/S0065-3233(05)70007-3

Burridge, K., & Feramisco, J. R. (1981). Non-muscle α-actinins are calcium-sensitive actin-binding proteins. *Nature*, *294*(5841), Article 5841. https://doi.org/10.1038/294565a0

Chin, E. R., Olson, E. N., Richardson, J. A., Yang, Q., Humphries, C., Shelton, J. M., Wu, H., Zhu, W., Bassel-Duby, R., & Williams, R. S. (1998). A calcineurin-dependent transcriptional pathway controls skeletal muscle fiber type. *Genes & Development*, *12*(16), 2499–2509. https://doi.org/10.1101/gad.12.16.2499

Clark, K. A., McElhinny, A. S., Beckerle, M. C., & Gregorio, C. C. (2002). Striated muscle cytoarchitecture: An intricate web of form and function. *Annual Review of Cell and Developmental Biology*, *18*, 637–706. https://doi.org/10.1146/annurev.cellbio.18.012502.105840

Cornvik, T., Dahlroth, S.-L., Magnusdottir, A., Flodin, S., Engvall, B., Lieu, V., Ekberg, M., & Nordlund, P. (2006). An efficient and generic strategy for producing soluble human proteins and domains in E. coli by screening construct libraries. *Proteins*, *65*(2), 266–273. https://doi.org/10.1002/prot.21090

Delling, U., Tureckova, J., Lim, H. W., De Windt, L. J., Rotwein, P., & Molkentin, J. D. (2000). A calcineurin-NFATc3-dependent pathway regulates skeletal muscle differentiation and slow myosin heavy-chain expression. *Molecular and Cellular Biology*, *20*(17), 6600–6611. https://doi.org/10.1128/MCB.20.17.6600-6611.2000

Djinović-Carugo, K., Young, P., Gautel, M., & Saraste, M. (1999). Structure of the alpha-actinin rod: Molecular basis for cross-linking of actin filaments. *Cell*, *98*(4), 537–546. https://doi.org/10.1016/s0092-8674(00)81981-9

Drozdetskiy, A., Cole, C., Procter, J., & Barton, G. J. (2015). JPred4: A protein secondary structure prediction server. *Nucleic Acids Research*, *43*(W1), W389–W394. https://doi.org/10.1093/nar/gkv332

Edlund, M., Lotano, M. A., & Otey, C. A. (2001). Dynamics of α-actinin in focal adhesions and stress fibers visualized with α-actinin-green fluorescent protein. *Cell Motility*, *48*(3), 190–200. https://doi.org/10.1002/1097-0169(200103)48:3<190::AID-CM1008>3.0.CO;2-C

Faulkner, G., Lanfranchi, G., & Valle, G. (2001a). Telethonin and Other New Proteins of the Z-Disc of Skeletal Muscle. *IUBMB Life*, *51*(5), 275–282. https://doi.org/10.1080/152165401317190761

Faulkner, G., Lanfranchi, G., & Valle, G. (2001b). Telethonin and Other New Proteins of the Z-Disc of Skeletal Muscle. *IUBMB Life*, *51*(5), 275–282. https://doi.org/10.1080/152165401317190761

Faulkner, G., Pallavicini, A., Comelli, A., Salamon, M., Bortoletto, G., Ievolella, C., Trevisan, S., Kojić, S., Vecchia, F. D., Laveder, P., Valle, G., & Lanfranchi, G. (2000). FATZ, a Filamin-, Actinin-, and Telethonin-binding Protein of the Z-disc of Skeletal Muscle *. *Journal of Biological Chemistry*, *275*(52), 41234–41242. https://doi.org/10.1074/jbc.M007493200

Frank, D., & Frey, N. (2011). Cardiac Z-disc signaling network. *The Journal of Biological Chemistry*, *286*(12), 9897–9904. https://doi.org/10.1074/jbc.R110.174268

Franzot, G., Sjöblom, B., Gautel, M., & Djinović Carugo, K. (2005). The crystal structure of the actin binding domain from alpha-actinin in its closed conformation: Structural insight into phospholipid regulation of alpha-actinin. *Journal of Molecular Biology*, *348*(1), 151–165. https://doi.org/10.1016/j.jmb.2005.01.002

Frey, N., Barrientos, T., Shelton, J. M., Frank, D., Rütten, H., Gehring, D., Kuhn, C., Lutz, M., Rothermel, B., Bassel-Duby, R., Richardson, J. A., Katus, H. A., Hill, J. A., & Olson, E. N. (2004). Mice lacking calsarcin-1 are sensitized to calcineurin signaling and show accelerated cardiomyopathy in response to pathological biomechanical stress. *Nature Medicine*, *10*(12), Article 12. https://doi.org/10.1038/nm1132

Frey, N., Frank, D., Lippl, S., Kuhn, C., Kögler, H., Barrientos, T., Rohr, C., Will, R., Müller, O. J., Weiler, H., Bassel-Duby, R., Katus, H. A., & Olson, E. N. (2008). Calsarcin-2 deficiency increases exercise capacity in mice through calcineurin/NFAT activation. *The Journal of Clinical Investigation*, *118*(11), 3598–3608. https://doi.org/10.1172/JCI36277

Frey, N., & Olson, E. N. (2002). Calsarcin-3, a novel skeletal muscle-specific member of the calsarcin family, interacts with multiple Z-disc proteins. *The Journal of Biological Chemistry*, *277*(16), 13998–14004. https://doi.org/10.1074/jbc.M200712200

Frey, N., Richardson, J. A., & Olson, E. N. (2000). Calsarcins, a novel family of sarcomeric calcineurin-binding proteins. *Proceedings of the National Academy of Sciences of the United States of America*, *97*(26), 14632–14637. https://doi.org/10.1073/pnas.260501097

Gautel, M., & Djinović-Carugo, K. (2016). The sarcomeric cytoskeleton: From

molecules to motion. *The Journal of Experimental Biology*, *219*(Pt 2), 135–145. https://doi.org/10.1242/jeb.124941

Goldstein, M. A., Michael, L. H., Schroeter, J. P., & Sass, R. L. (1986). The Z-band lattice in skeletal muscle before, during and after tetanic contraction. *Journal of Muscle Research and Cell Motility*, *7*(6), 527–536. https://doi.org/10.1007/BF01753569

Holmes, K. C. (1995). The actomyosin interaction and its control by tropomyosin. *Biophysical Journal*, *68*(4 Suppl), 2S-7S.

Huxley, H. E. (1969). The Mechanism of Muscular Contraction. *Science*, *164*(3886), 1356–1366. https://doi.org/10.1126/science.164.3886.1356

Ishida, T., & Kinoshita, K. (2007). PrDOS: Prediction of disordered protein regions from amino acid sequence. *Nucleic Acids Research*, *35*(Web Server issue), W460. https://doi.org/10.1093/nar/gkm363

Jacques, D. A., & Trewhella, J. (2010). Small-angle scattering for structural biology—Expanding the frontier while avoiding the pitfalls. *Protein Science : A Publication of the Protein Society*, *19*(4), 642–657. https://doi.org/10.1002/pro.351

Kikhney, A. G., & Svergun, D. I. (2015). A practical guide to small angle X-ray scattering (SAXS) of flexible and intrinsically disordered proteins. *FEBS Letters*, *589*(19PartA), 2570–2577. https://doi.org/10.1016/j.febslet.2015.08.027

Kn, N., N, Y., D, W., M, M., S, E., & Ah, B. (1999). A common nonsense mutation results in alpha-actinin-3 deficiency in the general population. *Nature Genetics*, *21*(4). https://doi.org/10.1038/7675

Luther, P. K. (2000). Three-dimensional structure of a vertebrate muscle Z-band:

Implications for titin and alpha-actinin binding. *Journal of Structural Biology*, *129*(1), 1–16. https://doi.org/10.1006/jsbi.1999.4207

Luther, P. K. (2009). The vertebrate muscle Z-disc: Sarcomere anchor for structure and signalling. *Journal of Muscle Research and Cell Motility*, *30*(5–6), 171–185. https://doi.org/10.1007/s10974-009-9189-6

Luther, P. K., Padrón, R., Ritter, S., Craig, R., & Squire, J. M. (2003). Heterogeneity of Z-band structure within a single muscle sarcomere: Implications for sarcomere assembly. *Journal of Molecular Biology*, *332*(1), 161–169. https://doi.org/10.1016/s0022-2836(03)00883-0

MacArthur, D. G., Seto, J. T., Raftery, J. M., Quinlan, K. G., Huttley, G. A., Hook, J. W., Lemckert, F. A., Kee, A. J., Edwards, M. R., Berman, Y., Hardeman, E. C., Gunning, P. W., Easteal, S., Yang, N., & North, K. N. (2007). Loss of ACTN3 gene function alters mouse muscle metabolism and shows evidence of positive selection in humans. *Nature Genetics*, *39*(10), 1261–1265. https://doi.org/10.1038/ng2122

Manalastas-Cantos, K., Konarev, P. V., Hajizadeh, N. R., Kikhney, A. G., Petoukhov, M. V., Molodenskiy, D. S., Panjkovich, A., Mertens, H. D. T., Gruzinov, A., Borges, C., Jeffries, C. M., Svergun, D. I., & Franke, D. (2021). ATSAS 3.0: Expanded functionality and new tools for small-angle scattering data analysis. *Journal of Applied Crystallography*, *54*(1), 343–355. https://doi.org/10.1107/S1600576720013412

Masaki, T., Endo, M., & Ebashi, S. (1967). Localization of 6S component of a alpha-actinin at Z-band. *Journal of Biochemistry*, *62*(5), 630–632. https://doi.org/10.1093/oxfordjournals.jbchem.a128717

McElhinny, A. S., Kazmierski, S. T., Labeit, S., & Gregorio, C. C. (2003). Nebulin:

The nebulous, multifunctional giant of striated muscle. *Trends in Cardiovascular Medicine*, *13*(5), 195–201. https://doi.org/10.1016/s1050-1738(03)00076-8

Miles, A. J., Drew, E. D., & Wallace, B. A. (2023). DichroIDP: A method for analyses of intrinsically disordered proteins using circular dichroism spectroscopy. *Communications Biology*, *6*(1), Article 1. https://doi.org/10.1038/s42003-023-05178-2

Miles, A. J., Ramalli, S. G., & Wallace, B. A. (2022). DichroWeb, a website for calculating protein secondary structure from circular dichroism spectroscopic data. *Protein Science*, *31*(1), 37–46. https://doi.org/10.1002/pro.4153

Mills, M., Yang, N., Weinberger, R., Vander Woude, D. L., Beggs, A. H., Easteal, S., & North, K. (2001). Differential expression of the actin-binding proteins, alpha-actinin-2 and -3, in different species: Implications for the evolution of functional redundancy. *Human Molecular Genetics*, *10*(13), 1335–1346. https://doi.org/10.1093/hmg/10.13.1335

North, K. N., & Beggs, A. H. (1996). Deficiency of a skeletal muscle isoform of alpha-actinin (alpha-actinin-3) in merosin-positive congenital muscular dystrophy. *Neuromuscular Disorders: NMD*, *6*(4), 229–235. https://doi.org/10.1016/0960-8966(96)00361-6

Noureddine, M., & Gehmlich, K. (2023). Structural and signaling proteins in the Z-disk and their role in cardiomyopathies. *Frontiers in Physiology*, *14*, 1143858. https://doi.org/10.3389/fphys.2023.1143858

Pappas, C. T., Bhattacharya, N., Cooper, J. A., & Gregorio, C. C. (2008). Nebulin interacts with CapZ and regulates thin filament architecture within the Z-disc. *Molecular Biology of the Cell*, *19*(5), 1837–1847.

https://doi.org/10.1091/mbc.e07-07-0690

Receveur-Brechot, V., & Durand, D. (2012). How Random are Intrinsically Disordered Proteins? A Small Angle Scattering Perspective. *Current Protein & Peptide Science*, *13*(1), 55–75. https://doi.org/10.2174/138920312799277901

Ribeiro, E. de A., Pinotsis, N., Ghisleni, A., Salmazo, A., Konarev, P. V., Kostan, J., Sjöblom, B., Schreiner, C., Polyansky, A. A., Gkougkoulia, E. A., Holt, M. R., Aachmann, F. L., Žagrović, B., Bordignon, E., Pirker, K. F., Svergun, D. I., Gautel, M., & Djinović-Carugo, K. (2014). The Structure and Regulation of Human Muscle α-Actinin. *Cell*, *159*(6), 1447–1460. https://doi.org/10.1016/j.cell.2014.10.056

Sanger, J. W., Wang, J., Fan, Y., White, J., & Sanger, J. M. (2010). Assembly and Dynamics of Myofibrils. *BioMed Research International*, *2010*, e858606. https://doi.org/10.1155/2010/858606

Sanger, J. W., Wang, J., Holloway, B., Du, A., & Sanger, J. M. (2009). Myofibrillogenesis in skeletal muscle cells in zebrafish. *Cell Motility*, *66*(8), 556–566. https://doi.org/10.1002/cm.20365

Scheuermann, T. H., & Brautigam, C. A. (2015). High-precision, automated integration of multiple isothermal titration calorimetric thermograms: New features of NITPIC. *Methods (San Diego, Calif.)*, *76*, 87–98. https://doi.org/10.1016/j.ymeth.2014.11.024

Schiaffino, S., & Reggiani, C. (2011). Fiber types in mammalian skeletal muscles. *Physiological Reviews*, *91*(4), 1447–1531. https://doi.org/10.1152/physrev.00031.2010

Sjöblom, B., Salmazo, A., & Djinović-Carugo, K. (2008). α-Actinin structure and regulation. *Cellular and Molecular Life Sciences*, *65*(17), 2688–2701.

https://doi.org/10.1007/s00018-008-8080-8

Sponga, A., Arolas, J. L., Schwarz, T. C., Jeffries, C. M., Rodriguez Chamorro, A., Kostan, J., Ghisleni, A., Drepper, F., Polyansky, A., De Almeida Ribeiro, E., Pedron, M., Zawadzka-Kazimierczuk, A., Mlynek, G., Peterbauer, T., Doto, P., Schreiner, C., Hollerl, E., Mateos, B., Geist, L., … Djinović-Carugo, K. (2021). Order from disorder in the sarcomere: FATZ forms a fuzzy but tight complex and phase-separated condensates with α-actinin. *Science Advances*, *7*(22), eabg7653. https://doi.org/10.1126/sciadv.abg7653

Squire, J. M. (1997). Architecture and function in the muscle sarcomere. *Current Opinion in Structural Biology*, *7*(2), 247–257. https://doi.org/10.1016/S0959-440X(97)80033-4

Studier, F. W. (2005). Protein production by auto-induction in high-density shaking cultures. *Protein Expression and Purification*, *41*(1), 207–234. https://doi.org/10.1016/j.pep.2005.01.016

Takada, F., Vander Woude, D. L., Tong, H. Q., Thompson, T. G., Watkins, S. C., Kunkel, L. M., & Beggs, A. H. (2001). Myozenin: An alpha-actinin- and gamma-filamin-binding protein of skeletal muscle Z lines. *Proceedings of the National Academy of Sciences of the United States of America*, *98*(4), 1595–1600. https://doi.org/10.1073/pnas.98.4.1595

Takahashi, K., & Hattori, A. (1989). Alpha-actinin is a component of the Z-filament, a structural backbone of skeletal muscle Z-disks. *Journal of Biochemistry*, *105*(4), 529–536. https://doi.org/10.1093/oxfordjournals.jbchem.a122701

Uversky, V. N. (2002). What does it mean to be natively unfolded? *European Journal of Biochemistry*, *269*(1), 2–12. https://doi.org/10.1046/j.0014-2956.2001.02649.x

von Nandelstadh, P., Ismail, M., Gardin, C., Suila, H., Zara, I., Belgrano, A., Valle, G., Carpen, O., & Faulkner, G. (2009). A Class III PDZ Binding Motif in the Myotilin and FATZ Families Binds Enigma Family Proteins: A Common Link for Z-Disc Myopathies. *Molecular and Cellular Biology*, *29*(3), 822–834. https://doi.org/10.1128/MCB.01454-08

Wang, J., Fan, Y., Dube K, D., Sanger, J. M., & Sanger, J. W. (2014). Jasplakinolide reduces actin and tropomyosin dynamics during myofibrillogenesis. *Cytoskeleton (Hoboken, N.J.)*, *71*(9). https://doi.org/10.1002/cm.21189

Wang, J., Shaner, N., Mittal, B., Zhou, Q., Chen, J., Sanger, J. M., & Sanger, J. W. (2005). Dynamics of Z-band based proteins in developing skeletal muscle cells. *Cell Motility and the Cytoskeleton*, *61*(1). https://doi.org/10.1002/cm.20063

Wright, P. E., & Dyson, H. J. (2015). Intrinsically disordered proteins in cellular signalling and regulation. *Nature Reviews Molecular Cell Biology*, *16*(1), Article 1. https://doi.org/10.1038/nrm3920

Ylänne, J., Scheffzek, K., Young, P., & Saraste, M. (2001). Crystal structure of the alpha-actinin rod reveals an extensive torsional twist. *Structure (London, England: 1993)*, *9*(7), 597–604. https://doi.org/10.1016/s0969-2126(01)00619-0

SUMMARY

FATZ-1 is a Z-disc protein expressed in fast-twitch fibres, which has multiple interacting partners such as α-actinin-2, the major player of the Z-disc, whose primary role is to cross-link the actin filaments at the boundaries of the sarcomere. In addition to α-actinin-2, FATZ-1 binds to myotilin, telethonin, the PDZ domain of ZASP and enigma family, filamin-C and the phosphatase domain of calcineurin. FATZ-1 plays an essential role in Z-disc signalling since it is a negative modulator of the calcineurin/NFAT signalling cascade that controls the muscle fibre composition in response to biomechanical stress. It may also play an essential role in the Z-disc assembly during the initial stages of myofibrillogenesis since it is present with α-actinin-2 and myotilin in the Z-bodies, the Z-disc precursors. Other FATZ isoforms exist, such as FATZ-2 in cardiac muscle and slow-twitch fibers, and FATZ-3 in fast-twitch fibres. The three isoforms bind the same proteins and perform similar roles in the Z-disc. They share conserved regions in the N-terminal and C-terminal, annotated as CD1 and CD2 in their sequence. The central region, called the GRR, is more variable and has a compositional bias towards glycine, a signature for disordered regions. Interestingly, none of the isoforms have structural homologs or canonical domains predicted. Several interactions have been mapped to the FATZ-1 CD2 region. To interact with all those binding partners, FATZ-1 may need multiple binding sites accessible, or competitive binding mechanisms would regulate their binding.

This project performed a biophysical and structural characterization of FATZ-1 alone and in complex with α-actinin-2 to understand its contribution to the Z-disc structure and assembly. We focused on answering the following questions. 1) What is the molecular architecture of FATZ-1? 2) How can the molecular architecture of FATZ-1 support its function? 3) What is the binding affinity of the complex FATZ-1/α-actinin-2? 4) What are the molecular bases of the complex FATZ-1/α-actinin-2? 5) How does the molecular architecture of the complex FATZ-1/α-actinin-2 contribute to the Z-disc structure?

A FATZ-1 construct having a deletion of the first 91 residues called FATZ1Δ91 was used to characterize the structure of FATZ-1. This construct was less sensitive to degradation and precipitation than the full-length, allowing us to establish

expression and purification protocols at a large scale to obtain enough protein for biophysical and structural studies. The experimental data obtained by SEC-MALS showed that FATZ1Δ91 is a monomer in solution. Furthermore, CD, NMR and SAXS experiments were employed to characterize its structural properties. The experimental evidence indicated that FATZ1Δ91 is an intrinsically disordered protein with a residual secondary structure. The EOM analysis suggested that a conformational ensemble can better describe the FATZ1Δ91 structure.

The construct FATZ1Δ91 was also used to study the interaction with α-actinin-2 since it comprises the entire CD2 region where the binding region of α-actinin-2 has been previously described. A co-purification protocol was developed to obtain the complex by size exclusion chromatography as a stable complex in solution in sufficient amounts to perform binding and structural experiments. ITC experiments were performed with α-actinin-2 full-length and half-dimer constructs to determine the binding constants of the complex FATZ-1/α-actinin-2. The binding assays with α-actinin-2 full-length and half-dimer provided Kd values of the complex with one and two binding sites. In collaboration with Dr. Friedel Drepper and Prof. Bettina Warsheid at the University of Freiburg, it was identified the contact residues at the binding interface employing chemical cross-linking combined with MS. The relevance of the proposed contact residues was tested using a FATZ1Δ91 mutant, designed to abolish the electrostatic interactions between two of the paired residues. In SEC-MALS and ITC, the FATZ1Δ91 mutant could still bind α-actinin-2, forming a stable complex but with relatively lower affinity than FATZ1Δ91 wild-type. The attempt to disrupt the complex using two-point mutations was unsuccessful, leading us to hypothesize that additional residues might be involved in the binding interface between FATZ-1 and α-actinin-2. The ITC data supported this hypothesis, revealing a strong affinity between these two binding partners.

CD and SAXS experiments were performed to obtain structural information on the complex FATZ-1/α-actinin-2. It was observed that there was no increment in the secondary structure content of the complex upon binding of FATZ1Δ91 to α-actinin-2. Moreover, the Kratky plots of the complex FATZ-1/α-actinin-2 suggested that FATZ1Δ91 remains flexible after binding α-actinin-2.

FATZ-1's flexibility is be compatible with having multiple binding partners, being part of a signalling pathway and recruiting proteins into the Z-disc during assembly. Since FATZ-1 has numerous binding partners in the CD2 region, providing flexible regions rather than compact globular domains may represent an advantage in performing multiple interactions. The high affinity of the complex FATZ-1/α-actinin-2 may allow the FATZ-1 to stay anchored to α-actinin-2 while interacting with other binding partners that would exchange in its CD2 region in response to signalling events or according to the Z-disc assembling stages.

ABSTRAKT

FATZ-1 ist ein Protein, das in der Z-Scheibe von schnell zuckenden Muskelfasern exprimiert wird und mehrere Bindungspartner wie α-Actinin, Filamin-C, Telethonin, ZASP, Myotilin und Calcineurin hat. FATZ-1 ist als negativer Modulator der Calcineurin/NFAT-Signalkaskade, die die Muskelfaserzusammensetzung als Reaktion auf biomechanische Belastungen steuert, ein wesentlicher Akteur bei der Z-Scheiben-Signalgebung. Darüber hinaus könnte FATZ-1 eine wesentliche Rolle beim Aufbau der Z-Scheibe spielen, indem es mit α-Actinin-2 interagiert, da der Komplex in den frühen Stadien der Myofibrillogenese auftritt, wo er andere Proteine an die Z-Scheibe rekrutieren kann. Der C-terminale Bereich stellt eine funktionelle Domäne dar, in der mehrere Bindungspartner interagieren. Wie die Struktur von FATZ-1 mehrere Bindungspartner unterstützen und die Rekrutierung anderer Proteine an der Z-Scheibe erreichen kann, während sie gleichzeitig an α-Actinin-2 bindet, muss noch herausgefunden werden. Wir haben eine Strukturstudie des Komplexes FATZ-1/α-Actinin-2 durchgeführt, um seinen Beitrag zur Struktur und Funktion der Z-Scheibe zu verstehen. Da Vorhersagen auf große unstrukturierte Bereiche in FATZ-1 hindeuteten, setzten wir verschiedene biophysikalische Methoden wie CD und SAXS ein, um seine Struktur zu untersuchen. Wir fanden heraus, dass FATZ-1 die Merkmale eines intrinsisch ungeordneten Proteins mit einem Restgehalt an Sekundärstruktur aufweist und besser als Konformationsensemble beschrieben werden kann. Darüber hinaus fanden wir heraus, dass FATZ-1 und α-Actinin-2 einen hochaffinen Komplex mit zwei verschiedenen Bindungsereignissen bilden. Wir identifizierten Kontaktreste der Bindungsschnittstelle des Komplexes FATZ-1/α-Actinin-2 durch chemische Quervernetzung in Kombination mit Massenspektrometrie. Schließlich legen unsere CD- und SAXS-Daten nahe, dass FATZ-1 nach der Bindung an α-Actinin-2 eher flexibel als kompakt bleibt. Unsere Studie stellt die Hypothese auf, dass die hohe Affinität des Komplexes FATZ-1/α-Actinin-2 und die Flexibilität von FATZ-1 für den Zusammenbau der Z-Scheibe und die Signalübertragung von Vorteil sein könnten, da FATZ-1 an der Z-Scheibe verankert bleiben kann, während es mit anderen Bindungspartnern interagiert, die in seiner CD2-Region als Reaktion auf Signalereignisse oder in Abhängigkeit von den Entwicklungsstadien der Z-Scheibe ausgetauscht werden würden.